12-2017

In Vitro Diabetic-Hypertensive Cellular-Response Evaluation Model for In-Stent Restenosis

Varun Chawla
Clemson University

IN VITRO DIABETIC-HYPERTENSIVE CELLULAR-RESPONSE EVALUATION MODEL FOR IN-STENT RESTENOSIs

---

A Dissertation
Presented to
the Graduate School of
Clemson University

In Partial Fulfillment
of the Requirements for the Degree
Doctor of Philosophy
Bioengineering

---

by
Varun Chawla
December 2017

Accepted by:
Dr. Martine LaBerge, Committee Co-chair
Dr. Agneta Simionescu, Committee Co-chair
Dr. Dan Simionescu
Dr. Eugene M. Langan III

Abstract

Drug-eluting stents have revolutionized the field of interventional cardiology and with the advent of their second-generation, percutaneous coronary intervention with drug-eluting stents is the clinically preferred method. These stents have shown remarkable performance in reducing neointimal hyperplasia and thus, clinical manifestation of restenosis. Despite significant technological advances in DES, high-risk patient populations are still affected by in-stent restenosis. Diabetes and hypertension are the two most common patient-specific complications that result in the development of restenosis even in DES era. Currently, percutaneous interventional approaches are not designed specifically to address the pathophysiological progression of restenosis in diabetic and hypertensive patients and as a result these high-risk patient cohorts continue to experience poorer prognosis. Absence of diabetes and/or hypertension specific stents or percutaneous interventional approaches is in part due to less emphasized basic research on understanding cellular response in diabetes and hypertension associated conditions owing to the lack of *in vitro* testing platforms capable of capturing the clinically relevant cellular response.

Diabetes is characterized by hyperglycemia, insulin resistance and requires external insulin administration. Chronic high-glucose acclimation resulted in significantly greater phenotypic modulation of vascular smooth muscle cells under clinically relevant loading. In the current dissertation, an *in vitro* model has been developed simulating conditions observed in diabetic and hypertensive patients to better evaluate the response of VSMC, predict in-stent restenosis and evaluate the efficacy of sirolimus. This model combined insulin administration and elevated circumferential strain associated with diabetes and hypertension respectively, with low wall-shear stress induced by the presence of stent struts. Cellular response under these conditions closely simulates clinical conditions, in comparison to the current gold standard of conventional static

cultures. Additionally, this model allows for a better understanding of VSMC response subjected to diabetes and hypertension simulated conditions during dynamic mechanical loading.

Using this novel approach of combining mechanical loading and patient-specific biochemical environment, this dissertation successfully demonstrates significantly greater phenotypic modulation of chronic high-glucose acclimated rat aortic smooth muscle cells due to insulin administration under clinically relevant mechanical forces. Evaluation of phenotypic modulation was performed by comparing cell-cycle progression, induction of apoptosis, expression of contractile-state associated proteins all of which demonstrated significantly greater modulation with insulin administration under dynamic loading ($p < 0.0001$ for all).

Hypertension-associated elevated mechanical strain resulted in a proliferative phenotype ($p < 0.001$), induced apoptosis ($p < 0.001$) and reduced the expression of contractile state proteins ($p < 0.001$). Subjecting cells to insulin administration under hypertension-associated cyclic mechanical strain with low-flow shear stress further enhances dedifferentiation of RASMCs. The combined effects of hypertensive mechanical forces and insulin administration associated with diabetes management significantly affected cell response where cells under hypertensive loading during insulin administration demonstrated significantly greater percentage of cells in the S ($p< 0.0001$) and G2/M phase ($p< 0.0001$). These conditions also resulted in significantly reduced expression of contractile markers (p-value < 0.0001 for αSM-actin and SM22α). As a model application, sirolimus a commonly used drug in stents was evaluated under diabetic-hypertensive conditions. Lower efficacy of sirolimus was observed under these conditions which necessitates development and identification of novel drugs and therapeutic targets, to address the greater phenotypic modulation associated with these patient-specific conditions and may also explain the poorer outcomes of sirolimus -eluting stents in diabetic patients requiring insulin administration and presenting with hypertension. The proposed cell-response evaluation model provides a tool to

investigate cellular and molecular mechanisms, testing novel drug and identifying important molecular targets for the specific patient cohort.

Acknowledgements

I would like to extend my sincerest thanks to my academic advisors – Dr. Martine LaBerge and Dr. Agneta Simionescu for all their support and guidance through my graduate school education and beyond. It is their patience and unrestricted support that always encouraged me to persevere. Sincere thanks to Dr. Dan Simionescu for providing critical insights that helped me shape this project to its potential and Dr. Eugene Langan III, for his guidance on clinical relevancy of the project. I am thankful to all the administrative and research staff at Clemson Bioengineering, Godley-Snell animal research facility, Machine shop, IBIOE for all the help they have given to me.

On a personal front, I am thankful to my family – Dad & Ma, Anubhav, Geetika and the most recent addition to our family, Yohaan. All of you have provided me the courage and moral support to venture into the unknown and have most definitely stood by my decisions even in the toughest of times. To all my friends, especially – Devanshu Gambhir and Tori Kleinbort - You have been a great source of support for me. I cannot thank you all enough for supporting me in meltdowns and putting up with me for so many years.

This exciting journey has restructured me in so many domains of life and I have learned so much from it that I am truly humbled. In the end, I would like to concur “If I have seen further, it is by standing on the shoulders of giants” – Isaac Newton 1675.

Table of Contents

Table of Contents (continued) Page

List of Figures, Tables and Equations

Page

Page

Page

Page

List of Abbreviations

RASMC – Rat aortic smooth muscle cells

VSMC – Vascular smooth muscle cell

D – Dimethylsulfoxide

DW – DMSO with wortmannin

DI – DMSO with insulin

DWI – DMSO with insulin and wortmannin

U - Unloaded

CT – Cyclic tensile

CTS – Cyclic tensile strain with low wall-shear stress

CTSS – Cyclic Tensile shear with low wall-shear stress and sirolimus

HTS – Hypertensive strain with low wall-shear stress

HTSS – Hypertensive strain with low wall-shear stress and sirolimus

BA – Balloon angioplasty

BMS - Bare metal stent

DES – Drug eluting stent

BP- Blood pressure

SBP- Systolic blood pressure

DBP-Diastolic blood pressure

HT – Hypertension

ISR – In-stent restenosis

Chapter 1: Background

1.1 Blood Vessel Anatomy:

The structure of the blood vessel has been anatomically structured to support multitude of functions including nutrient transport and gas exchange. Within the systemic circulation system, arteries carry oxygenated blood away from the heart downstream via smaller vessels. Arterioles, the smallest arteries, branch into tiny capillaries which are the site of nutrient and waste exchange owing to their thin structure. Similarly, deoxygenated blood is transported back to the heart via venules, veins and ultimately back to the heart to enter the pulmonary circuit. Different types of blood vessels vary slightly in their structures, but they share the same general features. Arteries and arterioles have thicker walls than veins and venules because they are closer to the heart and receive blood that is surging at a far greater pressure. In the larger vessels, blood transport occurs relatively quickly which, in addition to thicker vessel walls, results in poorer exchange of nutrients and waste. Anatomically, this problem is addressed by vasa vasorum or vessels of the vessel which fundamentally provide the nutrient exchange for the cells of larger blood vessels. Owing to differences in pressure, vasa vasorum are located closer to the lumen in veins whereas in the outer layer for arteries (1).

Blood vessels closer to the heart are known as elastic or conducting arteries typically larger than 10 mm in diameter and rich in elastic fibers. Moving away from the heart, the elastin content decreases while the amount of vascular smooth muscle cell increases resulting in muscular or distributing arteries ranging from 0.1 to 10 mm. Downstream these arteries further split into arterioles and eventually capillaries. A blood vessel is structured into three main layers or tunics:

Intima, *Media* and *Externa:*

a. *Tunica Intima:* As the innermost layer of a blood vessel, the intima is comprised of simple squamous epithelium called endothelium, which is a continuous layer throughout the entire vascular system, including the chambers of the heart. The endothelium is responsible for multitude functionalities such as regulating capillary exchange, altering blood flow through endothelin mediated vascular smooth muscle cell contraction, nitric oxide mediated vascular tone regulation among others. The endothelial monolayer is bound to the basement membrane or basal lamina (~80 nm thick) that effectively provides strength while maintain flexibility and permits materials to pass through owing to its permeable nature. The basement membrane primarily consists of type IV collagen and laminin. The intimal layer in aorta and coronary arteries may also include a sub-endothelial layer of connective tissue and axially oriented smooth muscle cells. Endothelial cells are usually flat and elongated in the direction of the blood flow, often about 0.2-0.5 μm thick, 10-15 μm wide and 25-50 μm long. Cells are interconnected by both tight junctions and gap junctions which regulate transport of substances across the endothelium and allow cell-cell communication via transport of metabolites respectively (2). In a healthy blood vessel, an intact endothelium ensures a non-thrombogenic luminal surface. The outer layer of tunica intima consists of connective tissue comprising primarily of elastic fibers to provide flexibility and collagenous fibers to provide mechanical strength. For larger arteries, a distinct elastic fiber layer is also present towards the boundary with tunica media, known as internal elastic lamina. Openings within this lamina permits exchange of materials between the tunics (1).
b. *Tunica Media:* The thickest layer of a blood vessel, the tunica media primarily consists of vascular smooth muscle cells that are responsible for muscular contraction and relaxation of the blood vessel, Type I, III and V collagen, and proteoglycans. The cells are supported

by connective tissue consisting of elastic fibers or elastin mostly arranged in circular sheets whereas presence of longitudinal fibers is more prominent towards the outer side of the layer. The cellular layer is supported by a framework of collagenous fibers that also bind to the inner and out tunics. Contraction and relaxation of circumferentially arranged muscular cells maintains the vascular tone of a blood vessel through processes known as vasoconstriction and vasodilation which are chemically and mechanically driven phenomenon. Like endothelial cells, smooth muscle cells also communicate via gap junctions. Their intracellular myofibrils are typically oriented along the axis of the cell. In elastic arteries, the medial smooth muscle cells are organized into 5-15 μm-thick concentric layers that are separated by thin fenestrated sheets of elastin, which supports radial transport of metabolites (1)(2).

c. *Tunica Externa (Adventitia):* Separated from the medial layer by the external elastic lamina, the outermost layer or adventitia comprises of collagenous fibers and fibroblasts. Fibroblasts are responsible for regulating the connective tissue, particularly type I collagen. The outermost layer of the externa is not distinctively visible but blends with the surrounding connective tissue around the blood vessel. The thickest layer for veins and the site for vasa vasorum in arteries, the outermost layer ensures stability and position of the blood vessel and prevents over distension of the vessels.

1.2 Blood-vessel mechanical forces:

During a single cardiac cycle, oxygenated blood is transported in a pulsatile manner from the heart to the aorta for distribution to the systemic circuit. Multiple forces act together in a healthy blood vessel as a result of blood flow from the heart and can adjust according to the diseased state of the vessel to ensure hemostasis. These forces can be from blood flow (shear), arterial distension and

contraction (vascular tone) and hydrostatic fluid pressure. Application of these forces induce stresses in the longitudinal, radial and circumferential directions and represents the intricate interplay between solid mechanics and fluid dynamics of the blood vessel. As depicted in the image, the radial pressure (P) in the lumen is balanced by circumferential tensile stress (σ) in the artery wall and is defined by Laplace's law, which assumed the blood vessel to be thin-cylinder, where 'r' is the radius and 'h' is thickness of the vessel (Figure 1).

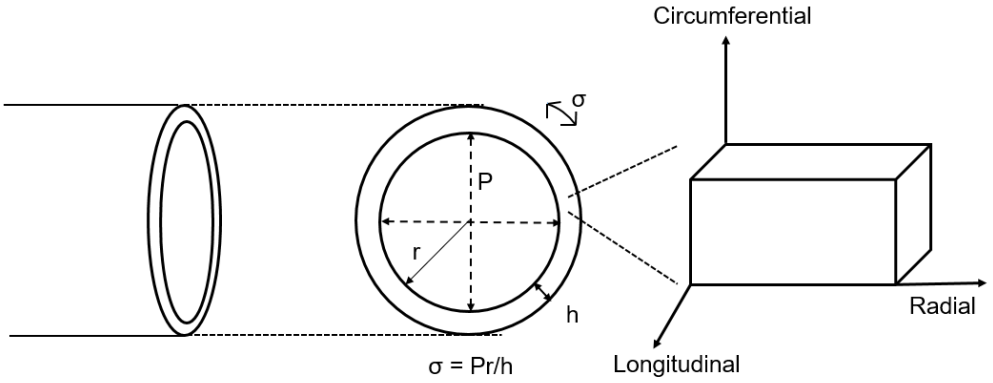

Figure 1: Principle stresses for thin-wall cylinder with Laplace's model (Adapted and modified from Lee et al) (3)

In three-dimension, most biological materials exhibit non-linear mechanical behavior and as the stress on a biological material is increased, the increment of strain for each increment of stress decreases, so that the material becomes stiffer and is one of the reasons why angioplasty often requires balloon pressures over 50 times greater than mean arterial blood pressures (3). Since blood vessels are not made up of a single material, defining their mechanical behavior with a single number is an oversimplification. Three-dimensionally, blood vessels have different arrangement of collagen and elastin fibers that results in different stress-strain relationship depending upon the direction of applied force or anisotropic and may require over 20 variables to accurately define the

mechanical properties. Blood-vessels also have a time-dependent response to the applied forces where if tensile stress is placed on the tissue, it will continue to elongate for some period of time until a new equilibrium strain is reached and essentially demonstrate a time-dependence of stress-strain relationship called viscoelasticity. Prolonged balloon inflations beyond critical fracture point and delayed elastic recoil are clinical cases where viscoelastic nature of the blood-vessel material comes into play (3). For arterial wall, the intraluminal surface is subjected to mean pressures of about 13.3 kPa (100 mmHg) and pulse pressure of ~ 5.3 kPa (40 mmHg). Physiologically, arterial wall is subjected to < 10% circumferential strain whereas in the longitudinal direction, arteries are stretched by 30-50% as confirmed by arterial contraction immediately after excision. The arterial diameter varies by ~ 10% in addition to significant change in arterial length as well (4).

Blood flow through small vessels is defined by the Haagen-Poiseuille flow or laminar flow through circular tubes where typical blood-flow rates are in the range of 300-400 mL/min. Behavior of fluid flow is impacted by the diseased state of the vessel and it has been well established that areas of low-wall shear stress or zones of no-flow are the primary sites of atherosclerotic lesion initiation and progression (5). In general, fluid flow can be steady or unsteady in nature with steady flow having a flow-velocity that does not alter with time while, time-dependent change occurs in unsteady flow conditions (6). Larger arteries are sites of unsteady flow conditions whereas small arteries and capillaries are considered to have steady flow conditions.

Flow through a cylindrical tube or vessel may be characterized as laminar, transitional or turbulent which is a result of the various forces acting on the fluid. Through a cylindrical tube, flow particles experience two primary forces – inertial and viscous forces. The ratio of these two forces is a dimensionless constant defined as the Reynolds number (Re), where ρ is the fluid density (kg/cm^3), U is velocity (cm/s), d is diameter (cm) and μ is viscosity ($dyne*sec/cm^2$) (7).

$$\mathrm{Re} = \frac{\text{Inertial forces}}{\text{Viscous forces}} = \frac{\rho U d}{\mu} \qquad \{1\}$$

A fluid volume entering a long tube has a flat velocity profile at the entrance of the tube and as fluid moves into the tube and further away from the entrance, the velocity profile begins to have a curvature near the wall and has a magnitude of zero at the wall (no slip condition) whereas the profile at the center remains flat. Beyond an arbitrary point (defined as fully developed point or F-D line), the fluid profile becomes parabolic. The section of the tube before the FD-line is called the entrance length or flow development region. For laminar flow (Re < 1200), fluid is assumed to move in concentric cylindrical shells and since the radial and tangential velocities are negligible, fluid essentially remains the same radial position throughout the tube. Fluid enters the tube (volumetric flow rate, Q) and its development is governed by two constraints: a. Due constant cross-sectional area of the tube, the average velocity at any position along the tube is constant; and b. Fluid particles adjacent to the wall are motionless with respect to the wall. The motionless "shell" of fluid adjacent to the wall retards the motion of the next shell though shearing forces acting in the direction opposite to the direction of flow and on the surface area of the shell resulting in shear stress. Since the motion of the second shell is retarded by the first and in tandem subsequent shells however, due to continuity constraint, the fluid near the center is accelerated to maintain the same average velocity as that at the entrance (figure 2).

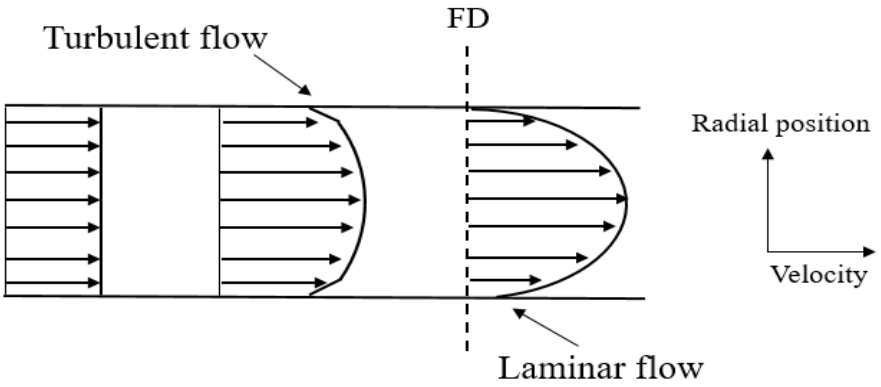

Figure 2: *Velocity profile through a straight tube. Image modified from original* (7).

This simultaneous retardation and acceleration continues until the profile becomes parabolic at the FD-line For laminar flow, the entrance length is given by 'X' (7).

$$X = 0.03d(Re) \qquad \{2\}$$

For fully-developed laminar flow in a circular tube, the volumetric flow rate 'Q' thought the tube is related to the pressure drop (Δp) measured over a length 'L' by the following expression (7):

$$\frac{\Delta p}{L} = 128 \frac{\mu}{\pi d^4} Q \qquad \{3\}$$

where Q = volumetric flow rate; μ = fluid viscosity; d = tube diameter and is called the Haagen-Poiseuille equation. Vascular walls are composed biologically active substances – cells and extracellular matrix which are sensitive to shear stress exerted by the fluid flow. For the parabolic profile, shear stress is defined as (7):

$$\tau = \mu \frac{dU}{dr} \qquad \{4\}$$

where U is the velocity (cm/s), r is the radius of the blood vessel (cm) and μ is the fluid viscosity (dynes*s/cm^2). Wall shear stress can be estimated at the vessel-wall by the volumetric flow-rate for a well-defined channel. Shear stress for a cylindrical vessel can be estimated by (7):

$$\tau_W = \frac{4\mu Q}{\pi R^3} \qquad \{5\}$$

Where 'τ_W' is the wall-shear stress (dynes/cm^2), μ is the fluid viscosity (dynes*s/cm^2), Q is the volumetric flow-rate (cm^3/sec) and R is the radius of the blood vessel (cm). Throughout the cardiac system blood-vessels of differing radius exist however, typical mean arterial values of shear stress range from 6 to 40 dynes/cm^2 but can vary from 0 to well over 100 dynes/cm^2 depending upon the location in the vasculature (8,9). Shear stress is known to be maintained within the 10-20 dynes/cm^2 range for most blood-vessels (10). Circumferential stress (σ_ϑ)is defined by the following equation:

$$\sigma_\theta = \frac{PR}{h} \qquad \{6\}$$

where P = transmural pressure, R = radius; h = thickness whereas axial wall stress is defined by

$$\sigma_z = \frac{f}{\pi h(2R + h)} \qquad \{7\}$$

As a consequence of elevated blood pressure, elevated levels of circumferential stress is exerted on the vessel wall.

1.3 Atherosclerosis:

Coronary artery disease arising from atherosclerosis is the leading cause of death and morbidity worldwide. Fundamentally, it is chronic inflammatory process of the arterial wall that occurs at favorable sites due to disturbed laminar flow. Structurally, atherosclerotic lesions are symmetrical

focal thickenings of the innermost layer of the artery consisting primarily of cells, connective-tissue elements, lipids and debris. Blood-borne inflammatory and immune cells constitute an important part of the atherosclerotic lesion with the remainder of the cells being endothelial and vascular smooth muscle cells. Accumulation of lipid-laden cells, also called fatty-streaks, underneath the endothelium precedes atheroma formation and is the earliest type of lesion consisting of only monocyte-derive macrophages and T-lymphocytes with appearance as early as infants and young childhood (11,12).

1.3.1 Endothelial dysfunction/denudation

The primary role of the endothelium is to maintain vascular homeostasis by a variety of regulatory substances including nitric oxide (NO), prostaglandins, angiotensin and endothelin-1. Pathophysiological observation in humans and animal models led to conclusions whereby endothelial dysfunction/denudation is the earliest step of atherosclerosis. When stimulated, endothelial cells can upregulate cell-adhesion molecules such as intercellular adhesion molecule 1 (ICAM-1), vascular adhesion cell molecule 1 (VCAM-1), P-selectin to promote attachment and rolling of circulating leukocytes and platelets. Common stimulants include elevated levels of low-density lipoprotein (LDL), very-low density lipoprotein (VLDL) and their oxidized forms, free radicals from cigarette smoking, hypertension, Diabetes mellitus, elevated plasma homocysteine concentrations or combination of these and other factors (13,14).

1.3.2 Acute and Chronic Inflammatory Response

Due to endothelial dysfunction/denudation, multiple vasoactive molecules, cytokines and growth factors are secreted which, combined with greater endothelial permeability results in attachment, rolling and diapedesis of monocytes at the site of dysfunction. Transmigration of monocytes, and their subsequent differentiation to macrophages, results in the initiation of an inflammatory

response at injured sites whereby macrophages uptake oxLDL resulting in the formation of foam cells. Further, macrophages secrete cytokines and growth factors (MCF-1 & 7) which ultimately encourage recruitment of more leukocytes from the circulation (15). As the inflammatory response continues unabated in the presence of the stimulants, more and more inflammatory cells accumulate at the injury site which further promote migration and proliferation of vascular smooth muscle cells that eventually are intermixed with the area of inflammation to form an intermediate lesion (14).

1.3.3 Vascular smooth muscle cell migration

Secretion of growth factors and cytokines at the site of injury by inflammatory cells results in phenotypic modulation, migration and proliferation of vascular smooth muscle cells to the lesion site. As this response continues uninhibited, more and more VSMCs populate the lesion with greater extracellular remodeling because of matrix metalloproteinase secretion by VSMCs and macrophages. VSMCs are believed to confer plaque stability and their subsequent apoptosis at advanced stages results in destabilization of the fibrous plaque which is more prone to rupture thus, resulting in clinical manifestation of stroke or myocardial infarction (16).

1.3.4 Altered hemodynamics

Despite numerous contributing factors to the development of atherosclerosis, local hemodynamic alterations play an extremely important role as atherosclerosis is a geometrically focal disease preferentially affecting the outer edges of vessel bifurcations where wall shear stress is low. From the earliest theories on co-localization of low shear stress and atherosclerosis, Caro et al (17) successfully demonstrated that low shear stress invoked a pro-atherosclerotic response in endothelial cells. Additional investigations subsequently supported the finding that low wall-shear stress, directional changes in flow, flow separation and stasis promote atherosclerosis development

since regions of the vascular tree free of these changes in flow were spared of atherosclerosis (18,19).

Direct measurements and fluid mechanical models of the susceptible regions have revealed shear values on the order of ± 4 dynes.cm^{-2} compared with greater than 12 dynes.cm^{-2} in the protected areas. Atherosclerotic lesions have been reported to co-localize with regions of low shear stress throughout the arterial tree from carotid artery bifurcation to the coronary, infrarenal and femoral artery vasculatures (18,19).

Flow analysis and carotid endarectomy pathological sections have been reported to show the greatest plaque thickness in the outer wall of the carotid sinus where flow shows stasis and shear is low in magnitude and also demonstrates direction-reversal (20).

Biological manifestation of shear stress is primarily through its effect on endothelium and eventually how the endothelial monolayer responds to alterations in shear stress. Shear stress resulting from second-to-minute time-scale variation in flow increase secretion of prostacyclin (21) and nitric oxide (22,23), both of which hinder platelet activation (24) and attenuate smooth muscle cells proliferation (25). Physiological levels of shear stress (> 15 dynes.cm^{-2}) decreases in vitro endothelial cell turnover reducing basal rate of proliferation and the rate of apoptosis form growth factor depletion (26,27). Whereas, low wall-shear stress (0-4 dynes.cm^{-2}) has been reported to promote endothelial cell proliferation and apoptosis (28) in addition to greater secretion of Platelet derived growth factor (PDGF) (29). Greater expression of inflammatory mediators such as Monocyte chemotactic protein-1 (MCP-1) (30) under low shear stress conditions further demonstrates the impact of WSS whereby areas of low shear promote endothelial dysfunction and support local inflammatory response. Essentially, shear stress alterations towards lower levels

make a passive, non-thrombogenic surface of the endothelium a dynamically responsive vascular element producing autocrine and paracrine factors (29).

1.3.5 Lesion progression

The initial lesion (type I) contains enough atherogenic lipoprotein to elicit an increase in macrophages and formation of scattered macrophage foam cells and consists of the first microscopically and chemically detectable lipid deposits in the intima and cellular reactions associated with such deposits. The precursors of advanced lesions are divided into three morphologically characteristic types. Type I, II and III are focal in nature, relatively small and contain abnormal amounts of lipoproteins and cholesterol esters (31).

Type II lesions include fatty streaks, which may appear as yellow-colored streaks, patches or spots on the intimal surface of arteries. These lesions are distinctly more defined than type I and consists primarily of macrophage foam cells stratified in adjacent layers with intimal smooth muscle cells, now containing lipid droplets as well. Location in the arterial tree in which type II lesions can be observed are relatively constant and predictable out of which a sub-group of lesions start progressing towards type III lesions and are called type IIa lesions. Interestingly, for coronary arteries the location of type IIa lesions co-localizes with the early type I lesions during childhood. The larger sub-group of type II lesions, which are thin and contain a few smooth muscle cells are commonly categorized as the progression-resistant or Type IIb lesions (31).

The designation of Type II lesion applies only to lesions that form the morphological and chemical bridge between type II lesions and atheromas (classified as type IV). These contain freer cholesterol, fatty acid, sphingomyelin, lysolecithin and triglyceride than type II lesions. Early in life, progression-prone locations shelter type IIa lesion and with aging these are the sites where type III lesions and atheroma-type lesions are found (31).

With type IV lesions or atheroma, a dense accumulation of extracellular lipid occupies an extensive but well defined region of the intima and is known as the lipid core. The characteristic core appears to develop from an increase and the consequent confluence of the small isolated pools of extracellular lipid that characterize type III lesions. Lipid cores thicken the arterial wall and are generally large enough to be visible when lesions are examined however, type IV lesions often fail to narrow the lumen. Macrophages, macrophage foam cells and lymphocytes are more densely concentrated in the lesion periphery. The tissue between the core and the surface endothelium corresponds to the proteoglycan-rich layer of the intima (32).

When the nearly normal cover of lipid core later undergoes an increase in fibrous tissue (mainly collagen), the lesion is then labeled type V which have prominent new fibrous connective tissue. If the new tissue is part of a lesion with a lipid core (type IV), this type of morphology is referred to as fibroatheroma or type Va lesion. A type V lesion in which the lipid core and other parts of the lesion are calcified is called type Vb lesion and a type V lesion in which a lipid cores is absent and lipid in general is minimal may be referred to as type Vc or fibrotic lesions. Type V lesions may also develop fissures, hematoma and/or thrombus (32).

Morbidity and mortality from atherosclerosis is largely due to type IV and type V lesions in which disruption of the lesion surface, hematoma or hemorrhage and thrombotic deposits have developed. Type IV or V lesions with one or more of these features is classified as a type VI lesion. These can be further categorized based on lesion features where, type VIa - disruption of the surface; type VIb – hematoma or hemorrhage; type VIc – thrombosis. A type VIabc lesion contains all the previously mentioned features (32).

1.3.6 Imaging of Atherosclerosis:

Current standard imaging techniques are plaque-centric and recent developments in imaging modalities the overall approach is moving more toward appreciation of the complexities that lead to the development of atherosclerotic lesions. Majority of the patients afflicted with atherosclerosis never experience overt clinical symptoms related to the disease which explains why more than 50% of the patients who die suddenly because of coronary heart disease lack any presentation of symptoms. Imaging techniques for atherosclerosis can be used to detect anatomic and physiological consequences of long-standing atherosclerosis and thus, provide detail on plaque composition and molecular activity in addition to estimation of biomechanical stresses.

Coronary angiography (Invasive): For diagnosis of atherosclerosis, invasive angiography is most often performed where selective intubation of the coronary ostia is performed with a catheter introduced via a peripheral sheath. A contrast dye is injected to produce radio-opaque contrast under x-ray fluoroscopy. The high-diagnostic accuracy afforded by superior spatial (0.1-0.2 mm) and temporal (10 millisecond) resolution remains unmatched by non-invasive methods and remains the gold standard technique when considering revascularization (33). However, evaluation of percentage diameter stenosis by means of invasive coronary angiography has limited value in predicting future cardiac events and thus, novel promising methods are under development such as 3-dimensional coronary angiography in which the gantry is mechanically rotated thus providing a multitude of X-ray projections during a single contrast injection (34).

Intravascular ultrasound (IVUS): IVUS is a minimally invasive imaging modality that uses miniaturized crystals incorporated at the catheter tip to provide real-time, high-resolution, cross-sectional images of the arterial wall and lumen with an axial resolution of about 150 μm and lateral resolution of 300 μm (35). Lumen and vessel dimensions – plaque area, vessel area, plaque

distribution, lesion length and remodeling index can be accurately predicted. In comparison to angiography, IVUS provides more details on the lesion characteristics and can identify plaques which are at a high risk of rupture and increasingly becoming the gold standard in trial evaluating plaque progression or regression in the coronary arteries. However, the main limitation of IVUS remains to be differentiation of plaque composition especially in areas of low echo reflectance (fibrous tissue, fibro-fatty tissue, thrombus). Additional modifications to the current IVUS techniques include backscatter IVUS (IB-IVUS) and virtual histology IVUS (VHIVUS) which uses color coded maps of plaque composition to improve plaque compositional characterization (35).

Optical coherence tomography (OCT): Another invasive technique which has a unique high-resolution imaging mode that uses low coherence, near infrared light for intravascular imaging of the coronary arteries. With an excellent spatial resolution (10-20 μm; 10x IVUS) and histological controls, OCT has been shown to be superior to IVUS in detecting important features of vulnerable plaque components. Additionally, it enables quantification of macrophages within fibrous caps thus allowing development of relationship between systemic inflammation and macrophage density in fibrous tissues. Since blood significantly attenuates emitted infrared light, requirement of saline flushes or balloon occlusion of the artery is necessary for adequate imaging. In addition, data acquisition is time consuming and is confined to focal lesion exploration (35).

Calcium score (Non-invasive): Presence of coronary artery calcifications (CAC) confirms the presence of atherosclerosis and it has been well established that visible CAC on invasive coronary angiography is associated with risk of cardiovascular events. CAC scores are evaluated by the widely-established electron-beam computed tomography (EBCT) (36) and more recently has been performed with multiscale computed tomography (MSCT). Extensive calcification can be present in the absence of luminal narrowing and thus, the specificity of CAC scores for obstructive CAD is low (35).

Computed tomography: Multi-detector CCTA is a useful first-line diagnostic test for appropriately selected patients with symptoms of angina and a low-to-moderate probability of CAD and in this context it has excellent negative predictive value thus, providing a remarkable mean to exclude CAD when clinical diagnosis is doubtful (33). Currently, CCTS is not superior to clinical risk ± CAC scores in asymptomatic patients nonetheless, it is an accurate test with good sensitivity to detect anatomically significant CAD when compared with invasive angiography (37). With multi-slice CT, an improved approach of differentiating plaque composition has been established however, this technique is associated with radiation exposure and the resolution also is inferior compared to invasive imaging (35).

Magnetic resonance imaging: Currently, MRI can differentiate atherosclerotic tissue without exposure to radiation using features such as chemical composition, water content, molecular motion or diffusion. Good correlation has been identified between fibrous cap integrity on MRI and histo-pathological specimens. It is a very useful technique to evaluate plaque progression following lipid-lowering therapy. However, plaque imaging of the coronary arteries with MRI remains challenging since deep location, motion and respiratory artifacts, and small caliber vessels are difficult to visualize (35).

Molecular imaging with nuclear techniques: Dedicated tracers enable nuclear imaging techniques such as single photon emission tomography (SPECT) and positron emission tomography (PET) target distinct mediators and regulators involved in the cascade of atherosclerosis. Feasibility of tracing molecular markers of MMP release, Apoptosis and F18-flurordeoxyglucose (FDG) are currently being explored for identification of vulnerable lesions (35).

1.3.7 Clinical Intervention

For atherosclerotic lesions requiring intervention, three main procedures are commonly used- Balloon angioplasty alone or with Stent-implantation, Coronary artery bypass graft (CABG).

Coronary Artery Bypass Graft: For multi-vessel lesions, diabetes mellitus, severe ventricular dysfunction patients, coronary arterial or vein graft is a suitable surgical procedure. Polymeric grafts made from Dacron, polyester or polytetrafluoroethylene (PTFE) are available. Complications associated with the surgical procedure make this as a high-risk option and typically is the end resort for multi-lesion cases. In addition, problems such as donor-site morbidity, systemic prevalence of atherosclerosis are common with natural graft procedures. With syndetic/polymeric grafts, material biocompatibility issues mandate lifelong anti-thrombotic regime and hemodynamic differences at the site of anastomosis can result in intimal hyperplastic response.

Angioplasty: This procedure involves compression of the atherosclerotic plaque to restore flow. During this procedure, a catheter is inserted usually into the femoral artery with a deflated balloon on a catheter tip. The most commonly used materials for manufacturing balloons are polyethylene (PE) or polyethylene terephthalate (PET). Balloons are available in different diameters and length depending upon the lesion site. At the lesion site, a balloon is inflated with saline typically to pressures of about 5-15 atm. Mechanistically, balloon expands until the deployment forces equals vessel wall circumferential force resulting in reopening of the blood vessel (38).

Stenting: A stent is a mesh-like scaffold that prevents the negative recoil of blood vessel after angioplasty. The expansion of a stent to its yield strength ensures that the stent does not collapse. Commonly used materials for stents include stainless steel, cobalt-chromium, platinum-titanium alloys, nickel-titanium, tantalum alloys. In addition to providing a scaffold for prevention of negative recoil, stents have also been designed to slowly release drugs to control neointimal

hyperplasia. First-generation drug-eluting stents include Paclitaxel eluting stents (Taxus, PES) and Sirolimus eluting stents (Cypher, SES). Paclitaxel cause microtubular arrest through polymerization of alpha and beta-tubulin in the cytoskeleton. Paclitaxel causes the cell cycle arrest at the G2/M phase of mitosis.

In contrast, sirolimus inhibits the mammalian target of rapamycin (mTOR) and thus causes cell cycle arrest at the G1 phase. A common clinical problem with first-generation DES was the late-stent thrombosis and inflammation in response to the thick polymer coating (39). Second generation DES include Zotarolimus-eluting stent (Endeavor, ZES) and Everolimus-eluting stents (Xience V, EES) and bio-degradable polymer coated biolimus-ES (40).

1.4 Restenosis:

The major complication associated with PCI is Restenosis or re-narrowing/collapse of the blood vessel which eventually necessitates revascularization or need for another intervention. Binary angiographic restenosis is defined as the re-narrowing of the vessel lumen to > 50% occlusion, usually within 3-6 months after PCI. Clinical restenosis is characterized by recurrent angina pectoris requiring target vessel revascularization (TVR) (41). Restenosis is a common problem after balloon angioplasty with rates up to 50-60% (42). With advent of bare metal stents, the overall rates of restenosis have drastically reduced owing to the success of stents in preventing negative remodeling but still remain as high as 25-30 % with bare metal stents (BMS) and lower with drug eluting stents (DES) (43). In spite of major advances in interventional cardiology, restenosis remains a consistent clinical problem owing to in-stent restenosis. Even with drug-eluting stents, in-stent restenosis has been reported clinically especially in complex lesions. This has been, in part, explained by the late catch phenomenon where vascular smooth muscle cells re-initiate

proliferation and phenotypic modulation after the initial burst release of the drug has been removed from the site.

1.4.1 Pathophysiology

Fundamentally, restenosis is a maladaptive response of the coronary artery to the trauma induced during PCI procedures and comprises of the characteristic wound healing responses – thrombosis, inflammation, cellular proliferation and extracellular matrix production that together contribute to post-procedural lumen loss over approximately 6 months (44). Lumen loss after balloon angioplasty can be separated into 3 distinct stages – early loss associated with elastic recoil, late loss due to negative remodeling and neointimal hyperplasia (45).

Elastic recoil is a dynamic and progressive phenomenon that occurs immediately following PCI and results in an immediate lumen loss with clinical reports of up to 34% lumen loss 15 minutes after angioplasty (46) and may even lead to a 50% loss in lumen gain post angioplasty (47). With the advent of stent-implantation, lumen loss due to elastic recoil has been significantly reduced albeit, there may be occurrence of sub-optimal lumen diameter primarily due to improper stent-positioning.

Immediately following angioplasty, fracture of the atherosclerotic plaque exposes the thrombogenic contents of the plaque to the flowing blood thus, triggering platelet activation and thrombosis. The barotrauma from a PCI also results in endothelial denudation/damage and results in loss of antithrombotic factors (e.g. nitric oxide, prostacyclin and tissue plasminogen activator) further contributing to platelet adhesion and aggregation (44). Platelets, upon activation, release mitogens including thromboxane A_2, serotonin and platelet-derived growth factors (PDGF) which ultimately results in phenotypic modulation of vascular smooth muscle cells resulting in their migration to the intimal region, proliferation and synthesis of extracellular matrix (43).

Negative remodeling may also contribute the development of restenosis as replacement of hyaluronic acid with collagen in the extracellular matrix is believed to result in scar tissue formation (45).

With stent-implantation, elastic recoil is virtually eliminated and neointimal hyperplasia is the main mechanism responsible for lumen narrowing and subsequently in the events leading up to in-stent restenosis. Early phase of in-stent restenosis (ISR) immediately after intervention results in relocation of the plaque, reorganization of thrombus and an acute inflammatory response where thrombus formation seems to be as a consequence of endothelial disruption ultimately leading to deposition of fibrin and platelets at the site of injury (48). Thus, an increased leukocyte trafficking is evident at the stent location with their subsequent migration into the intimal layer. Corroborating platelets, monocyte/macrophages and VSMCs results in an increased production of adhesion molecules, cytokines, chemoattractants and growth factors ultimately leading to greater recruitment of inflammatory cells from the circulation (49).

With the increasing use of DES, especially in complex lesions such as lesions in left main artery, bifurcations, small vessel vein grafts, chronic total occlusions and diabetic patients, ISR rates of up to 10% have been reported (50,51). The time frame to restenosis after DES may be longer as compared to BMS due to the application of anti- proliferative drugs with repots of up to 12 months (52). Various factors, like BMS, have been implicated in the development of ISR with DES including diabetes, lesion length, vessel diameter, implantation factors. In addition to these, factors such as resistance to antiproliferative drugs, hypersensitivity reactions to the polymer and metal, circulating levels of MMPs, low wall-shear stress, polymer release kinetics have also been demonstrated to contribute to ISR development (53). Further, different types of DES have also been shown to affect the phenotype of VSMCs with synthetic phenotype more frequent with BMS and

paclitaxel-eluting stents (PES), intermediate with Zotarolimus-eluting stent (ZES) and Sirolimus-eluting stents (SES), contractile with tacrolimus- eluting stent (TES) (54).

1.4.2 Role of Endothelial Cells: Mechanical injury from coronary intervention leads to denudation of the endothelium and subsequently leads to a sequel of events resulting in VSMC migration and proliferation. Re-endothelialization is a critical step to completion of the wound healing response to PCI-induced injury of the vessel wall. Endothelial dysfunction is commonly observed at sites of regenerating endothelium resulting in reduced nitric oxide action. Studies with drugs that enhance endothelium-derived relaxing factors or diminish endothelium derived contracting factor production have been shown to control restenosis (55). Further, the extent of the denuded area is also contributive to re-endothelialization and hence intimal hyperplasia as small denuded areas heal more quickly (56).

1.4.3 Role of Platelets, Macrophages and VSMCs: Proliferation and migration of vascular smooth muscle cells from the medial layer over time results in the formation of neointima. As described previously, increased trafficking of inflammatory cells and platelets at the site of injury leads to an increase in local concentration of growth factors and cytokines which stimulate phenotypic modulation of VSMCs possibly due to degradation of the basement membrane via MMPs secreted by macrophages.

1.4.4 Role of Hemodynamics: In stented vessels, low wall-shear stress has been inversely correlated with neointimal thickening using 3D-reconstruction and finite element analysis (57,58). Further, Wenetzel et al also showed similar results in 14 patients after stent implantations in coronary arteries (59). VSMCs respond to shear stress variations such that low wall-shear stress contributes to VSMC proliferation and hence neointimal formation whereas high shear shows an opposite

effect (60). Further evidence exists in studies where reduced number of stent wires and strut thickness have resulted in less of vessel area exposed to low shear stress (61).

1.4.5 Classification of Restenotic lesions

Based on the angiographic patterns observed clinically a well-established lesion classification system exists for in-stent restenosis according to the geographic distribution of intimal hyperplasia in reference to the implanted stent (62). Patterns predicted using this classification system is very well accepted by the surgical community in predicting the long-term need for repeat revascularization and pre-intervention ISR pattern serves as an independent predictor of future target vessel failure/repeat revascularization with 19%, 35%, 50% and 98% for class I, II, III, IV respectively (64).

i. Class I (Focal ISR group) – Lesions are ≤ 10 mm in length and are positioned at the unscaffolded segment (i.e. articulation gap), the body of stent, the proximal or distal margin (but not both) or combination of these sites (multifocal ISR).
ii. Class II (Diffuse intrastent) – Lesions are > 10mm in length and are confined to the stent(s) without extending outside the margins of stent(s).
iii. Class III (Diffuse-proliferative) – Lesions are > 10 mm in length and extend beyond the margin(s) of the stent(s).
iv. Class IV (Total occlusion) – Lesions have a flow grade of zero.

1.4.6 Predictors of Restenosis

Predictors for restenosis have been categorized as patient-related factors, vessel-related predictors and procedure-related factors. Various patient-related factors including high serum levels of C-reactive protein (CRP) & Interleukin-6 (IL-6), previous angioplasty. However, the most consistent patient-related factor is the presence of Diabetes with a 30-50% increased risk of developing

restenosis. Vessel-related factors such as vessel diameter and lesion length independently serve to predict the incidence of in-stent restenosis with larger diameter/shorter lesions demonstrating significantly lower restenosis rates (63). Finally, procedure-related factors such as stent-strut thickness, stent fracture, stent length and minimum lumen diameter serve as significant clinical predictors of restenosis (51). Thinner-struts are hemodynamically more favorable as compared to thicker struts. With increase in stent length, rate of In-stent restenosis (ISR) have been reported to be nearly double for stent lengths > 35 mm (64).

Introduction of drug-eluting stent has successfully reduced the overall rates of revascularization in comparison to bare-metal stents however, routine angiographic surveillance 6 – 8 months after stent implantation has revealed ISR rates of 30.1% 14.6% and 12.2 % for BMS, first-generation DES, second-generation DES respectively (65). Despite significantly greater rates of revascularization associated with BMS, these stents are still used clinically in cases where DES are not affordable or where bleeding is a major risk-factor due to extensive anti-platelet therapy required with DES. ISR with DES is on the rise primarily due to wide clinical acceptance of this technology. ISR rates can range from 3-20% depending upon the type of DES used, lesion complexity, lesion location (66). In general, it may take longer to develop ISR with DES primarily due to delayed onset of intimal hyperplasia owing to phasing out of the bulk of drug beyond 6 months (52). Factors which serve to be predictors in development of ISR with DES are similar to BMS – diabetes, lesion length, vessel diameter, implantation factors. Novel factors such as resistance to antiproliferative drugs, hypersensitive reactions to the polymeric layer and metallic ions, altered hemodynamics, release kinetics have also been reported to contribute to ISR development (65,66). The main predictors for developing ISR with DES are:

a. Patient-specific: Higher rates of ISR have been reported in patients with comorbidities like metal allergy, local hypersensitive reactions to drug or the polymer on DES, age, female gender, diabetes mellitus, chronic kidney disease, multivessel coronary artery disease, hypertension amongst other (67,68). Specifically, diabetes associated complications such as hyperglycemia, insulin resistance and insulin administration alongside hypertension have been consistently reported to risk-factors for developing ISR even with the use of DES (69,70).

   The two common class of drugs that are used for DES are cytostatic drugs like sirolimus and its analogues – which fundamentally arrest progression of cell-cycle by causing inhibition of the mammalian target for rapamycin (mTOR) complex and cytotoxic drugs like paclitaxel – which specifically bind to the bet-tubulin subunit of microtubules ultimately preventing microtubular depolymerization (71). Genetic mutations rendering cellular-resistance to these drugs and thus, influencing the sensitivity to these drugs have been reported (72,73).

   Hypersensitive response to stents was initially observed with early BMS where 316L stainless-steel stents were reported to cause these allergic reactions owing to release of nickel and molybdenum ions from stents (74). These were eventually addressed by using stents made of cobalt-chromium alloy which demonstrated significantly lower release of nickel and molybdenum ions. With DES, there were three principle components have been reported to potentially cause hypersensitivity reactions – metallic platform, polymer coating and drug (75).

b. Lesion-specific: Lesion characteristics such as lesion length, smaller reference artery diameter, ostial lesions, initial plaque burden, residual plaque after implantation and neo-

atherosclerosis have been reported to negatively affect the outcomes of stent implantation. Lesion are typically focal in nature for DES with the exception of diabetic patients which present with more diffused type lesions (76).

c. Procedural-specific: Procedure-specific problems that may result in ISR with DES include – stent undersizing, incomplete lesion coverage, stent under-expansion and malapposition. Stent under-expansion results from poor expansion of stent during implantation and may not be detected angiographically. Typically, higher calcification of the lesion or inability to fully expand the balloon inside the stent are primary suspects which result in stent under-expansion. Clinically, excellent expansion as evidenced by ≥90% minimum lumen area in comparison to the reference lumen area prevent clinical manifestation of stent under-expansion (77).

Malapposition is a condition where stent-struts are not completely apposed to the blood vessel – there is clear space between the stent struts and arterial intima where blood can be detected. This complications cannot be detected angiographically and typically occurs with the usage of under-sized stents or in arteries that have significant tortuosity and fluctuations of reference arterial lumen diameter within the treated segments and encourages thrombosis (78).

Non-uniform drug distribution owing to local blood flow alterations, strut overlap and polymer damage may result in neointimal growth in regions of low drug availability. Computational models have demonstrated these factors to influence the local drug distributions (79). Non-compliant lesions and difficult delivery may strip the polymeric layer of the stent ultimately compromising drug-elution kinetics. Additional variability can

stem from metal-to-artery ratio which commonly is different for different DESs. All of these alone or in combination may result in focal areas within the stented segment with less than optimal drug release eventually contribution to the development of ISR (80).

Barotrauma outside stented segment as a result of balloon dilation during stent deployment has been reported to be the primary site of restenosis with sirolimus eluting stent placement (81). These geometrical-miss were effectively reduced through different strategies - by deploying a short balloon to pre-dilate the lesion site, using single stent long enough to cover the entire lesion length, post-dilations within the stented regions using short, high pressure balloons (66).

Neo-atherosclerosis is defined as the condition where atherosclerotic lesions have been identified within the stented regions of the blood vessel. It has recently gained attention due to its common prevalence with the use DES owing to incomplete endothelial healing from delayed release of drug by the stent. Neoatheroslcerosis is a frequent finding in DES and occurs earlier than in BMS and is suspected to be a pro-thrombotic factor in stented regions. Investigations have reported incidence of neoatheroslcerosis to be significantly greater in DES lesions (31%) as compared to BMS lesions (16%) with detection as early as 420 days with DES in comparison to 2160 days with BMS (82).

1.5 Diabetes and Restenosis:

With a total economic burden of $245 billion in direct and indirect costs, diabetes is amongst the leading cause of deaths in the US (83) and combined with cardiovascular disease, about 68% of

deaths are related to complications of diabetes and CVD and patients afflicted with diabetes have a 4 to 6-fold increased risk of developing cardiovascular disorders (84).

Pathophysiologically, diabetes can result due to autoimmune response to beta-pancreatic cells which are responsible for secreting insulin (type 1); peripheral insulin resistance in skeletal and adipose tissue (type 2); pregnancy induced (gestational); drug or chemical induced (anti-retroviral therapy and second-generation anti-psychotic drugs). Out of these, the two most commonly observed forms of diabetes are type 1 and 2 and represent almost the entire burden on healthcare with type 2 diabetes accounting for about 90% cases (National diabetes fact sheet, CDC). T1D is characterized by a prolonged autoimmune attack of pancreatic beta cells carried by autoreactive T-cells and these patients are unable to secrete insulin in response to a glucose load manifesting hyperglycemia. Type 2 diabetic patients develop desensitization of insulin receptors ultimately rendering peripheral insulin resistance. A direct consequence of insulin resistance is the dysfunctional glucose transport across target cells and dysfunctional lipid metabolism. Hyperglycemia, hyperinsulinemia, dyslipidemia are common clinical features of T2D patients and as the disease progresses significant reduction in beta-cells functions conjoins to exacerbate insulin resistance (85).

As mentioned in the previous section, diabetes remains to be the most consistent patient-specific risk factor or predictor for developing ISR even in the DES era. Studies from early PCI procedures on angioplasty in diabetics demonstrated restenosis rates to be almost twice as much as in non-diabetic patients (63% vs 36%). These observations were initially correlated to late vessel occlusion however, even after adjusting for late vessel occlusion, diabetic patients still demonstrated greater restenosis rates (86). Clinical trials comparing restenosis post BMS implantation between diabetic and non-diabetic patients demonstrated higher rates of both angiographic restenosis (diameter stenosis $\geq$ 50% determined angiographically) (87–90) and clinical restenosis (requiring target

lesion revascularization) (88,91,92). Since restenosis post stent implantation is primarily due to exaggerated neointimal hyperplasia, these investigations concluded diabetic patients to be associated with greater neointimal proliferation and increased tissue remodeling (93). In fact clinically diabetes mellitus is the only patient-specific risk factor equivalent to 15 years of cardiovascular ageing (94).

First generation DES reduced the overall rates of restenosis when compared to BMS alone in all patients including those afflicted with diabetes due to the cytostatic or cytotoxic drug release from the platform however, emergence of stent thrombosis resulted in safety concerns especially late onset after a majority of the drug has been released and high-risk patients. Clinical investigations have indicated a favorable survival rate with BMS in diabetic patients as compared to first-generation sirolimus eluting stents with additional evidence indicating higher relevance of adverse cardiac events (95,96).

Despite the advances in drug-eluting stent technology with second-generation DES, patients with diabetes undergoing revascularization continue to have worse outcomes compared with nondiabetic patients with studies demonstrating less pronounced clinical advantage of second generation drug eluting stents, especially in insulin requiring diabetic patients (97). Restenotic lesions characterized at 1 year post DES implantation by optical coherence tomography revealed thicker neointima in case of diabetic patients with evidence of direct association with poorly managed blood glucose levels ($\geq$ 7% HbA_{1C} levels) (98). Major clinical trials with DES in diabetic patients have been summarized in table 1.

Clinical Trial	Outcome
SYNTAX (Taxus stent) (99)	Increased cardiac events after PCI in diabetic patients
FREEDOM (Taxus stent) (100)	CABG superior to PCI for diabetic patients
SPIRIT V (Xience V vs TAXUS) (101)	Paclitaxel-eluting stents increase In-stent late loss in diabetic patients
Pooled analysis of SPIRIT II, III, IV and COMPARE (Taxus vs Xience V EES) (102)	EES vs PES resulted in no difference for diabetic patients while EES led to decreased mortality, myocardial infarction, stent thrombosis and TLR for non-diabetic patients
ENDEAVOR IV (103)	In-stent restenosis (%) was greater in diabetic patients treated with Zotarolimus-eluting stents
E-FIVE (104)	Higher rates of cardiac events, TLR, target vessel failure and stent thrombosis in diabetic patients at 1 year follow-up
NAPLES-DIABETES (105)	Higher TLR rates in diabetic patients ultimately resulting in greater cardiac events with Zotarolimus-eluting stents
Pooled analysis of International global RESOLUTE (ZES) program (106)	Insulin requiring patients had rates of target lesion revascularization (13.7%)

Table 1: Major clinical trials evaluating the performance of DES in diabetic patients (107)

1.5.1 Contribution of Hyperglycemia

Various clinical studies have demonstrated the impact of poor glycemic control associated with increased restenosis resulting in higher rates of target lesion revascularization. In addition to long-term glycemic management, clinical studies have also underscored the importance of maintaining procedural glycemic control since pre-procedure hyperglycemia (> 128 mg/dL) resulted in 33.8% target-vessel revascularizations at 9 month follow up (108,109). Further, the importance of managing pre-procedure glycemic control was further demonstrated in patients who had good long-term glycemic control ($HbA_{1C} \leq 7\%$) but had elevated pre-procedure glucose concentrations (> 128 mg/dL), as these patients had greater restenosis rates (110). Although the exact mechanisms of these effects were never explored, hyperglycemia was successfully demonstrated to be associated with restenotic lesion development and progression (111).

Hyperglycemia in general, has been shown to increase platelet activation and aggregation through upregulation of PKC activity (112), direct osmotic effects (113) and through induction of non-enzymatic glycation of platelet surface proteins (113). Additional studies have indicated increased expression of P-selectin and CD40 ligands by platelets under hyperglycemic conditions (114,115). Evidence exists for activation and increased expression of pro-coagulant tissue factors by endothelial cells though the NF-KB pathway via hyperglycemia induced advanced glycated-end-products (AGE) and reactive oxygen species (ROS) (116). Hyperglycemia directly reduces tissue plasminogen activator (t-PA) ultimately contributing to initiation and development of thrombus (117). For vascular healing, endothelial progenitor cells are believed to play an important role in re-endothelialization of damaged intimal layer post-injury with evidence of circulating EPCs being captured for regeneration of the endothelial lining (58). Hyperglycemia has been shown to

adversely affect this process since high-glucose (12.5 mM) resulted in cellular senescence of EPCs and potentially induced apoptosis as well though the p38 MAPK pathway (118).

Neointimal progression is primarily driven by proliferation and migration of smooth muscle cells ultimately leading to restenosis. In vitro investigations have demonstrated greater proliferation of vascular smooth muscle cells under high-glucose through elevated basic fibroblastic growth factor (bFGF) (119), elevated transforming growth factors alpha (TGF-α) (120), upregulation of osteopontin release (121), increased polyol pathway flux (122), upregulation of protein kinase C (123), direct increase in DNA (124), increased IGF-1 responsiveness resulting in enhanced proliferation and migration (125), suppression of AMP activated protein kinase (AMPK) resulting in activation of mammalian target of rapamycin (mTOR) (126,127), upregulation of MAPK, PI3K/AKT and NFKB (128). Even in animal models of diabetes, hyperglycemia has been shown to cause higher cell proliferation 3-days post arterial injury in comparison to controls (129). These studies demonstrate the influence in hyperglycemia in regulating the intimal response.

1.5.2 Contribution of insulin administration and insulin resistance

In the United States alone, approximately 1 in 4 diabetic patients are treated with insulin and insulin treated DM represents a higher-risk group of patients (130). These patients typically have prolonged duration of diabetes that is difficult to control alongside greater than normal levels of HbA_{1C}. Insulin requiring patients additionally present additional complications – hypertension, dyslipidemia and exogenous insulin administration has been shown to be a powerful cardiovascular risk factor in patients with type 2 diabetes. (131). Kronmal et al reported measurements of fasting serum insulin levels to be strongly correlated to developing coronary heart disease. In addition, patients with higher levels of insulin (906 – 2400 pmol/L) were almost 6-fold likely of developing

coronary complications (132). Although the exact mechanisms are not properly understood, poorer outcomes are considered to be a multi-factorial problem where insulin is suggested to be pro-inflammatory and accelerate atherosclerosis (133), increase thrombogenesis (134), and impair fibrinolysis (135). Circulating insulin levels in the body can vary due to multiple factors including but not limited to age, glucose load, lifestyle, body mass index, insulin resistance, hyperglycemia, pancreatic beta cell function etc. In healthy lean individuals circulating venous (or arterial) fasting insulin concentrations are about 18 – 90 pmol/L (136) however, under diabetic conditions these values can range from anywhere between 194 – 2000 pmol/L. These variations are primarily driven by the glucose load and insulin concentration tend to be towards 2000 pmol/L after 1 hour of glucose administration (137).

In the context of restenosis, multiple clinical trials have demonstrated insulin to be associated with poorer outcomes after PCI procedures (previously summarized in table 1). These studies indicate poorer outcomes of intervention especially in patients requiring external insulin administration. In animal models of diabetes requiring insulin administration, greater neointimal response to balloon injury (138) and stent implantation (139). Further, hyperinsulinemia has been reported to induce proliferation of VSMCs in experimental models of diabetes (140,141). Insulin itself is considered to be a weak mitogen but it is known to potentiate expression of platelet derived growth factor and insulin-like growth factor (142,143). Insulin has also been shown to augment the influence of PDGF and thus, promoting further stimulation (144).

Insulin resistance is a state in which peripheral tissues have decreased sensitivity to insulin ultimately leading to increased circulating insulin levels to maintain normal glucose concentration. Most patients affected by insulin resistance are also accompanied by central obesity, arterial

hypertension, dyslipidemia and other cardiovascular risk factors. Presence of multiple of these complications is clinically identified as metabolic syndrome. Insulin mediates its effects through two distinct pathways – AKT/PKB for metabolic effects and Ras/Raf/MAP kinase for mitogenic effects (145–147). A disturbance of the metabolic signal pathways via IRS/PI3K/AKT is present in insulin resistance in type 2 diabetes whereas the mitogenic pathway of the insulin signal via MAPK is not affected. Thus, with insulin resistance, a reduced cellular action of insulin is found concerning the metabolic but not mitogenic effects of insulin (148). As diabetes progress, there is significant loss in insulin secretion by beta cells and consequently, a loss of beta cells mass is also observed (149).

Like skeletal muscle tissue and adipocytes, VSMCs are also sensitive to the metabolic effect of insulin. Insulin has been shown to regulate glucose uptake and metabolism in VSMCs thus, establishing them as insulin sensitive (150,151). Glucose transporters (GLUT4), which are primarily responsible for transport of glucose across insulin-sensitive tissues have been detected in the vasculature (152). Upon stimulation with insulin, vesicles fuse with plasma membrane via exocytosis and consequently result in increased cell-surface expression of glucose transporter. This increase results in proportional increase in glucose transport across cells to maintain glucose homeostasis. This mechanisms involves a tyrosine phosphorylation cascaded that is triggered by the binding of insulin to IRS and includes activation of PI3K/AKT (153). Figure 4 displays the very basic pathway depicting the mitogenic and metabolic actions of insulin on muscle cells.

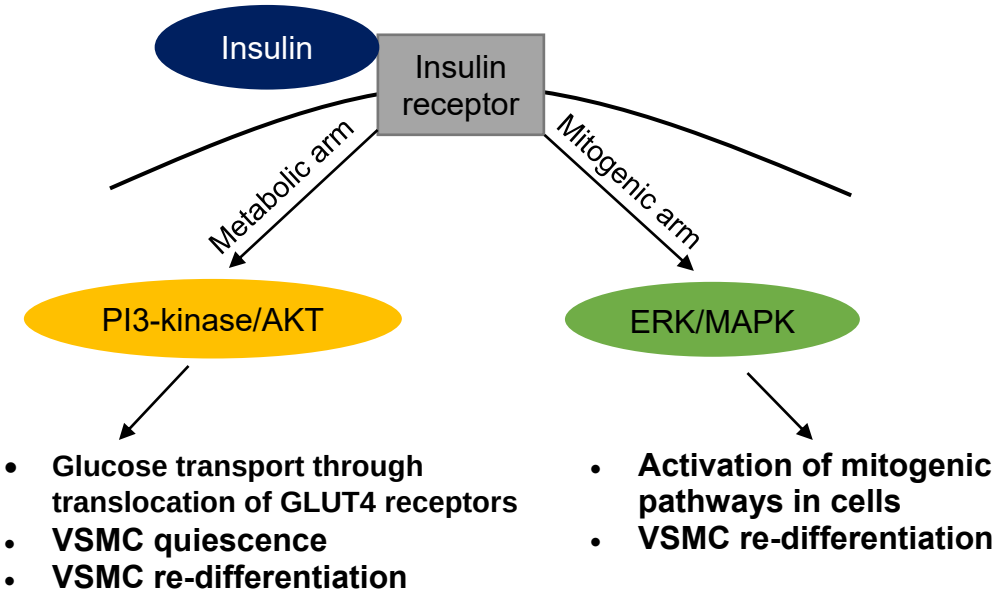

Figure 3: *Metabolic and mitogenic actions of insulin on smooth muscle cells*

1.6 Hypertension and Restenosis

Systemic arterial hypertension is the condition of persistent, non-physiological elevation of systemic blood pressure (BP). Current clinical standards dictate resting systolic blood-pressure to (SBP) ≥ 140 mmHg whereas diastolic pressure to be ≥ 90 mmHg (154). The exact causal factors of hypertension are not entirely clear however, in general genetic, environmental and behavioral factors are known to influence development of hypertension which in the long run influences cardiovascular disease since hypertension is also amongst major causal risk factors for CVD – including heart disease, vascular disease and stroke, and renal disease. About 30.9% of the US population are affected by hypertension (155). Although, blood-pressure elevation from the normal values of 120/80 mmHg (SBP/DBP) is considered to hypertension, there are generally four different categories of hypertension (154).

a. Normal (SBP < 120 mmHg and DBP < 80 mmHg)
b. Prehypertension (SBP 120-139 mmHg or DBP 80-89 mmHg

c. Stage 1 hypertension (SBP 140-159 or DBP 90-99 mmHg

d. Stage 2 hypertension (SBP ≥ 160 or DBP ≥ 100 mmHg

Primary hypertension accounts for the majority (>90%) of cases of human hypertension which stems from a complex interaction of a multitude of factors including but not limited to increased sympathetic nervous system activity, psychological stress, high sodium intake, inappropriate renin-angiotensin secretion, deficiency of vasodilator peptides, nitric oxide, diabetes mellitus, insulin resistance, obesity, altered ion transport among others.

Clinically, hypertension is also a patient-specific risk associated with poorer prognosis of PCI with hypertensive patients affected by greater restenosis (156). In addition, high SBP levels both in clinical (peri-procedural) and invasive (intra-procedural) measurements have been associated with greater risk of restenosis for single vessel disease (69). Chronic hypertension in experimental animals and in human subjects has been well documented to result significant wall thickening (157), hypertrophy of medial smooth muscle cells and increased connective tissue content (158–160). A direct consequence of elevated blood pressure on the vessel wall is elevated circumferential strain which may increase by as much has 30% thus, resulting in altered VSMC proliferation, hypertrophy and deposition of extracellular matrix – particularly collagen (161,162).

1.7 Cellular-response to drugs from stents

DES are essentially biomaterials capable of delivering drugs locally and in a controlled manner to eradicate the increased neointimal proliferation owing stent implantation, which is the primary cause of restenosis. As stents are placed within the blood vessel – it results in deep, local and prolonged injuries to the blood vessel layers and denudation of the endothelial layer. Sullivan et al

have demonstrated the extent of injury to the internal elastic lamina to be correlated to neointimal proliferation where greater damage was associated with poorer outcome (163). The barotrauma results in release of growth factors which dictate VSMCs to enter G1/S phase of cell-cycle thereby encouraging migration and proliferation into the intima (164). Lack of endothelium further encourages an inflammatory response subsequently culminating in greater proliferative response of VSMCs. Thus, activation of VSMCs served to be the therapeutic target for DES. Essentially, two classes of drug have been commonly used for DES – Cytostatic (Sirolimus and analogues) and Cytotoxic (Paclitaxel). The most common DES used clinically are summarized in table 2 (164).

Table 2: Major DES used clinically

Stent	Technology/Polymer coating	Limitations
CYPHER (Sirolimus)	Non-erodible poly(ethylene-co-vinyl acetate) and poly(n-butyl methacrylate) carrier : 67% polymer and 33% drug	• Late stent-thrombosis • Hypersensitivity • Inflammatory
TAXUS (Paclitaxel)	Triblock polymer – Translute™ using a poly(styrene-b-isobutylene-b-styrene) tetra polymer	• In-stent thrombosis • Hampers re-endothelialization • Hypersensitivity
Endeavor (Zotarolimus)	Biocompatible phosphorylcholine coating on Co-Cr alloy base. Zotarolimus – extremely lipophilic and is not solubilized with blood flow	• Diabetes • Small vessel • Dual anti-platelet therapy
Xience V™ (Everolimus)	Better stent platform – high flexibility and deliverability, better compliance.	• Diabetes • Small vessel

	More polar nature reduces the tissue concentration of the drug. Uses a hydrophilic poly(vinylidene fluoride-co-hexafluoropropylene) which has improved compatibility at the adluminal surface	• Cost • Dual anti-platelet therapy

Paclitaxel (taxanes) was initially approved by the FDA for its anti-neoplastic use for ovarian cancer treatment in 1992. Currently, it is still used for intravenous treatment of lung, breast and ovarian cancer (164). Paclitaxel promotes polymerization of the α and β subunits of tubulin by reversibly and specifically binding the β subunit of tubulin. As a result of polymerization, paclitaxel stabilizes microtubules which are required for G2 transition into the M phase of the cell cycle in VSMCs (figure 4). The drug successfully blocks cellular proliferation at the G2/M phase. Due to its highly lipophilic nature, paclitaxel is easily taken up in the vasculature. Paclitaxel leads to an almost complete growth inhibition within a dose range of 1.0 – 10.0 mmol/L even with short duration of exposure (~ 20 minutes)(165).

Sirolimus was discovered in soil samples as a naturally occurring product in *Streptomyces hygroscopicus*. It is a 31-memebr macrocyclic lactone that was initially approved by the FDA as an immunosuppressant agent (166). Sirolimus and its analogues (Zotarolimus and Everolimus) inhibit SMC proliferation by binding the cytosolic FK-binding protein 12 (FKBP12). This prevents activation of the mammalian target of rapamycin (mTOR) and ultimately leads to interruption of the cell-cycle progression in the G1/S phase (167). The mTOR is a large evolutionarily conserved

member of the phosphatidylinositol kinase (PIK) related kinase family that regulated protein translation, cell-cycle progression and cell-proliferation.

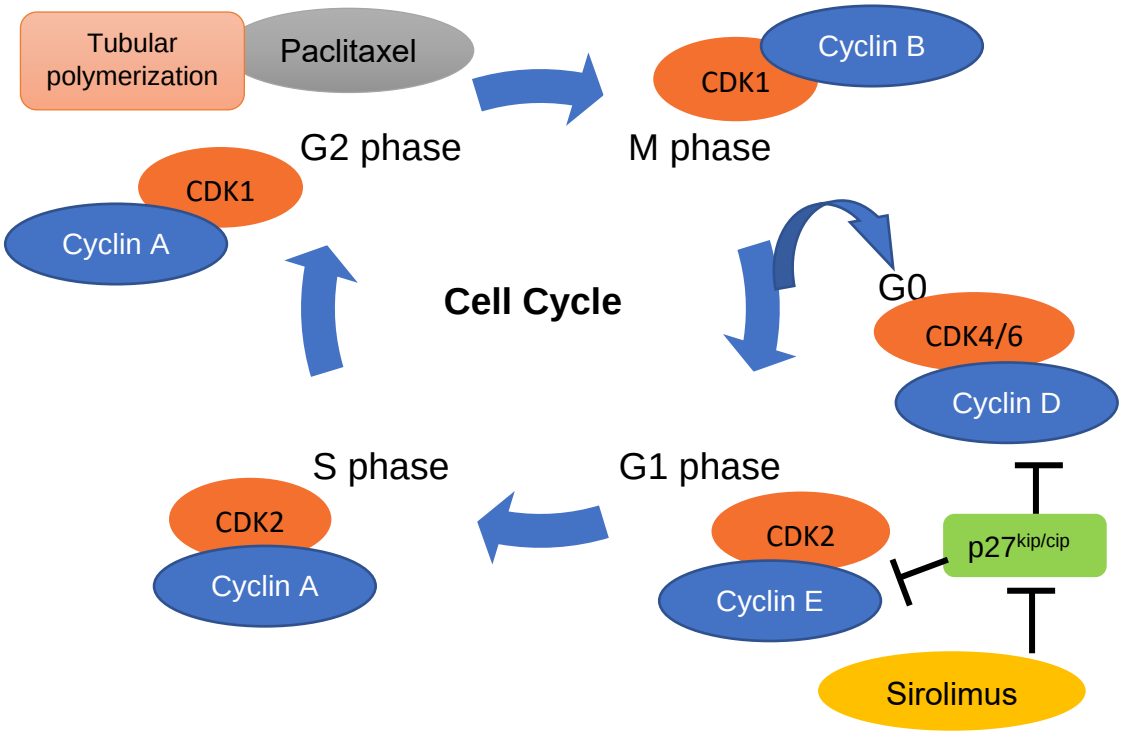

Figure 4: Schematic representation of cell-cycle targets of paclitaxel and sirolimus.

Within the cell-cycle (figure 5), cyclin-dependent kinase (CDK) activity is reduced ultimately reducing phosphorylation of the retinoblastoma protein. CDK inhibitors $p27^{kip1}$ mediates sirolimus' anti-proliferative and anti-migratory properties in smooth muscle cells (168). In response to growth factors or mitogens, $p27^{kip1}$ levels decrease thus allowing higher activity of CDKs ultimately manifesting into progression within the cell-cycle. During mitogen deprivation, $p27^{kip1}$ levels increase resulting in reduced activity of CDKs which prevents progression within the cell-cycle (169). Thus, sirolimus inhibits mitogen-induce downregulation of $p27^{kip1}$ in addition to inhibition of $p70^{S6k}$ phosphorylation (170) and activity, phosphorylation of the eukaryotic translation initiation factor 4E-binding protein (171).

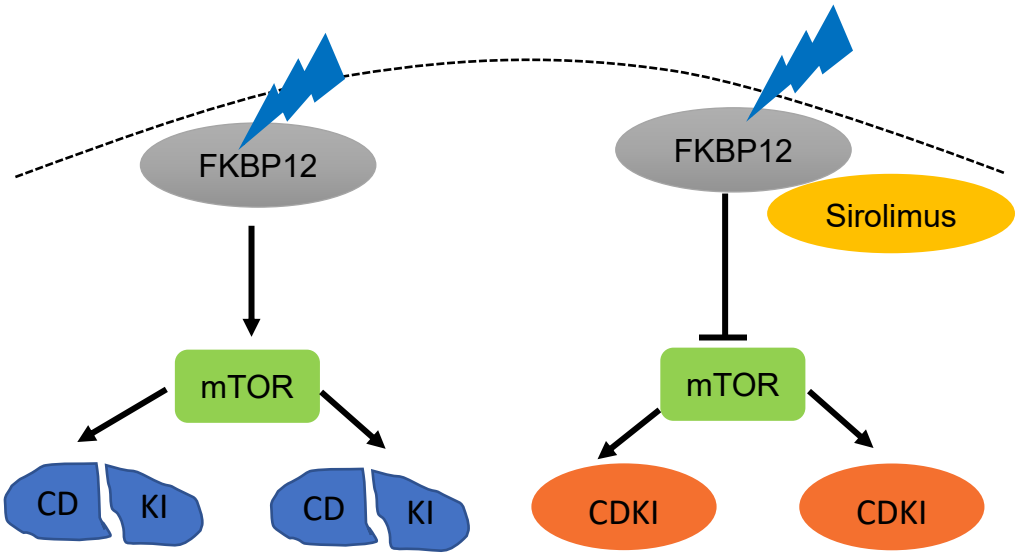

Figure 5: Schematic representation of mechanism of sirolimus induced cell-cycle arrest.

Sirolimus has been shown to demonstrate anti-proliferative effects on VSMCs in a dose-dependent manner in the range of 0.1 – 100 ng/mL. These effects were explored in both porcine and human venous smooth muscle cells (172). With VSMC migration, concentrations > 0.1 ng/mL have been reported to be significantly effective in controlling migration. In addition, 50 ng/mL sirolimus was shown to be effective in controlling neointimal hyperplasia in ex-vivo models although statistical significance was not achieved (173). Wessely et al measured sirolimus concentration in blood after deployment of drug-eluting stents with a custom coating system and reported concentrations in the range of 10-30 µg/L (or ng/mL). This range also captured the release profile of Sirolimus-eluting stent as well, which had very similar release kinetics as the custom system. In addition, both the custom system and SES resulted in similar neointimal outcome after 30 days indicating the custom system and SES to be very similar and following similar kinetics (174).

Summary

Pathophysiology of In-stent restenosis and Contribution of VSMCs: Restenosis is a maladaptive response of the blood vessel to the trauma induced by PCI procedures with the sequence of events-thrombosis, inflammation, VSMC proliferation and migration and extracellular matrix production (175). In-stent restenosis is primarily driven by exaggerated neointimal hyperplasia, since the metallic scaffold prevents negative recoil of the blood vessel, as observed in case of stand-alone angioplasty (2). In the early phase, immediately after an intervention, relocation of plaque, reorganization of thrombus and an acute inflammatory response is observed which, although resolves in a few days to week, results in the onset of the late phase where phenotypic modulation of VSMCs leads to their migration into the intima and subsequent proliferation and synthesize copious amounts of extracellular matrix thus, increasing the bulk of the neointimal tissue (18).

The vessel trauma caused during implantation of a stent leads to denudation of the endothelial lining followed by delayed healing, which in case of drug eluting stent, may take up to 48 months for complete re-endothelialization (3,4). Under these conditions, VSMCs may be directly subjected to shear forces from blood flow which are normally experienced by endothelial cells. Further, neointimal thickness in stented blood vessels has been correlated with areas of flow separation, zones of recirculation or point of flow-reattachment where average wall shear stress can be as low as < 5 dynes.cm $^{-2}$ (7). In case diabetic patients, it is further complicated by endothelial dysfunction which may further delay intimal healing in addition to being a consistent risk factor for developing atherosclerosis and additional 'pro-restenotic' factors (e.g. hyperglycemia, hyperinsulinemia, insulin resistance, hypertension etc.) working concomitantly with altered hemodynamics, which may contribute to exaggerated neointimal hyperplasia observed commonly in this patient population.

Mechanical forces and VSMC-response: In normal and healthy blood vessels, vascular cells are subjected to cyclic strain due to pulsatile nature of blood flow in addition to wall shear stress, owing to the viscosity of blood. The typical range for cyclic strain has been reported to 1-2 e^6 dynes/cm^2 (20) along with typical mean arterial shear stresses from 6-40 dynes.cm^{-2} depending upon the anatomical location (21). Application of physiological levels of cyclic strain (≤10%) have been shown to promote quiescence and prevent proliferation of VSMCs (22), whereas higher strain levels may promote dedifferentiation and proliferation of these cells and may even cause apoptosis (23) as compared to static cultures, thus substantiating the relevance of cyclic-strain application in mechanosensitive cells.

Stent implantation leads to variations in arterials geometry thus resulting in areas of localized turbulence which, in turn, can result in creation of zones of separation/areas stagnation which are associated sub-optimal wall shear stress, typically less than < 5 dynes/cm^2 (7). In addition, pre-clinical investigations with stent-implantation in animal models have previously demonstrated areas of low and oscillatory wall shear stress to be correlated with neointimal thickening within stented vessels (24). These observations are consistent with 3-dimensional mesh analysis studies in human arterial post-angioplasty analysis (25). Further, contribution of local wall shear stress post-PCI can be appreciated from the radical change in stent-strut design with older stents with thicker and squared-struts were found to be inferior to newer stents with thinner and rounded struts. At a cellular level, VSMCs subjected to physiological shear stresses have been shown to reduce proliferation and phenotypic modulation (26) whereas low wall shear stress promoting smooth muscle cell proliferation (27).

These clinical and pre-clinical observations demonstrate the versatility of VSMC response thus underscoring the need to evaluate cellular-response under clinically relevant mechanical loading conditions. In the currently proposed research project, a previously designed and characterized vascular simulator was employed (28) which is capable of concomitant application of physiologically relevant cyclic strain and low wall-shear stress, typifying dynamic loading on vascular cells post stent implantation in patients.

In vitro response-evaluation modeling can be extremely beneficial in determining the exact mechanism involved and developing causal relationship between stimulus and response, primarily due to lack of precise experimental control with animal models and impracticality of such investigations in humans. However, in vitro investigations pertinent to neointimal hyperplasia and In-stent restenosis are currently limited to studies focused towards evaluating drug-toxicity and efficacy under static unloaded conditions which fail to recapture the mechanically-dynamic environment observed clinically.

Although, in vitro investigations with dynamic loading have contributed significantly to the current understanding of VSMC-response under different regimes, prior investigations have failed to incorporate disease-related biochemical and biomechanical modifications especially those associated with diabetic and hypertensive patients. Patient-specific complications continue to impact the prognosis of DES implantation even with second-generation stents.

Chapter 2: Research Overview

2.1 Research aims and rationale:

Diabetes remains as the prime patient-specific risk factor in case of Balloon Angioplasty (BA) (8), Bare-metal stent (BMS) (9,11) and Drug-eluting stent implantation (DES) (13,58) with clinical evidence of exaggerated neointimal hyperplasia for all interventional procedures, as compared to the non-diabetic patient population. Consistent with BMS implantation (14), insulin-treated diabetic patients have been associated with greater rate of target lesion failure as compared to non-insulin treated diabetes with Resolute-Zotarolimus eluting stent (R-ZES), which is the only FDA-approved DES for diabetic patients, thus indicating the contribution of insulin to the development of restenosis despite the similar rate of stent-thrombosis (15).

In pre-clinical investigations, diabetes has been demonstrated to positively correlate with neointimal thickness (16,176). In support of the clinical observations in diabetic patients requiring insulin administration, rat models of diabetes have been demonstrated to exhibit greater neointimal hyperplasia post balloon angioplasty, upon insulin administration (4). A multitude of diabetes specific complications have been linked to an exaggerated NIH and *despite various clinical and pre-clinical investigations indicating contribution of diabetes-associated complications to neointimal development post-PCI, current interventional approaches do not account for variations in cellular-response associated with diabetes primarily due to lack of knowledge on exact mechanisms in these complicated conditions***.** This gap in knowledge can be associated to lack of precise variable-control in animal models and impracticality of investigating causal relations in human subjects. Thus, in vitro studies can be utilized to abridge this knowledge gap and further the current understanding of ISR in diabetic patients. This dissertation project proposes a in vitro

cellular-response specific test model which has successfully combined implant-associated altered mechanical forces with patient-specific complications through the following aims:

Aim 1: *Development and characterization of diabetic cellular-response evaluation model for in-stent restenosis*

Hypothesis: Insulin administration will promote proliferation and dedifferentiation of chronic high-glucose acclimated RASMC under physiologically relevant circumferential stretch with low wall-shear stress and this effect will be enhanced in case of partially induced insulin administration.

Rationale: Insulin is commonly administered under clinical settings to achieve normoglycemia in diabetic patients. Since diabetic patients requiring insulin-mediated glycemic control have significantly greater rates of revascularization post PCI, insulin administration and partial insulin resistance may contribute to the poorer response to PCI procedures. As neointimal hyperplasia is primarily driven by VSMC proliferation and phenotypic modulation, subjecting VSMC to dynamic loading conditions under diabetes related insulin administration and selective insulin resistance will capture the clinically relevant response more accurately. Blocking the phosphatidylinositol-3-kinase (PI3K) enzyme with wortmannin is a known approach to hamper glucose transport across cells, a cellular complication associated with insulin resistance. Thus, by blocking the "metabolic" arm of insulin receptor mediated glucose transport this approach captures partial insulin resistance.

Aim 2: *Development and characterization of hypertensive-diabetic cellular-response evaluation model for in-stent restenosis*

Hypothesis: The application of elevated mechanical strain with low-shear stress will result in greater dedifferentiation of RASMCs and insulin administration will augment this effect. In

addition, due to a proliferative effect of these factors, equimolar concentration of sirolimus will result in poor regulation of VSMC phenotype.

Rationale: A vast majority of diabetic patients are also afflicted with hypertension with substantial clinical evidence indicating high blood pressure leading to greater restenosis. Elevated blood pressure results in greater circumferential strain exerted on the vascular wall, and in case of denuded endothelium, directly on VSMCs. Higher than normal circumferential strain has been shown to promote VSMC proliferation and migration (177) thus, hypertension-associated cyclic strain should corroborate in phenotypic modulation of VSMCs during partially induced insulin resistance and insulin administration.

2.2Research significance

2.2.1 In vitro cell-response testing platform: The current standard of testing cellular response to clinical complications is primarily limited to static cultures which not only fails to capture the relevant response but also does not represent the clinical conditions. Mechanosensitive cells such as vascular smooth muscle cells (VSMC) are very responsive to subtle changes in blood vessel mechanics and hemodynamic alterations resulting from percutaneous coronary intervention (PCI) procedures such as balloon angioplasty and stent-implantation. The mechanical injury from these interventional procedures significantly affects local cellular responses such that VSMCs, which physiologically are exposed to circumferential strain are now, in addition, directly exposed to wall shear stress from blood flow. Various clinical and pre-clinical studies have established significant evidence demonstrating the contribution of these mechanical cues in VSMC-response (178). However, incorporation of these mechanical forces within basic cell culture investigations still remains uncommon and a vast majority of basic science studies designed to explore causal

mechanisms, are still confined to static-unloaded culturing approaches thus, fail to combine disease-associated complications in vitro. Consequently, a major drawback of these investigations is the lack of correlation of cellular-response in cell culture studies with pre-clinical or clinical observations. Our approach successfully incorporates clinically relevant cyclic strain and stent-associated low wall-shear stress at an in vitro level representing clinically relevant cellular response more accurately.

2.2.2 Combining patient-related complications with in-vitro culturing approach: Diabetes has been a consistent patient-specific risk factor for developing neointimal hyperplasia (NIH) ultimately leading to restenosis for all coronary interventions. Even in the drug eluting stent era, diabetic patients show more incidence of restenosis as an outcome of endovascular procedures. Current in vitro cell-response evaluating approaches to mitigate restenosis do utilize VSMCs isolated from various diabetic sources (179) however, these approaches fail to include relevant mechanical loading. Further, there is significant variation in cellular-response between different diabetic models alongside lack of correlation with clinical response (138)(176)(129). In addition, the current test model successfully subjects VSMCs to hypertension-related elevated circumferential strain while maintain diabetes-associated insulin administration.

Our approach of combining diabetes-related biochemical complications such as chronic high-glucose, insulin administration and selective insulin-resistance with stent-related hemodynamic alterations uniquely combines patient related factors and clinically relevant mechanical forces in vitro. In addition to diabetes, patient afflicted with hypertension are also at a higher risk with clinical reports of poorer outcomes of PCI in patients with diabetes and hypertension (180). Our approach of applying hypertension-related cyclic strain under diabetes-related insulin resistance

and insulin administration will capture the clinical response of such patients more accurately, as compared to static cultures. All the factors specified: diabetes, hypertension and hemodynamic alterations independently affect VSMC-response and drug efficacy however, a combination approach where all these are tested together has not been conducted yet. Such combinations are not feasible in animal models owing to lack of proper experimental control for cause and effect in addition to impracticality of conducting these investigations in humans.

2.2.3 Testing drug-efficacy under pathophysiological conditions: Currently, in vitro studies contribute primarily to evaluating the toxicity of drugs intended to control restenosis however, with our modeling approach, drug efficacy in controlling VSMC proliferation and phenotypic modulation was tested under diabetes-hypertensive conditions thus, providing a more clinically accurate environment at an in vitro level. This diabetic-hypertensive cellular-response evaluation model may be utilized to investigate cellular and molecular mechanisms that may be contributive to restenosis in a diabetic-hypertensive environment and can also be utilized for testing and trial of novel therapeutic targets and drugs aimed at reducing restenosis in these patients before evaluating them in animal models. Future exploration of pathways and therapeutic targets with this model will be extremely useful in reducing the lack of correlation between cellular-response and clinical observation with improved clinical efficacy of anti-restenotic drugs.

2.3 Research Innovation

2.3.1 Correlation to Clinical Relevance: Our current approach combines two of the fundamental contributors of in-stent restenosis namely 1) altered hemodynamics due to stent design and 2) patient-specific biochemical complications such selective insulin-resistance alongside insulin administration. This approach is unique since it incorporates diabetes-associated cellular response

with the physiologically relevant mechanical forces and thus captures the clinical condition of diabetic patients, with endovascular stents, in vitro more accurately. Further, increased cyclic strain characteristically associated with elevated blood pressure was employed to represent the VSMC-response more accurately for diabetic patients with hypertension thus, simulating coexistent patient-specific conditions under clinically relevant conditions. This methodology combines implant related mechanical forces with patient specific complications of diabetes and hypertension at an in vitro level which continue to be the patient cohort majorly affected by In-Stent Restenosis (ISR), even in the second-generation drug eluting stent era.

2.3.1 In vitro modeling of diabetes and hypertension associated complications: Wortmannin has previously been employed for evaluating the contribution of phosphatidylinositol-3-kinase enzyme in various cell and molecular pathways, PI3K/Akt inhibitory approach was utilized in order to induce selective insulin-resistance since this pathway has been demonstrated to hamper insulin-mediated glucose transport across cellular membrane. The phenomenon of insufficient insulin-mediated glucose transport is clinically defined as the peripheral insulin resistance in which fat, liver and muscular cells are unable transport and eventually metabolize glucose from the circulation ultimately leading to hyperglycemia, hyperinsulinemia and elevated triglyceride levels (94). In accordance with pathophysiology of peripheral insulin resistance, we attempted to block the PI3K/Akt pathway in order to partially mimic these clinically relevant conditions at cellular levels and thus have employed the approach of partial insulin resistance.

Insulin administration is a commonly employed strategy to ensure euglycemia in diabetic patients and since substantial clinical evidence exists for higher rate of target lesion/vessel revascularization in diabetic patients requiring insulin and for the development of an in vitro diabetic model, VSMCs

were subjected to 10 ng/mL insulin during induction of quiescence and mechanical loading to recapitulate the clinical scenario.

A direct consequence of hypertension is elevated blood pressure which ultimately exerts greater force on the vessel-wall. In order to represent these conditions in vitro, our unique model incorporated higher than normal circumferential strain (~15%) with low wall-shear stress with or without insulin administration. Thus, providing a novel platform which combines the corroborating effects of diabetes and hypertension with stent-specific hemodynamic alterations to a certain degree, in order to provide a novel in vitro testing platform for cellular response evaluation under these patients-associated conditions.

2.3.2 Use of model for evaluating drug efficacy: As an application of In vitro diabetic-hypertensive model, cells were treated with 10 ng/mL sirolimus in the final phase. This was primarily performed to evaluate if diabetes or hypertension associated complications incorporated into the model influenced the efficacy of sirolimus in controlling proliferation and phenotypic modulation of VSMCs. Thus, providing a clinically relevant approach of drug-testing under patient-specific conditions in vitro.

Chapter 3: "Development and characterization of diabetic cellular-response evaluation model for in-stent restenosis"

Purpose: The current study explores the different treatments incorporated to capture the effect of insulin administration and insulin-resistance on chronic high-glucose acclimated rat aortic smooth muscle cell under dynamic loading. The aim of this study is to develop an in vitro cell culture diabetic model that captures the clinically relevant cellular response in diabetic patients within stented vascular regions afflicted with poor glycemic management requiring insulin administration.

Method: Passage 4 rat aortic smooth muscle cells (SMC) acclimated to chronic high-glucose (25 mM D-Glucose media, 3-4 weeks) were seeded on type I collagen coated silicon membranes and subsequently subjected to 0-7% circumferential strain with low wall-shear stress (0.3 dynes/cm^2) in contact with wortmannin (100 nM, 84 hours), insulin (10 ng/mL, 48 hours) or a combination of both to represent selective-insulin resistance, insulin administration, or combination respectively. Treatments were evaluated by comparing cell-cycle distribution, apoptosis, estimation of cellular hypertrophy, αSM actin, SM22α, p-AKT and p-ERK ½ expression.

Results: Combined application of circumferential strain and low wall-shear stress resulted in greater proliferation and phenotypic modulation of chronic high-glucose acclimated SMC during insulin administration compared to controls. A greater percentage of cells in the S ($p < 0.0001$) and G2/M phase ($p < 0.0001$) of the cell cycle, reduced apoptosis ($p < 0.0001$) indicating greater cell survival, greater cell hypertrophy estimated by higher cell-area ($p < 0.0001$) and lower aspect ratio ($p < 0.0001$), reduced expression of contractile-phenotype associated markers -αSM actin ($p < 0.0001$), SM22α ($p < 0.0001$), higher expression of proliferation associated p-ERK ½ ($p < 0.0001$) were observed in comparison to control. These results indicate that insulin administration demonstrates a corroborating effect in conditions of poor glycemic control under dynamic

mechanical loading. Wortmannin administration did not result in significant differences of the cellular response despite resulting in a significantly reduced expression of p-AKT ($p < 0.0001$) whereas insulin-wortmannin combination resulted in similar proliferation and phenotypic modulation as insulin alone.

Conclusion: Our experimental approach successfully integrates mechanical forces observed in a stented blood vessel with diabetic patient-related conditions such as chronic high glucose with insulin administration, in vitro. Cellular-response under these conditions has not been performed previously despite clinical relevancy and demonstrates the need to model cellular behavior under disease-associated conditions to further improve prognosis of percutaneous interventional approaches. Results from the current investigation demonstrate a differential cellular-response under diabetes associated insulin administration which is significantly augmented by clinically relevant mechanical loading. Future investigations should focus on exploring the precise mechanisms such that it can be incorporated as a therapeutic target. Additional patient-specific complications can also be combined with diabetes-associated conditions to further current understanding of VSMC-response under complex conditions.

3.1: Introduction:

Patients afflicted with diabetes and requiring insulin therapy represent a high-risk cohort for restenosis, with increased rates of target vessel failure after coronary revascularization even with second generation drug-eluting stents (70). Increased risk of restenosis is attributable to exaggerated intimal hyperplasia ultimately necessitating subsequent target lesion revascularization. In addition, percutaneous interventional procedures including angioplasty and stent implantation result in vascular barotrauma which ultimately leads to endothelial denudation and exposes underlying vascular smooth muscle cells to normally unseen shear forces in addition to physiological circumferential strain (178).

Physiologically, VSMCs experience circumferential stress due to vessel-distension associated with blood pressure (≤ 10%) which has been demonstrated to promote a contractile phenotype of VSMCs in contrast to high strain, which in turn has been reported to promote proliferation and de-differentiation of VSMCs (181–184). In addition, direct shear forces from blood flow have also been reported to influence VSMC phenotype with physiologically relevant shear stress reducing proliferation and promoting contractile phenotype (185,186) while low-wall shear stress leading to proliferation, migration and dedifferentiation (61,187). An altered cellular response in presence of mechanical forces further emphasizes the mechanosensitive nature of VSMCs and thus, necessitates mechanical loading of these cells to better capture their physiologically relevant -response.

Insulin administration and insulin-resistance have been previously reported to exert a pro-proliferative effect on vascular smooth muscle cells, with insulin-effects in a concentration dependent manner (141,188–190). Additional investigations have reported greater neointimal hyperplasia post balloon-injury and stent-implantation in pre-clinical models of diabetes (139,191).

However, effects of these diabetes-related complications have not been explored under physiologically-relevant circumferential strain and stent-associated low wall-shear stress. Under diabetes associated chronic high-glucose conditions, we have previously demonstrated the effect of chronic high glucose on phenotypic modulation of rat aortic smooth muscle cells (RASMCs) during dynamic loading (192). In the current study, additional complications of insulin administration and insulin-resistance, both of which are clinically relevant for diabetic patients undergoing PCI, are investigated.

In order to combine these patient-specific complications with dynamic loading, we subjected RASMCs to physiologically relevant insulin administration and induced insulin-resistance with circumferential strain and low wall shear stress. Current experimental approach attempts to conceptualize an in vitro diabetic model which successfully captures VSMC-response under insulin administration and insulin-resistance conditions more accurately in comparison to conventional static/unloaded conditions. We hypothesize that insulin administration will promote chronic-high glucose acclimated RASMC proliferation and dedifferentiation and this effect will be enhanced in case of partially induced insulin resistance. In future, this model can be utilized to explore the efficacy of novel anti-restenotic drugs in vitro and can also be combined with additional patient-specific complications to capture clinically relevant cellular-response more accurately.

3.2: Materials and Methods:

3.2a. Isolation of rat aortic smooth muscle cells: Rat aortas were harvested from 9-10 weeks old female Sprague-Dawley™ rats using a modified version of previously published protocol approved (193). The modified version was approved by Clemson University Institutional Animal Care and Use Committee (IACUC). Briefly, aorta isolated from rat, was transferred back to the laboratory

and immediately rinsed with 1x sterile Dulbecco's phosphate buffered solution (DPBS; Cellergo, 21-031-CV) at 37 ^{0}C for 1-2 minutes in order to remove blood clots and any unwanted tissue. Aorta were subsequently treated with Collagenase type-II (300U/mL, Worthington 4176) in sterile Dulbecco's modified essential medium (DMEM with 25 mM D-Glucose; Corning 10-013-CM) for 12-15 minutes to enable enzymatic degradation of the adventitial layer. Subsequently, using straight and angular forceps, tears in the adventitial layer were created to facilitate its easy removal. After successfully removing the adventitial layer, aorta was split open along its longitudinal axis thus, allowing easy scraping on the luminal side to remove the endothelial monolayer. Multiple 1x DPBS rinses were performed to ensure removal of any loose cells and tissue after which, aorta was chopped into small sections (about 1mm^2) and subjected to another enzymatic digestion containing type I collagenase - 10mg/mL, elastase (10 U/mL, Worthington 2292) treatment for 3-4 hours under gentle shaking conditions at 37 ^{0}C thus allowing complete dissolution of the extracellular matrix of the medial layer. At the end of enzymatic digestions, the suspension was centrifuged and cells were transferred to T-25 flasks in DMEM (containing 25 mM D-Glucose) supplemented with 10% fetal bovine serum (FBS; Corning 35-010-CV) and 1% Antibiotic-Antimycotic agent (Penicillin/Streptomycin; Cellgro 30-004-CI). The primary cell line was incubated for about a week before passaging and subsequent passaging was performed every two weeks until passage 4. Cells were recruited at passage 4 for all experiments, in order to remove any passage-associated variability.

3.2b. Preparation of silicone membranes and Cell seeding: For this work, two baseplates were used providing a total sample size of 6 test specimens per experiment. Biomedical-grade silicone membrane of 0.015-inch thickness (0.15" NRV G/G 40D, Specialty Manufacturing Inc., MI) were cut to fit the custom cell-culture assembly (Figure 6a) which were coated with type 1 collagen using

Teflon ring (2.75 cm^2 inner cross-sectional area and 1.2 cm height) centered on the silicone surface exactly above the loading post (Figure 6b). To minimize friction between the loading post and the silicone membrane, 0.2 ml of silicone lubricant (Loctite, 51360) was distributed evenly on the loading-post under aseptic conditions.

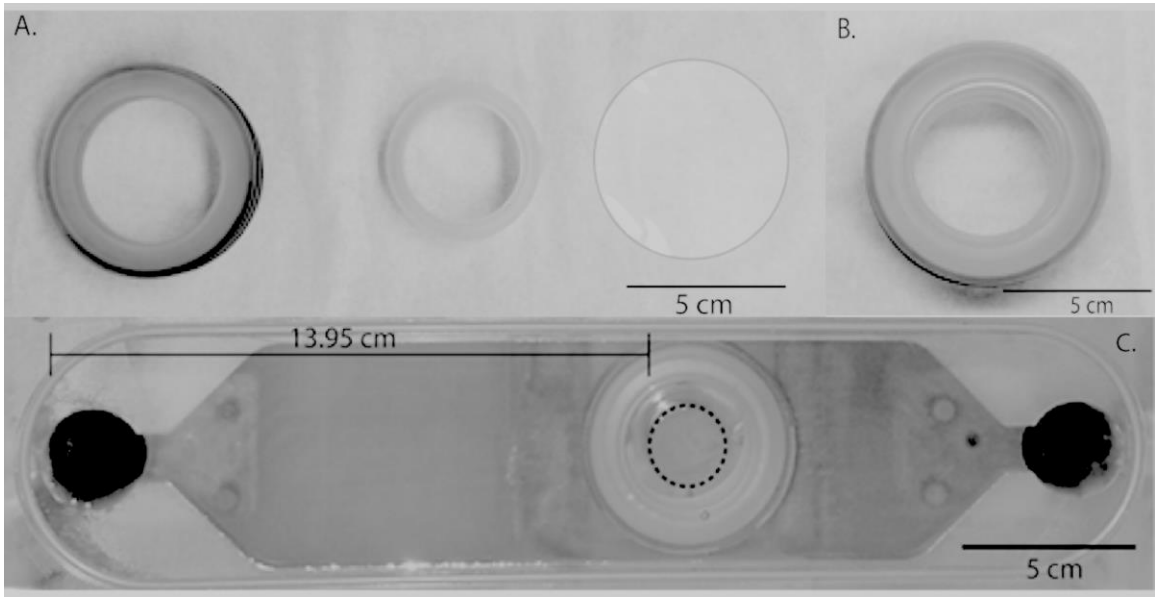

Figure 6 A: Components of the custom cell-culture assembly with outer ring, inner ring, silicone sheet (l-r); **B:** Cell-culture assembly prior to collagen coating; **C:** Singular channel of the simulator with cells seeded in the encircled area.

Passage 4 VSMCs cultured in media containing 25 mM D-Glucose were trypsinized (Corning, 25-050-CI) and counted using scepter cell-counter (Millipore, PHCC00000) and seeded at a density of 3.6 x 10^4 cells/cm^2 or 100,000 cells per well/loading station and allowed to attach and spread for 36 hours in cell culture media containing 10% FBS, 1% Ab/Am and 25 mM dimethyl sulfoxide (DMSO). After 36 hours, media was changed to DMEM containing 1% FBS, 1% Ab/m and 1% Dextran (Sigma, 9004-54-0) to induce quiescence and adjust media viscosity respectively. Briefly, cells were subjected to media supplemented with 10 ng/mL insulin (Sigma, I0516) during induction of quiescence and mechanical loading to represent insulin administration whereas for insulin-

resistance, cells were subjected to media supplemented with 100 nM wortmannin dissolved in DMSO (Sigma, W1628) during cell-seeding, induction of quiescence and loading (Table 3). DMSO was added to all treatments since it was required for dissolving wortmannin which was used for two treatments – wortmannin and insulin-wortmannin. Upon completion for every loading condition for each respective treatment, cells were rinsed with sterile 1x DPBS for 1-2 minutes and were subsequently detached using 1mL/well of trypsin-EDTA treatment and assayed using flow cytometry for cell-cycle and apoptosis analysis or protein extraction or fluorescent imaging for evaluating cellular hypertrophy.

Table 3: *Experimental treatments for aim 1*

Treatment / Loading	**Unloaded** (Cells seeded in 12-well plates)	**Cyclic Tensile (CT)** *(0-7 % cyclic strain, 0.5 Hz for 24 hours)*	**Cyclic Tensile Shear (CTS)** *(0-7 % cyclic strain, 0.5 Hz for 24 hours with shear from flow ~ 0.3 dynes.cm^{-2})*
DMSO Control (D)	**DU:** Cells in media containing 25 mM DMSO during seeding (36 hours), induction of quiescence (24 hours) and **unloaded** (24 hours).	**DCT:** Cells in media containing 25 mM DMSO during seeding (36 hours), induction of quiescence (24 hours) and **CT-loading** (24 hours).	**DCTS:** Cells in media containing 25 mM DMSO during seeding (36 hours), induction of quiescence (24 hours) and **CT-loading w/ low-shear stress** (24 hours).

DMSO w/ Wortmannin (100 nM) (DW)	**DWU:** Cells in media containing 25 mM DMSO + 100 nM Wortmannin during seeding (36 hours), induction of quiescence (24 hours) and **unloaded** (24 hours).	**DWCT:** Cells in media containing 25 mM DMSO + 100 nM Wortmannin during seeding (36 hours), induction of quiescence (24 hours) and **CT-loading** (24 hours).	**DWCTS:** Cells in media containing 25 mM DMSO + 100 nM Wortmannin during seeding (36 hours), induction of quiescence (24 hours) and **CT-loading w/ low-shear stress** (24 hours).
DMSO + Insulin (10 ng/mL) (DI)	**DIU:** Cells in media containing 25 mM DMSO during seeding (36 hours), 25 mM DMSO + 10 ng/mL insulin during induction of quiescence (24 hours) and **unloaded** (24 hours).	**DICT: :** Cells in media containing 25 mM DMSO during seeding (36 hours), 25 mM DMSO + 10 ng/mL insulin during induction of quiescence (24 hours) and **CT-loading** (24 hours).	**DICTS:** Cells in media containing 25 mM DMSO during seeding (36 hours), 25 mM DMSO + 10 ng/mL insulin during induction of quiescence (24 hours) and **CT-loading w/ low-shear stress** (24 hours).

DMSO w/ Wortmannin (100 nM) + Insulin (10 ng/mL) (DWI)	**DWIU:** Cells in media containing 25 mM DMSO + 100 nM Wortmannin during seeding (36 hours), 25 mM DMSO + 100 nM Wortmannin + 10 ng/mL insulin during induction of quiescence (24 hours) and **unloaded** (24 hours).	**DWICT:** Cells in media containing 25 mM DMSO + 100 nM Wortmannin during seeding (36 hours), 25 mM DMSO + 100 nM Wortmannin + 10 ng/mL insulin during induction of quiescence (24 hours) and **CT-loading** (24 hours).	**DWICTS:** Cells in media containing 25 mM DMSO + 100 nM Wortmannin during seeding (36 hours), 25 mM DMSO + 100 nM Wortmannin + 10 ng/mL insulin during induction of quiescence (24 hours) and **CT-loading w/ low-shear stress** (24 hours).

3.2c. Mechanical Loading: Cells were subjected to either physiological cyclic strain (0-7%) at 0.5 Hz (CT) or to cyclic tensile strain (0-7% at 0.5 Hz) and low wall shear stress (CTS, ~0.30 dynes.cm^{-2}) from externally supplied flow at 350 mL/min using a peristaltic pump (CTS) for all treatments (Table 3). Cyclic strain was applied using FlexCell-3000^{TM} system (Flexcell International, NC) where shear stress was provided by externally supplied flow at 350 mL/min using a peristaltic pump (Cole-Parmer). Physiologically, VSMCs are subjected to 0-7% cyclic strain in a healthy blood vessel and typically never experience direct blood flow. Typically, the loading frequency in previous investigations is 1 Hz but in the current investigation we used 0.5 Hz to represent physiological profile due to mechanical limits of the design where significant differences were observed in applied vs theoretical strain (Appendix B). Previous studies have indicated frequency of mechanical loading to be correlated with altered cell-response however, this effect was only observed for short-duration of loading with no difference in PI3/AKT or p-ERK 1/2 expression

levels (194). However, in case of endothelial dysfunction or damage the underlying layer of VSMCs now experiences shear stress from blood flow directly. After stent implantation, flow separation zones are created due to stent struts which can result in zones of no-flow or area of flow separation. The zones typically have very low wall shears-tress. All simulations were performed at 37 ^{0}C in an incubator (Fisher Scientific). Cells were subjected to unloaded/static conditions for each respective treatment (Control-C, Wortmannin-W, Insulin-I or Insulin + Wortmannin-InsW) whereby, these samples served as loading controls.

3.2d. Cell cycle analysis: Cell cycle analysis was performed using propidium iodide staining method using the Guava cell-cycle flow cytometric assay and manufacturer's protocol (Millipore, 4500-0220)(195,196). Briefly, cells were detached at the end of every simulation using trypsinized-EDTA and were centrifuged at 500x g for 5 minutes. Subsequently, cells were rinsed in 1x DPBS and re-centrifuged for 5 minutes at 500x g. Cells were redissolved in 200 µL of 1x DPBS and fixed in ice-cold 70% ethanol with gentle-intermittent shaking and stored at -20 ^{0}C for 48 hours at least. On the day of the assay, cells were removed from ethanol, rinsed in 1x DPBS and resuspended in 200 µL of guava cell-cycle reagent after which they were incubated in dark conditions for 30 minutes at room temperature. Finally, cells were assayed for their distribution within the cell cycle with Guava HT flow cytometer. For each sample, the threshold cellular count was set to 2000 events.

3.2e. Apoptosis analysis: Apoptotic analysis was performed using the TUNEL assay (Millipore 4500-0121), where cells undergoing apoptosis were incorporated with fluorescently labeled dUTP and subsequently assay for their intensity using Guava flow cytometer. Cells were detached and fixed in 70% ethanol similarly to cell-cycle analysis, for measuring apoptotic index for all

treatments and on the day of the assay, cells were first incubated with a reaction mixture containing dUTP monomers for 1 hour and subsequently incubated with Anti-BrDU antibody, according to manufacturer's protocol (196).

3.2f. Cellular Hypertrophy: Measurement of cellular hypertrophy was performed as described previously (192). Briefly, cells after each treatment were fixed and permeabilized with 0.2% Triton X-100 in PBS following which cells were incubated with rhodamine-phalloidin (P1951, Sigma; 1:2000) and DAPI (1:2000) in PBS. Cells were imaged using fluorescent microscope (Digital inverted microscope, EVOS f1, AMG). For each sample, five to six random field-of-view were recorded and analyzed per sample, resulting in a total sample size of 180 per experimental group. Cell area (indicative of cellular hypertrophy) and aspect ratio (major axis length to minor axis length ratio) were measured using ImageJ software (Open source imaging software from National Institute of Health). Mean cell area (μm^2) & aspect ratio were measured and analyzed for a sample size of 180 per treatment (192).

3.2g. Protein extraction and Western blotting: Protein quantification was performed using western blot analysis using a modified version of a previously described protocol (197). Whole cell lysates were prepared from the cells at the end of each simulation using extraction buffer (20 mM Tris 1% SDS, 0.5% Triton and 10 µL/mL protease inhibitor cocktail, Sigma P 8340). Total protein concentration was calculated using BCA-assay kit (Life Technologies, 23225) using BSA know standards as described by manufacturer. SDS-PAGE was performed using Mini-PROTEAN TGX 10% precast-gels (BioRad 4561034). For each well, 10 µg of total protein was loaded using 5x loading buffer and electrophoresis was performed at 110 V for 90 minutes. Protein samples were subsequently transferred to PVDF membranes (BioRad 1620177) at 100V for 75 minutes under

ice-cold conditions. Blots were blocked with 3% BSA in PBS and were probed with primary antibodies overnight at 4 ^{0}C (SM α-actin ab 119952, 1:500; SM-22α, ab10135 1:1500; α-tubulin, ab7291 1:1500; p-AKT 4060s Cell signaling technologies 1:1000; p-ERK ½ 4370s Cell signaling technologies 1:1000). Luminol was used as a chemiluminescence-substrate (Santa Cruz, SC-2048) reagent prior to blot-imaging. Densitometric analysis was performed using ImageJ software to quantify the amount of protein expressed. Prior to analysis, all protein bands were normalized with α-tubulin, which was the loading control.

3.2h. Statistical analysis: Statistical Analysis was performed with One-way ANOVA and Tukey's HSD post hoc for all data sets with 0.05 level of significance ($\alpha = 0.05$). All tests were performed with JMP 12 pro and plots were created with OriginPro 2017. "*" represents statistical significance when compared to control treatment within each respective loading. "#" represents statistical significance between treatments during CT and CTS loading.

3.3: Results

3.3a. Cell-cycle distribution: Cell cycle distribution was analyzed using the propidium-iodide staining method with Guava cell-cycle kit (n=6 for each treatment within every loading) which provides cellular-distribution within the cell-cycle depending upon fluorescent-intensity (198). Effect of treatment and loading was evaluated across the cell cycle and distributions within each phase – G1/G0, S and G2/M phase were compared. A higher cell-percentage in G2/M or S-phase represented a more proliferative response since all the cells were passage-matched and conditioned to quiescence state, prior to any simulation. All cells in the G1/G0 phase are represented with the first peak of histograms whereas cells in the G2/M phase were gated for double the intensity of G1/G0 phase. Cells between these two peaks were recorded as cells in the stationary phase or S-phase (Figure 7) and cell-cycle results are summarized in table 4.

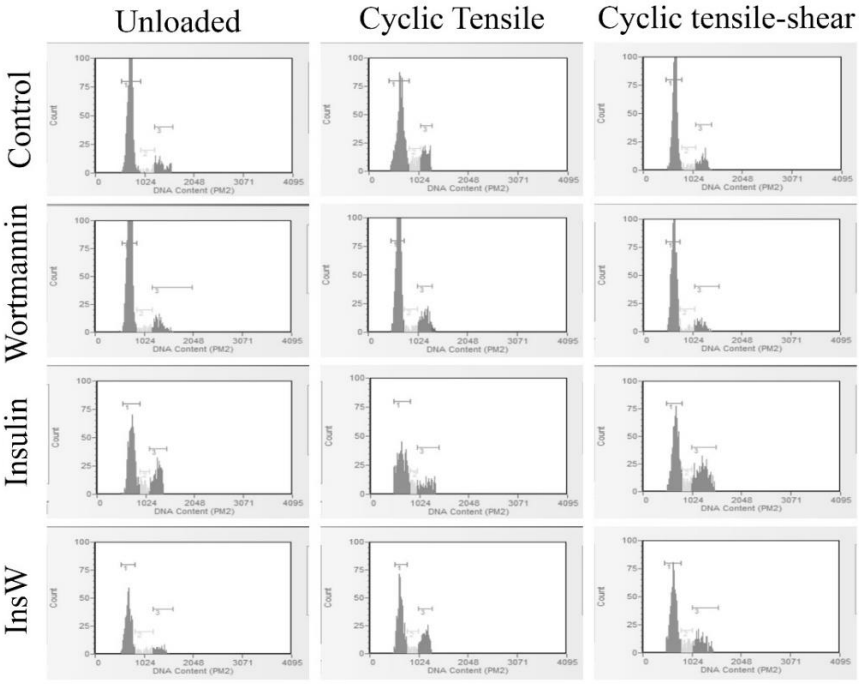

Figure 7: *Treatment and loading-wise cell-cycle distribution of cells. Each sample was assayed for 2000 cells. First peak represents % cells in the G1/G0 phase whereas second peak represents % cells in G2/M phase. All cells in between these two distinct peaks were categorized in the s-phase.*

Table 4: *Cell-cycle results*

Loading	Treatment	% Cells in G1/G0 phase (Mean±SD)	% Cells in S-phase (Mean±SD)	% Cells in G2/M phase (Mean±SD)	Sample Name
Unloaded	*Control*	77.05±3.56	5.35±1.05	15.15±1.63	**DU**
	Wortmannin	78.68±3.32	6.08±0.75	12.05±1.77	**DWU**
	Insulin	53.15±3.88	9.93±1.52	27.77±3.64	**DIU**
	InsW	64.73±6.63	8.58±0.95	26.47±1.93	**DWIU**
CT	*Control*	85.8±3.39	3.56±1.47	9.27±1.54	**DCT**
	Wortmannin	84.83±2.76	5.28±0.92	9.55±1.84	**DWCT**
	Insulin	67.55±5.94	9.97±1.64	25.75±2.06	**DICT**
	InsW	66.85±2.26	8.51±1.29	22.21±2.72	**DWICT**
CTS	*Control*	78.42±2.06	6.63±1.07	11.95±1.64	**DCTS**
	Wortmannin	75.05±6.81	7.81±1.77	14.62±2.35	**DWCTS**
	Insulin	53.1±3.56	9.43±1.76	37.47±2.25	**DICTS**
	InsW	56.01±4.92	7.49±1.00	26.70±3.01	**DWICTS**

Comparison of all treatments with DMSO control for each loading revealed that insulin treatment led to significantly lower % cells in the G1/G0-phase for all mechanical loading (p-value < 0.0001 for DIU vs DU; DICT vs DCT; DICTS vs DCTS, Figure 8) and a corresponding increase in %-cells in the S phase (p-value < 0.0001 for DIU vs DU; DICT vs DCT; DICTS vs DCTS, Figure 9) and G2/M phase (p-value < 0.0001 for DIU vs DU; DICT vs DCT; DICTS vs DCTS, Figure 10). Cellular-treatment with 100 nM wortmannin did not result in significantly different % cells in G1/G0 or S or G2/M phase, in comparison to DMSO control across all loadings. Similar to insulin treatment, InsW treatment also demonstrated significantly reduced % cells in the G1/G0-phase for mechanical loading (p-value < 0.0001 for DWIU vs DU; DWICT vs DCT; DWICTS vs DCTS) and a corresponding increase in %-cells in the S phase (p-value < 0.0001 for DIU vs DU; DICT vs DCT; DICTS vs DCTS) and G2/M phase (p-value < 0.0001 for DIU vs DU; DICT vs DCT; DICTS vs DCTS) however, the results were not significantly different from insulin-only treatment.

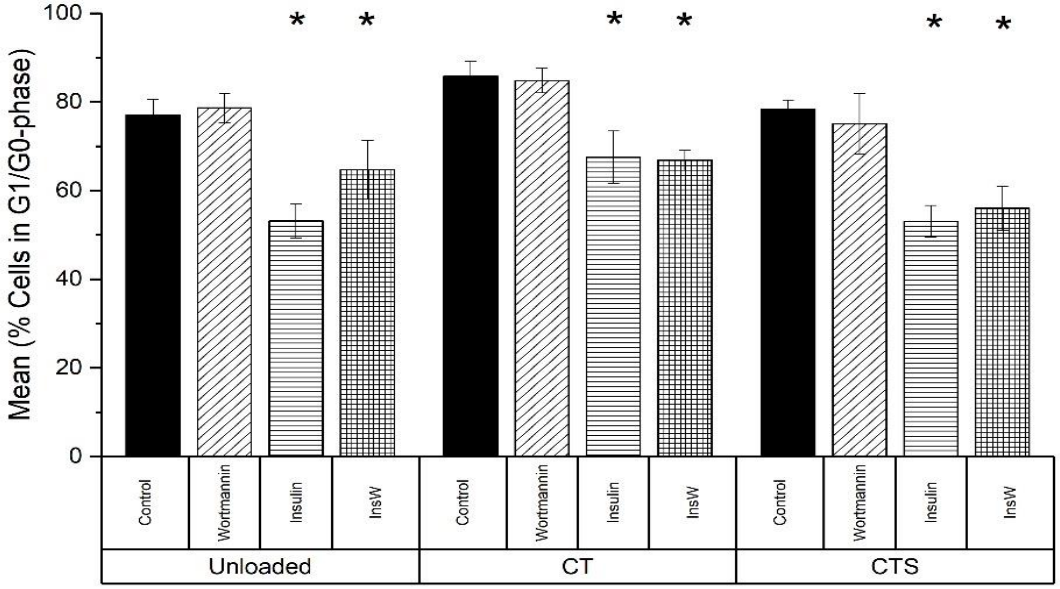

Figure 8: *Treatment-wise percentage of cells in the G1/G0 phase within each mechanical loading; Values represented as Mean ± SD for every treatment (n=6 for each). '*' represents statistical significance (p-value < 0.05) in comparison to 'control or DMSO' for every loading; '#' represents statistical significance (p-value < 0.05) in comparison to cyclic-tensile (CT). All comparisons performed with one-way ANOVA and Tukey's HSD.*

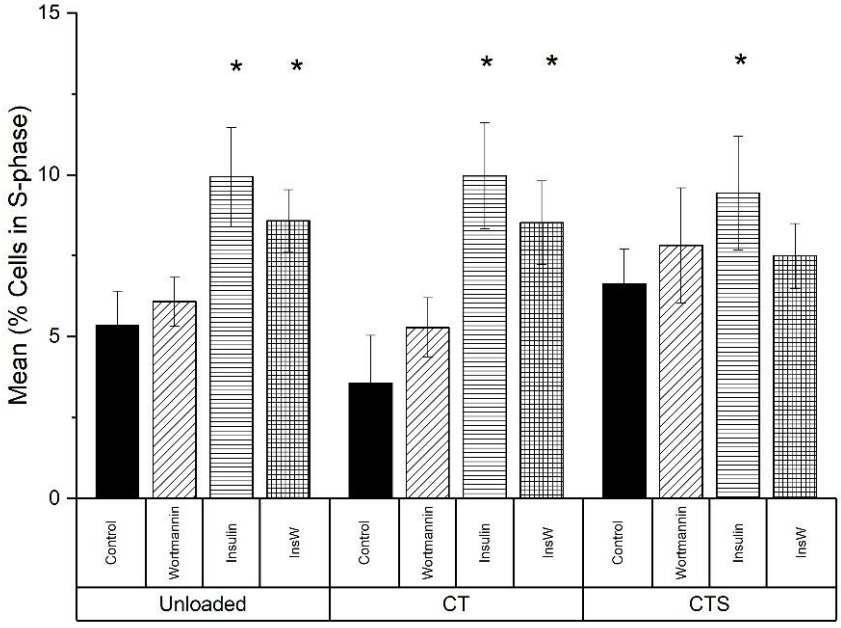

Figure 9: *Treatment-wise percentage of cells in the S- phase within each mechanical loading; Values represented as Mean ± SD for every treatment (n=6 for each). '*' represents statistical significance (p-value < 0.05) in comparison to 'control or DMSO' for every loading with one-way ANOVA and Tukey's HSD post-hoc comparison.*

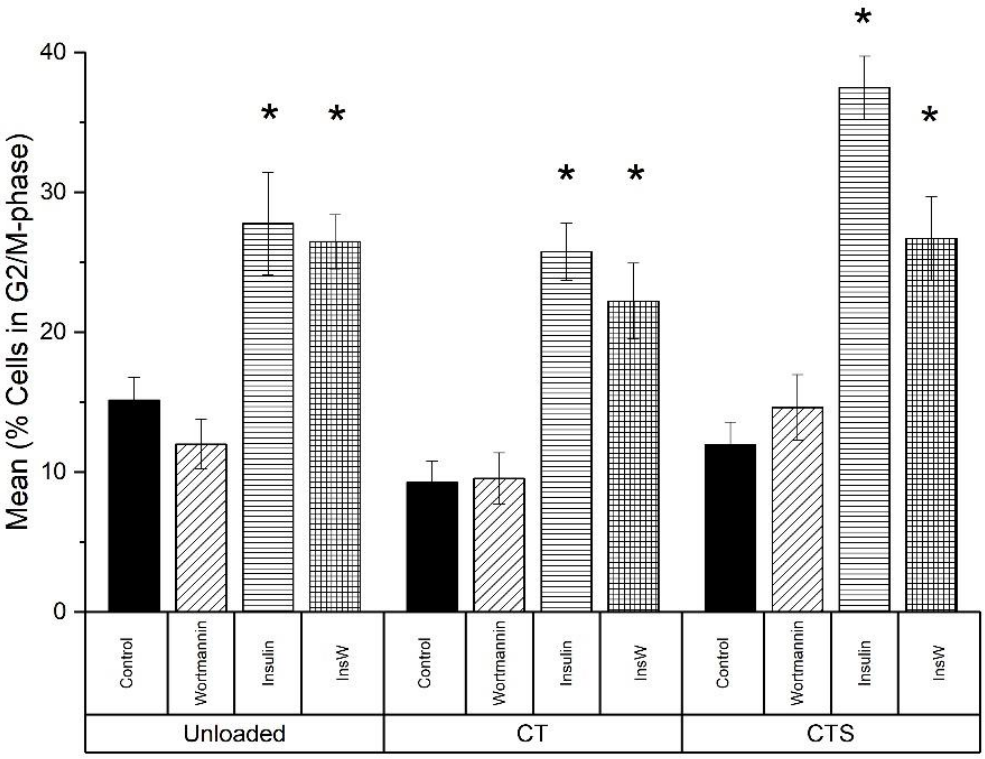

Figure 10: *Treatment-wise percentage of cells in the G2/M- phase within each mechanical loading; Values represented as Mean ± SD for every treatment (n=6 for each). '*' represents statistical significance (p-value < 0.05) in comparison to 'control or DMSO' for every loading; '#' represents statistical significance (p-value < 0.05) in comparison to cyclic-tensile (CT). All comparisons performed with one-way ANOVA and Tukey's HSD.*

Corroborating with the effects of insulin, concomitant application of low-shear stress and cyclic-strain further led to lower % of cells in the G1/G0-phase in comparison to CT only (p-value < 0.0001 for DICT vs DICTS and DWICT vs DWICTS) and a corresponding increase in % of cells in the S phase (p-value < 0.0001 for DICT vs DICTS and DWICT vs DWICTS) and G2/M phase (p-value < 0.0001 for DICT vs DICTS and DWICT vs DWICTS). In addition, insulin administration resulted in significantly greater % of cells during CTS loading in comparison to CT (p-value < 0.0001 for DICTS vs DICT) and in comparison to InsW treatment (p-value < 0.0001 for DICTS vs DWICTS). These observations indicate that under clinically relevant cyclic-strain and low-shear application, insulin exerts a pro-proliferative effect on RASMCs while selective-insulin resistance through wortmannin treatment did not influence cell-cycle progression.

3.3b. Apoptotic Index: For evaluating the total percentage of cells undergoing apoptosis samples were quantified by the TUNEL assay, using Guava flow cytometer (n=6 for each treatment per loading). Cell-distribution for each treatment within every loading is depicted in figure 11 where the first peak represents cells that are TUNEL-negative and the second peak for TUNEL-positive cells. Results are summarized in table 5 and plotted as percent apoptosis – defined as ratio of percent apoptotic cells to percent total cells (sum of apoptotic and non-apoptotic cells) (Figure 12).

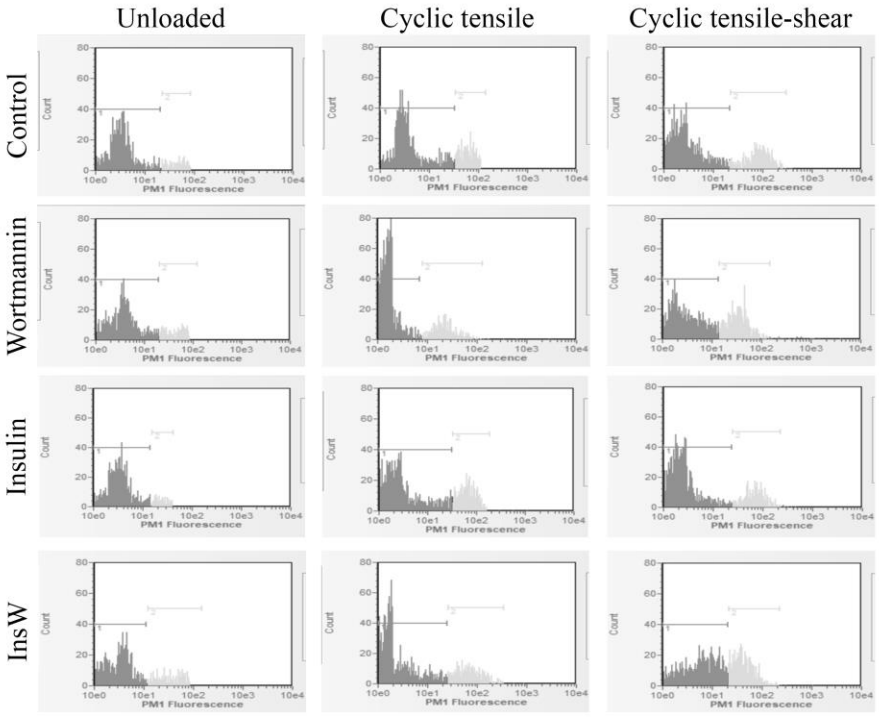

Figure 11: *Treatment and loading-wise TUNEL positive cell-distribution. Each sample was assayed for 2000 cells. First peak represents % cells in the negative for TUNEL statin whereas second peak represents % cells positive for TUNEL stain.*

Table 5: *Guava TUNEL results*

Loading	Treatment	% Apoptotic cells Mean ± SD	Sample Name
Unloaded	*Control*	10.97 ± 1.12	**DU**
	Wortmannin	15.97 ± 0.94	**DWU**
	Insulin	6.14 ±1.29	**DIU**
	InsW	16.26 ± 1.77	**DWIU**
CT	*Control*	19.29 ± 0.88	**DCT**
	Wortmannin	24.12 ± 1.35	**DWCT**
	Insulin	18.76 ± 1.03	**DICT**
	InsW	24.92 ± 1.58	**DWICT**
CTS	*Control*	29.12 ± 0.83	**DCTS**
	Wortmannin	36.01 ± 1.14	**DWCTS**
	Insulin	29.19 ± 2.49	**DICTS**
	InsW	39.47 ± 0.95	**DWICTS**

For unloaded samples, insulin treatment significantly reduced overall apoptosis however, this effect was not extended to CT or CTS loadings where the results were not significantly different from the DMSO control thus, demonstrating the contribution of mechanical loading in inducing cellular apoptosis. Wortmannin appeared to induce apoptosis since InsW treatment resulted in similar measurements as for wortmannin treatment, where InsW treatment led to significantly greater number of cells undergoing apoptosis as compared to DMSO control for all loadings (p-value < 0.0001 for DWIU vs DU; DWICT vs DCT; DWICTS vs DCTS) (figure 12). In addition, InsW treated cells did not exhibit significantly greater number of cells undergoing apoptosis in comparison to wortmannin treated cells thus, indicating wortmannin primarily resulted in greater apoptosis.

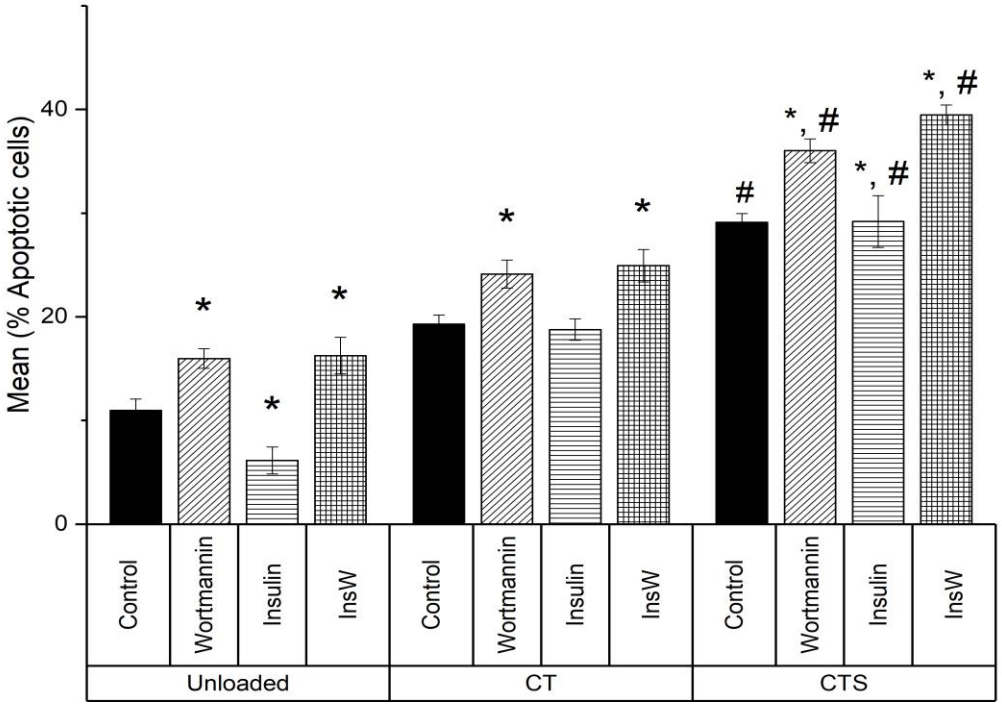

Figure 12: *Treatment-wise percent apoptosis within each mechanical loading; Values represented as Mean ± SD for every treatment (n=6 for each). '*' represents statistical significance (p-value < 0.05) in comparison to 'control or DMSO' for every loading; '#' represents statistical significance (p-value < 0.05) in comparison to cyclic-tensile (CT). All comparisons performed with one-way ANOVA and Tukey's HSD.*

Application of CT led to significantly greater number of cells undergoing apoptosis as compared to unloaded samples for all treatments (p-value < 0.0001 for CT vs U within each treatment) whereas application of low-shear stress further contributed to induction of apoptosis (p-value < 0.0001 for CTS vs CT within each treatment).

3.3c. Cellular hypertrophy: Cellular hypertrophy was evaluated by measuring the cell-area and aspect ratio (Ratio of major-axis length to minor-axis length) using image analysis with ImageJ software. Hypertrophic cells exhibit greater cell area either due to increased protein secretion or relatively loose F-actin fibers while rhomboid-shaped cells will have lower aspect ratio as compared to spindle-shaped cells thus indicative of synthetic phenotype (192). Results for cell-area and aspect ratio are summarized in table 6 and rhodamine-phalloidin stained images for all treatments within each loading is compiled in Figure 13.

Table 6: *Cell-area and aspect ratio results*

Loading	Treatment	Cell area (sq. μm) Mean± SD	Aspect Ratio Mean± SD	Sample Name
Unloaded	*Control*	5125.24 ± 94.05	1.67 ± 0.02	**DU**
	Wortmannin	5172.09 ± 107.11	1.75 ± 0.05	**DWU**
	Insulin	5372.98 ± 95.32	1.68 ± 0.03	**DIU**
	InsW	5512.38 ± 84.23	1.80 ± 0.04	**DWIU**
CT	*Control*	2460.64 ± 54.36	2.76 ± 0.08	**DCT**
	Wortmannin	2686.14 ± 99.03	2.46 ± 0.05	**DWCT**
	Insulin	3620.26 ± 80.31	2.05 ± 0.06	**DICT**
	InsW	3636.81 ± 79.97	2.09 ± 0.04	**DWICT**
CTS	*Control*	2994.73 ± 65.75	2.31 ± 0.05	**DCTS**
	Wortmannin	3097.84 ± 84.39	2.22 ± 0.06	**DWCTS**
	Insulin	4362.94 ± 88.67	1.84 ± 0.23	**DICTS**
	InsW	4464.68 ± 83.73	1.92 ± 0.03	**DWICTS**

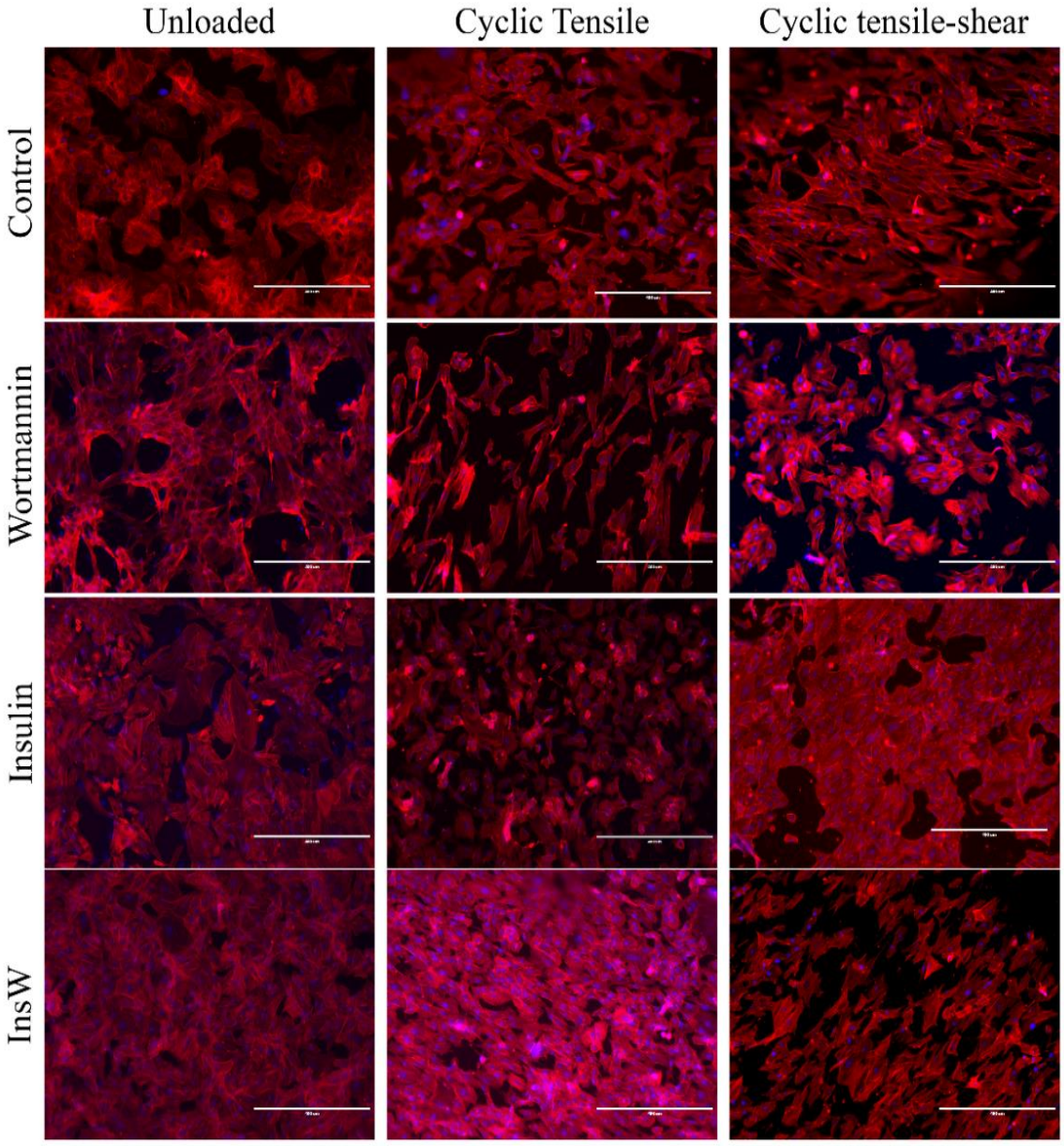

Figure 13: *Rhodamine-phalloidin stained images with treatments as rows and mechanical loadings as columns; Scale-bar 400 µm*

As demonstrated in figure 14, insulin treatment led to significantly greater cell-area for mechanically loaded samples in comparison to DMSO controls (p-value < 0.0001 for DICT vs DCT; DICTS vs. DCTS) thus, demonstrating a combined effect of insulin treatment and physiologically relevant mechanical loading where cells exhibit greater cell-area under loaded conditions. Further, wortmannin treatment did not result in significant change in cell-area independent of loading. Similar to the results from insulin during mechanical loading, InsW treatment resulted in significantly greater cell area, in comparison to controls (p-value < 0.001 DWICT vs DCT; DWICTS vs. DCTS) albeit, no significant differences between InsW and insulin treatment within each respective loading. These results indicate a relatively greater hypertrophic response in RASMCs due to insulin treatment under CT and CTS loading with no significant effect to due to selective insulin resistance.

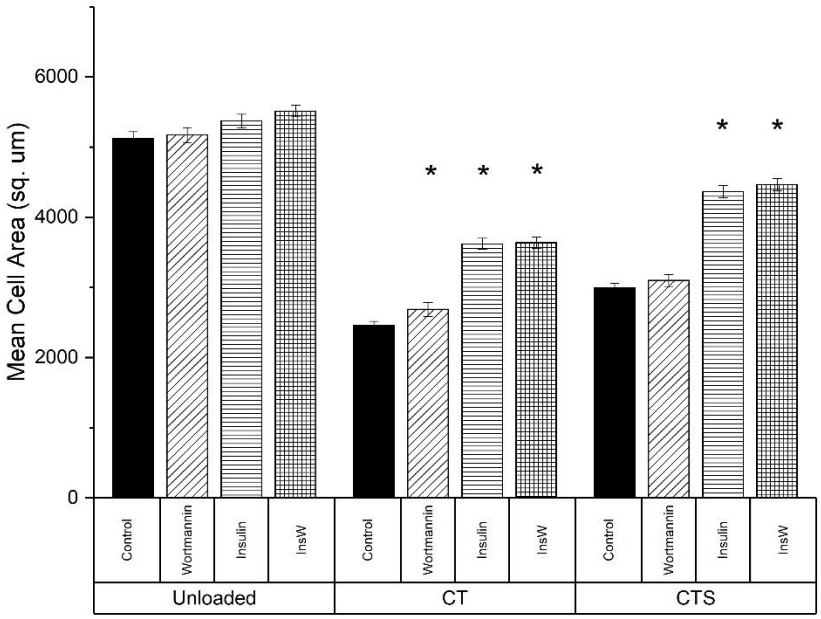

Figure 14: *Treatment-wise Cell area (sq. µm) within each mechanical loading; Values represented as Mean ± SD for every treatment (n=6 for each with 180 cells per sample). '*' represents statistical significance (p-value < 0.05) in comparison to 'control or DMSO' for every loading with one-way ANOVA and Tukey's HSD post-hoc comparison.*

In accordance with cell-area results, aspect ratio measurements (figure 15) demonstrated that insulin treatment led to a significantly lower aspect ratio for CT and CTS loading (p-value < 0.0001 for DICT vs DCT; DICTS vs DCTS) whereas wortmannin treatment did not induce significant

changes in aspect ratio across all loadings thus, supporting cell-area measurements. As with insulin, InsW treatment also demonstrated significantly lower aspect ratio for CT and CTS loading in comparison to control (p-value < 0.0001 DWICT vs DCT; DWICTS vs. DCTS). With no significant differences between insulin and InsW treatment across all loadings, selective insulin-resistance did not influence cellular hypertrophy whereas insulin treatment promoted cellular hypertrophy as estimated by significantly greater cell-area and correspondingly lower aspect ratio measurements.

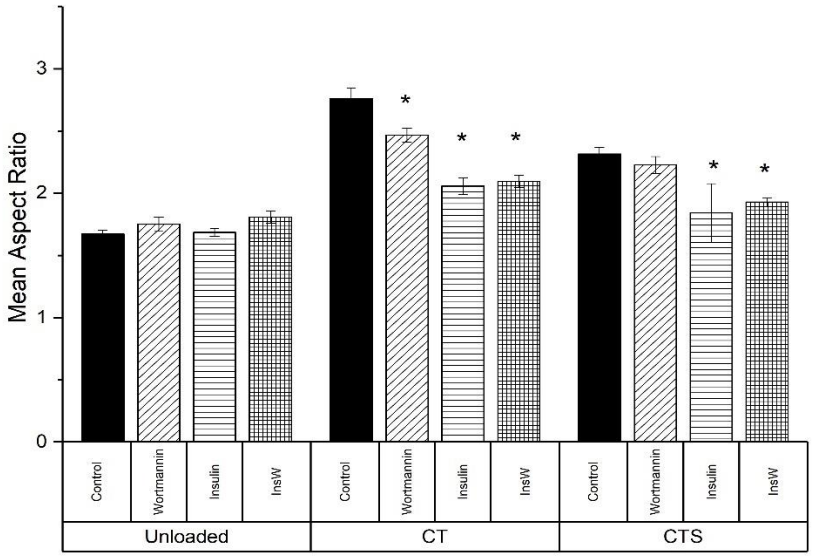

Figure 15: *Treatment-wise Aspect-ratio within each mechanical loading; Values represented as Mean ± SD for every treatment (n=6 for each with 180 cells per sample). '*' represents statistical significance (p-value < 0.05) in comparison to 'control or DMSO' for every loading with one-way ANOVA and Tukey's HSD post-hoc comparison.*

3.3d. Protein Expression: Protein expression was measured with western blotting and results were normalized to α-Tubulin (50 kDa), which served as the loading control. Smooth muscle cell-contractile state was evaluated by comparing the expression of contractile-state associated markers –α-SM actin and SM22 α with reduced expression decreases as cells switch to proliferative/synthetic phenotype. Further, to evaluate if wortmannin treatment was effective in inducing selective insulin-resistance, expression of phosphorylated-AKT (p-AKT) was evaluated

for all treatments whereas phosphorylated-ERK ½ (p-ERK ½) expression was evaluated to verify the potential molecular track through which the cellular response acts.

As shown in figure 16, insulin administration led to significantly lower expression of α-SM actin for unloaded, CT and CTS loading conditions in comparison to control (p-value < 0.0001 for DIU vs DU; DICT vs DCT; DICTS vs DCTS) thus, indicating a shift towards greater synthetic-state. Similar results with InsW treatment were observed where significantly lower α-SM actin expression was observed in comparison to DMSO controls across all loadings (p-value < 0.0001 DWIU vs DU; DWICT vs. DCT; DWICTS vs DCTS) further confirming insulin's effect in inducing a synthetic-state response.

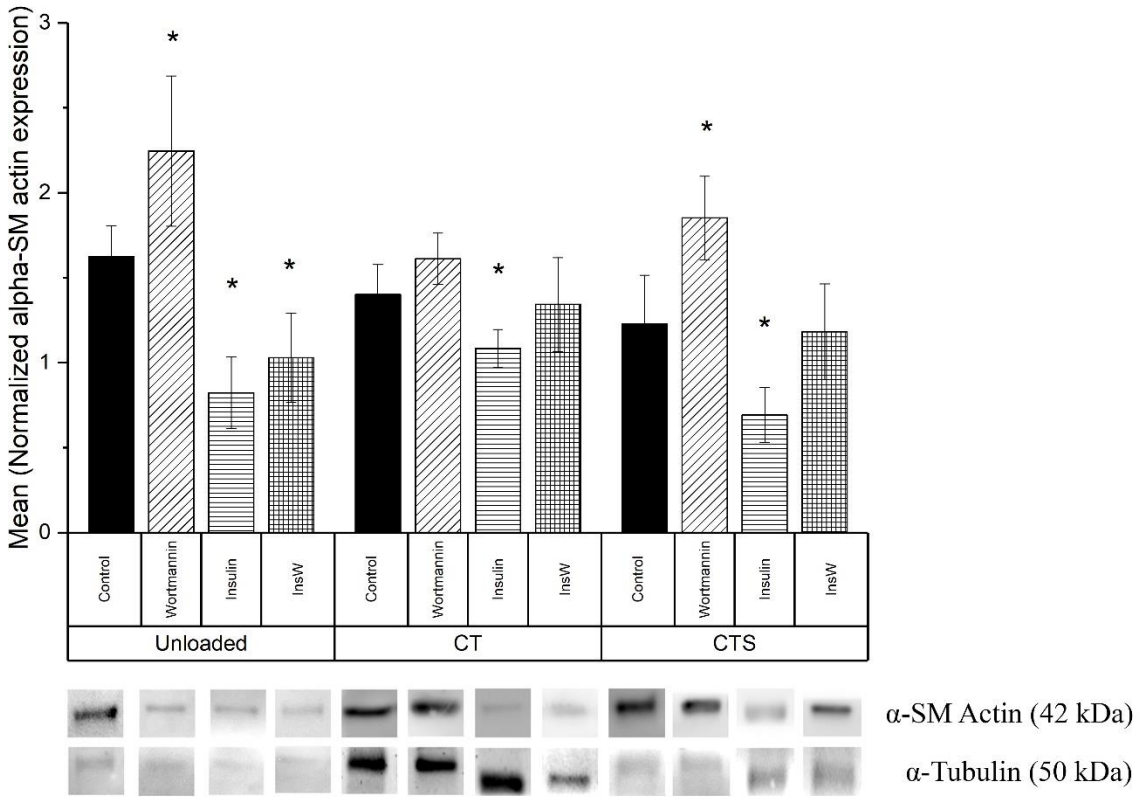

Figure 16: *Treatment-wise α-SM actin expression normalized to α-Tubulin expression within each mechanical loading; Values represented as Mean ± SD for every treatment (n=6 for each). '*' represents statistical significance (p-value < 0.05) in comparison to 'control or DMSO' for every loading with one-way ANOVA and Tukey's HSD post-hoc comparison.*

Wortmannin treatment led to greater expression of α-SM actin for unloaded (p-value < 0.0001 for DWU vs DU) and CTS loading (p-value < 0.0001 for DWCTS vs DCTS) thus, indicating a pro-contractile state shift of RASMCs under these conditions. With InsW treatment, results were observed to be very similar to insulin treatment where significantly lower expression of α-SM actin was observed across all loadings (p-value < 0.0001 for DWIU vs DU; DWICT vs DCT; DWICTS vs DCTS). However non-significant differences between insulin and InsW treatment indicate the involvement of insulin under these conditions whereby insulin promotes dedifferentiation of RASMCs overall.

Similarly, SM22 α expression results (Figure 17) indicate that insulin treatment led to significantly lower expression of SM22 α for unloaded (p-value < 0.0001 for DIU vs DU), CT (p-value < 0.0001 for DICT vs DCT) and CTS loading (p-value < 0.0001 for DICTS vs DCTS). In combination with the actin-expression results, these results indicate that insulin administration leads greater dedifferentiation of RASMCs since both the contractile-state associated markers have significantly lower expression. Wortmannin treatment did not result in significant changes in the expression of SM22 α across all loadings. In addition, InsW treatment led to significantly lower expression of SM22 α for unloaded (p-value < 0.0001 for DWIU vs DU), CT (p-value < 0.0001 for DWICT vs DCT) and CTS (p-value < 0.0001 for DWICTS vs DCTS) with no significant difference between InsW and insulin treatment. These results confirm that insulin treatment leads to greater phenotypic modulation of RASMCs towards the synthetic state and thus, demonstrates lack of influence of selective insulin-resistance in mediating a phenotypic change in RASMCs. Different mechanical loadings did not impact contractile-state markers for each respective treatment however, insulin administration led to lower α-SM actin and SM22 α expression with the application of shear when compared respective cyclic-tensile treatments (p-value < 0.0001 for DICT vs DICTS).

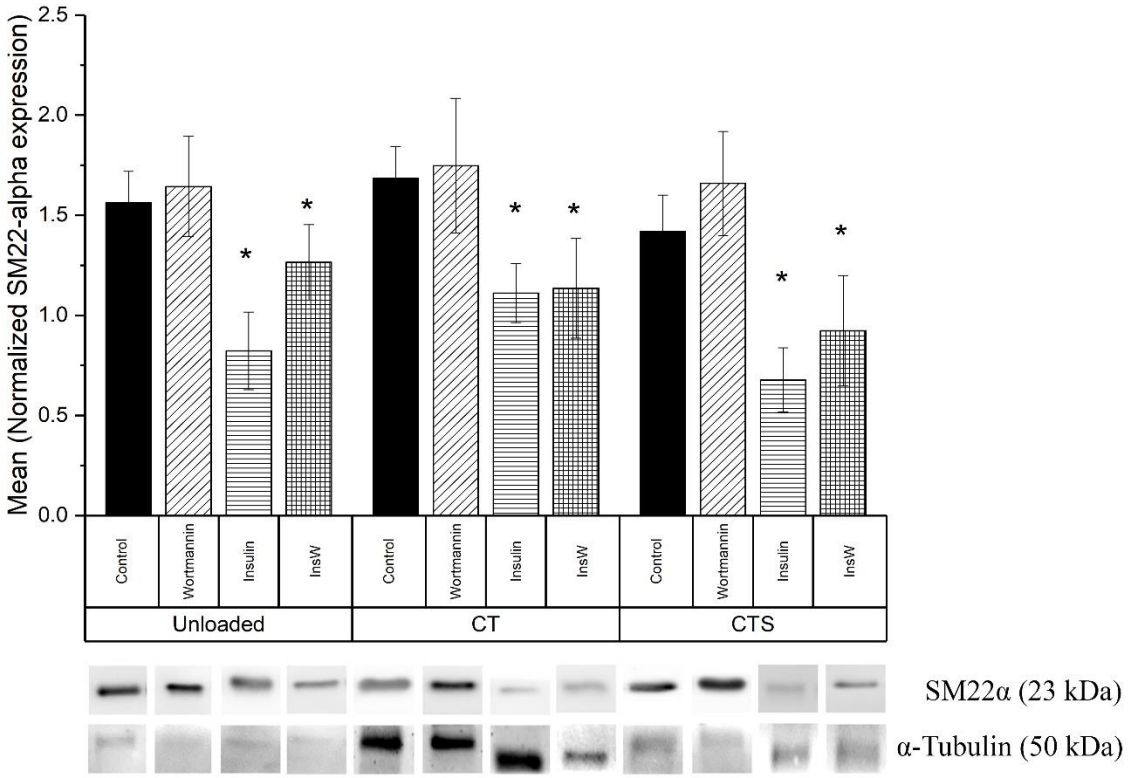

Figure 17: *Treatment-wise SM22α expression normalized to α-Tubulin expression within each mechanical loading; Values represented as Mean ± SD for every treatment (n=6 for each). '*' represents statistical significance (p-value < 0.05) in comparison to 'control or DMSO' for every loading with one-way ANOVA and Tukey's HSD post-hoc comparison.*

In order to confirm the efficacy of wortmannin in inducing selective insulin resistance through inhibiting phosphorylation of AKT, expression levels of p-AKT were compared for all treatments within each loading. As shown in figure 18, wortmannin treatment did in fact suppressed expression of p-AKT across all loadings with significantly lower for unloaded (p-value < 0.0001 for DWU vs DU), CT (p-value < 0.0001 for DWCT vs DCT) and CTS (p-value < 0.0001 for DWCTS vs DCTS). In addition, significantly reduced expression of p-AKT was also observed for InsW treatment for unloaded (p-value < 0.0001 for DWIU vs DU), CT (p-value < 0.0001 for DWICT vs DCT) and CTS (p-value < 0.0001 for DWICTS vs DCTS). These results indicate that 100 nM wortmannin treatment did reduce expression of p-AKT significantly across all loadings.

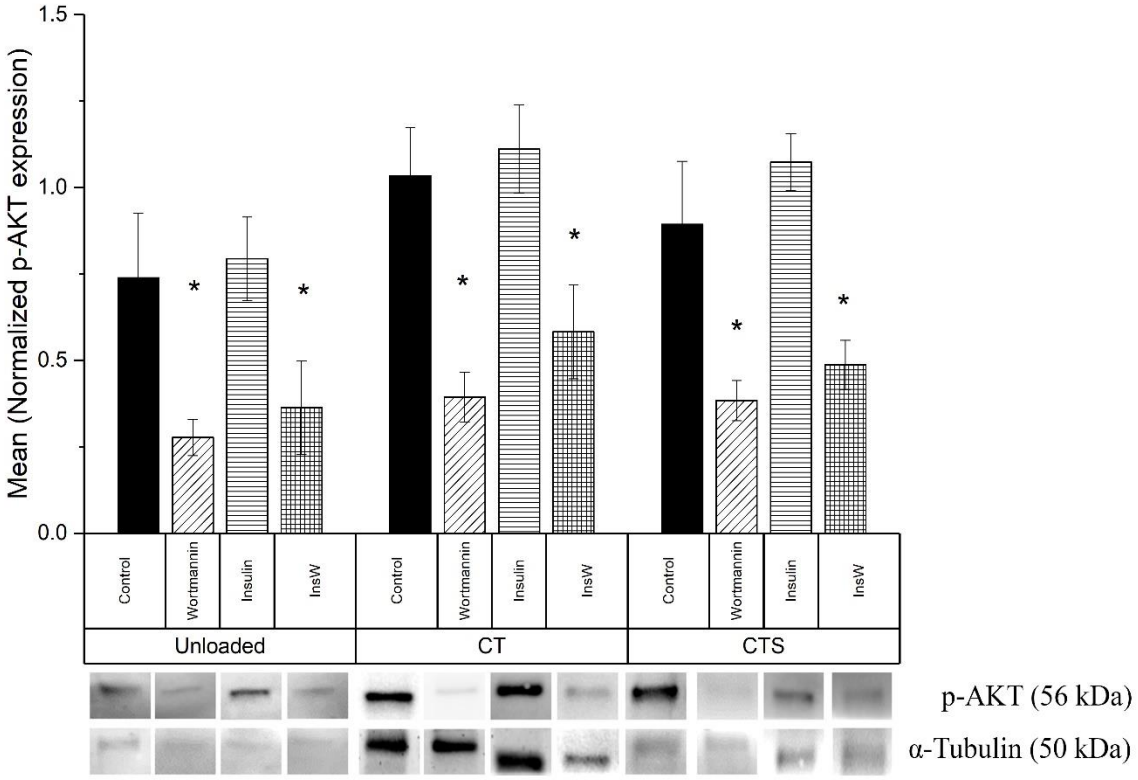

Figure 18: *Treatment-wise p-AKT expression normalized to α-Tubulin expression within each mechanical loading; Values represented as Mean ± SD for every treatment (n=6 for each). '*' represents statistical significance (p-value < 0.05) in comparison to 'control or DMSO' for every loading with one-way ANOVA and Tukey's HSD post-hoc comparison.*

Expression of p-ERK ½ were compared as a direct marker of cellular proliferation (Figure 19). ERK-1/2 phosphorylation is known to occur during cell cycle progression and cellular proliferation both of which are indirect indicators of phenotypic modulation. From figure 19, it can be observed that the insulin treatment led to a greater expression of phosphorylated p-ERK ½ for unloaded (p-value < 0.0001 for DIU vs DU), CT (p-value < 0.0001 for DICT vs DCT) and CTS (p-value < 0.0001 for DICTS vs DCTS). Similar results were observed for InsW treatment where significantly greater expression of p-ERK ½ was observed for unloaded (p-value < 0.0001 for DWIU vs DU),

CT (p-value < 0.0001 for DWICT vs DCT) and CTS (p-value < 0.0001 for DWCTS vs DCTS). With wortmannin treatment, expression of p-ERK ½ was not significantly different, independent of mechanical loading. This effect is further confirmed when comparing InsW and insulin treatment under CTS loading where insulin treatment led to significantly greater expression of p-ERK ½ in comparison to InsW treatment (p-value < 0.0001 for DICTS vs DWICTS).

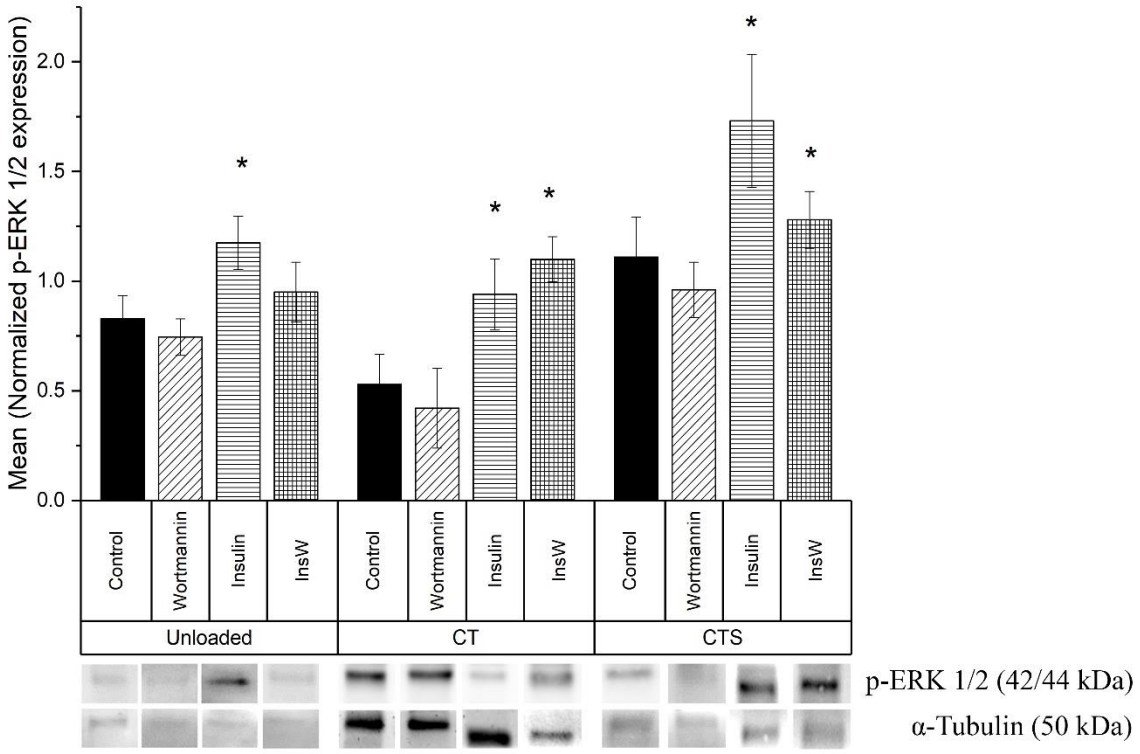

Figure 19: *Treatment-wise p-ERK 1/2 expression normalized to α-Tubulin expression within each mechanical loading; Values represented as Mean ± SD for every treatment (n=6 for each). '*' represents statistical significance (p-value < 0.05) in comparison to 'control or DMSO' for every loading with one-way ANOVA and Tukey's HSD post-hoc comparison.*

Overall results from this investigation are summarized in table 7 and demonstrate that inducing selective-insulin-resistance did not alter the phenotypic state of RASMCs significantly whereas insulin administration resulted in greater phenotypic modulation of RASMCs and much greater for insulin administration under clinically relevant mechanical loading conditions of cyclic strain and

low wall-shear stress as evidenced from greater number of cells in G2/M and S-phase of the cell cycle, greater apoptosis, reduced expression of contractile-state associated markers and greater expression of phosphorylated ERK-1/2. Combination of wortmannin with insulin administration did not result in significant changes in comparison to insulin groups. Thus, these results indicate a pro-proliferative/greater phenotypic modulation in RASMCs under clinically relevant mechanical loading when supplemented with insulin, while selective insulin-resistance did not influence proliferation or phenotypic modulation of RASMCs under these conditions.

Table 7: *Summary of all treatment and loading-wise comparison where each respective row represents a group ('Group' column) within treatments. Results represented were compared to the treatment-control (DMSO) for its respective mechanical loading (Unloaded or CT or CTS).*

Treatment	**Cell Cycle**	**TUNEL**	**Area**	**Aspect Ratio**	**Actin**	**SM22α**	**p-ERK 1/2**	**p-AKT**	**Group**
DMSO + Wortmannin (100 nM)		*		*	*			*	DWU
				*				*	DWCT
					*			*	DWCTS
DMSO + Insulin (10 ng/mL)	*	*			*	*	*		DIU
	*	*	*		*	*	*		DICT
	*	*	*	*	*	*	*		DICTS
DMSO + Wortmannin (100 nM) + Insulin (10 ng/mL)				*	*	*		*	DWIU
	*	*	*			*	*	*	DWICT
	*	*	*	*		*	*	*	DWICTS

3.4: Discussion

Clinical investigations have consistently demonstrated insulin administration a risk factor for developing in-stent restenosis (ISR) following angioplasty (199) for bare metal stents (91) and first (200) and second-generation drug eluting stents (102,106). Although the exact mechanisms resulting in greater neointimal hyperplasia in diabetic patients remains unclear, diabetes itself represents the most significant predictor of developing ISR owing to multiple co-existing complications such as hyperglycemia, insulin resistance, insulin administration, elevated triglyceride levels, hypertension, each resulting in significantly greater proliferation of vascular smooth muscle cells (201).

Previously we have demonstrated that chronic high glucose resulted in greater proliferation and phenotypic modulation of RASMCs under dynamic loading as compared to low glucose controls (192). Clinically, diabetic patients are afflicted with insulin resistance and may require insulin administration (202). In the current study, we investigated if clinically relevant insulin administration (10 ng/mL) and selective partial insulin resistance (wortmannin 100 nM) influenced dedifferentiation and phenotypic modulation of RASMCs under dynamic loading. We hypothesized that insulin administration will promote proliferation and dedifferentiation of chronic-high glucose acclimated RASMC and this effect will be magnified in case of induced insulin-resistance. In order to ensure that cellular passaging did not interfere with dedifferentiation of cells, we strictly employed passage 4 RASMCs for all the experiments in the study. Effects of combined mechanical loading with cyclic strain and low wall-shear stress under insulin administration and selective insulin-resistance have not been explored by others to our knowledge. This study was aimed at capturing cellular response for diabetes-specific conditions more accurately than conventional static/unloaded conditions using clinically relevant mechanical forces.

The process of cellular proliferation is governed by the progression of the cell and its components through the process of cell-cycle whereby, cells under non-proliferative or quiescent-state remain in the G1/G0 phase and do not pass this checkpoint. However, under the influence of proliferative triggers, cascade of molecules are activated, consequently moving to subsequent phases of S and then G2/M (203). Cell-cycle analysis using flow-cytometry revealed that the administration of insulin to chronic high-glucose acclimated cells resulted in a significantly lower percentage of cells in the G1/G0 phase (p-value < 0.0001 for DMSO control vs insulin across all loadings and concurrently greater percentage of cells in the S-phase (p-value < 0.0001 for DMSO control vs insulin across all loading) and the G2/M-phase (p-value < 0.0001 for DMSO control vs insulin across all loading) indicative of a proliferative response independent of mechanical loading. However, insulin administration associated low shear-stress and physiologically relevant circumferential strain observed locally after stent implantation resulted in significantly greater % cells in the G2/M-phase in comparison to cyclic-tensile loading. This observation is indicative of the significance of low shear-stress on cellular-response (p-value < 0.0001 for DICTS vs DICT). The current results support previously published work by others where insulin has been demonstrated to exert pro-proliferative effects on VSMCs (141,188,204) with greater neointimal hyperplasia (15,32) with clinical evidence (70,107). Induction of selective insulin-resistance by incubating cells with 100 nM wortmannin did not significantly alter %cells in the G1/G0,S or G2/M phase for all loadings indicating that further exploration of pathways is required before AKT phosphorylation can be leveraged to mimic insulin-resistance at the cellular level in RASMCs while subjected to clinically relevant circumferential strain and low wall-shear stress. In fact, in this study, inhibiting AKT phosphorylation with wortmannin did not influence cell-cycle progression of chronic high glucose acclimated RASMCs. These observations are further supported by non-

significant difference in cell-cycle progression due to InsW treatment in comparison to insulin treatment.

In order to evaluate the impact of treatments on induction of apoptosis, cells were analyzed for TUNEL expression using flow-cytometric assay. Application of mechanical forces has been previously reported to induces apoptosis in RASMCs (205). Our results are consistent with these observations where circumferential strain led to a significantly greater % TUNEL-positive cells in addition to higher % TUNEL-positive cells for concomitant strain and low shear stress. insulin administration led to lower apoptosis in comparison to DMSO controls under mechanical loading thus indicating pro-survival effect of insulin on RASMCs. Previous animal studies and in vitro investigations have demonstrated a pro-survival effect of insulin where insulin treatment led to a significant reduction in cells undergoing apoptosis (206). In the current investigation as well, insulin administration resulted in reduced apoptosis during unloaded conditions however this effect was not extended to CT or CTS loading hence underscoring the importance of mechanical loading. In contrast, wortmannin treatment resulted in significantly greater % TUNEL-positive cells for unloaded, CT and CTS thus, indicating pro-apoptotic effect of inhibiting AKT-phosphorylation. These results have been confirmed in previous investigation where wortmannin treatment was observed to promote apoptosis in VSMCs in vitro (206) and due to similar mechanical loading (192). Further, similar results were observed for InsW treatment where significantly greater % TUNEL-positive cells were observed across all loadings, in comparison to DMSO controls. However, these results were not significantly different than wortmannin treatment demonstrating lower efficacy of insulin in control apoptosis during partially insulin resistant state.

Cell-area and aspect ratio (major axis length to minor axis length) are indirect indicators of cellular hypertrophy where a hypertrophic response is estimated by greater cellular area and correspondingly lowered aspect ratio. Within the phenotypic continuum, VSMCs exhibit different

morphologies depending upon their differentiated state with contractile-state is associated with longer and narrower cells resulting in lower cell area and higher aspect ratio and synthetic-state is associated with greater cell area and lower aspect ratio (207). In the current investigation, insulin administration resulted in significantly greater cell-area and correspondingly lower aspect ratio for chronic high glucose acclimated cells subjected to physiological strain and low shear stress in comparison to DMSO controls (p-value < 0.0001 for DICTS vs DCTS). Using other indicators, previous investigations with insulin administration have demonstrated insulin to induce cardiac hypertrophy in animal models (208) and in vitro investigations with VSMCs (209). In addition, previous studies have also demonstrated a reduced hypertrophic response to physiologically relevant strain and application of low shear stress to these conditions resulted in greater hypertrophy (192,210). These results are in agreement with the current observation and provided investigational validation to our results. Wortmannin treatment did not significantly alter cell area or aspect ratio in the absence of insulin across all loading conditions and these results are consistent with previously reported results. Further non-significant differences between InsW and insulin treatment indicate that inhibiting phosphorylation of AKT may not influence cell area or aspect ratio.

Expression of contractile-state associated protein markers are a direct estimate of VSMC differentiation of the phenotypic continuum. In the current study, we investigated the expression of αSM actin and SM22α which are predominantly observed in the contractile phenotype of RASMCs and with dedifferentiation to a synthetic state, their expression is reduced. Administration of insulin resulted in a significantly reduced expression of αSM actin for unloaded (p-value < 0.0001 for DIU vs DU), CT (p-value < 0.0001 for DICT vs DCT) and CTS loading (p-value < 0.0001 for DICTS vs DCTS) in comparison to DMSO controls thus indicating greater phenotypic dedifferentiation of RASMCs due to insulin administration. Wortmannin treatment on the contrary resulted in greater significantly greater expression of αSM actin in comparison to DMSO controls for unloaded (p-

value < 0.0001 for DWU vs DU) and CTS loading (p-value < 0.0001 for DWCTS vs DCTS) indicative of relatively greater contractile-phenotype under these conditions. In addition, InsW treatment resulted in significantly reduced expression of actin in comparison to wortmannin treatment but were not significantly different than insulin treatment across all loadings. In agreement with αSM-Actin results, SM22α expression results also indicate a pro synthetic-state effect of insulin administration while a protective effect of wortmannin treatment with non-significant differences between InsW and insulin treatment. These results demonstrate insulin to be primarily responsible in inducing a synthetic state phenotype in chronic high glucose acclimated RASMCs independent of wortmannin treatment. Physiologically relevant circumferential strain has been reported to promote a contractile phenotype with greater expression of actin (183) whereas application of low shear stress in addition to physiological strain reduced the expression of contractile-state associate markers (210). Our results agree with previous cellular studies where a similar response of mechanical loading on actin expression has been reported. Cells isolated from neointimal lesions of diabetic animals requiring insulin administration and human arterial cells from diabetic patients have been reported to exhibit reduced expression of contractile state associated markers (176,211,212). In the current investigation, selectively inhibiting expression of p-AKT to induce experimental insulin resistance did not result in a significant difference in actin expression. This necessitates further investigation in deciphering the role of AKT inhibition in regulating contractile-state markers in smooth muscle cells.

Expression levels of p-AKT were evaluated to confirm if wortmannin treatment resulted in partial inhibition of AKT-phosphorylation. Wortmannin (100 nM) has been reported to irreversibly inhibit over 95% phosphorylation of AKT with small incubation times and was primarily the reason of selection (212). Treatment of chronic high glucose acclimated RASMCs with 100 nM of wortmannin significantly reduced the expression of p-AKT across all loadings with or without

insulin administration, in the current investigation. Although the wortmannin did not completely inhibit p-AKT expression, marked reduction in the expression levels were acceptable for the current exploratory model since they were significantly lower than the control treatment ($p < 0.0001$ for control vs wortmannin across all loadings).

VSMCs have been previously demonstrated to result in greater phosphorylation of ERK ½ proteins when undergoing cellular proliferation (212). Thus, in addition to cell-cycle progression, greater expression of these markers indicates a proliferative cellular-response. In the current investigation, insulin administration resulted in greater expression of p-ERK ½ markers for unloaded, CT and CTS loadings in comparison to DMSO controls. Wortmannin treatment however did not alter p-ERK ½ expression significantly under any loading in comparison to controls. Similar to insulin treatment, InsW treatment also resulted in significantly greater expression of p-ERK ½ across all loading conditions. Previously, in vitro studies have demonstrated that VSMCs undergoing proliferation exhibit greater phosphorylation of ERK ½ (212) and our results are in agreement with these observations further indicating that insulin exerts a pro-proliferative response on chronic high glucose acclimated RASMCs.

The currently proposed model successfully captures cellular-response under clinically relevant mechanical loading (0-7%) and implant associated low wall-shear stress (~ 0.3 dynes.cm^{-2}) in combination with diabetes-specific complications of chronic high-glucose acclimation (25 mM) and insulin administration (10 ng/mL). Physiologically, cells VSMCs area subjected to circumferential strain owing to pulsatile nature of blood-flow and also experience direct flow shear stress due to barotrauma from PCI, which results in endothelial damages and exposes the underlying smooth muscle cells to flow. Cellular-response under these conditions captures the clinically relevant-VSMC response more accurately than conventional static/unloaded conditions for diabetic patients implanted with arterial stents and requiring insulin administration. With the

proposed model, we have successfully shown that insulin administration has pro-proliferative effect on VSMCs and results in greater phenotypic modulation of chronic high glucose acclimated RASMCs under dynamic loading conditions.

3.5: Conclusion

Our experimental approach successfully integrates mechanical forces observed in a stented blood vessel with diabetic patient-related conditions such as chronic high glucose with insulin administration in vitro. Cellular-response under these conditions has not been performed previously despite clinical relevancy and demonstrates the need to model cellular behavior under disease-associated conditions to further improve prognosis of percutaneous interventional approaches. Chronic high-glucose acclimated passage 4 RASMCs were subjected to dynamic mechanical loading comprising of cyclic-tensile strain and low wall-shear stress under diabetes associated insulin administration and selective insulin resistance. Results underscore the relevance of subjecting mechanosensitive cells to dynamic loading and the current investigation successfully combines physiological circumferential strain with implant associated low wall-shear stress under patient-specific metabolic complications. The exploratory approach of incorporating selective insulin resistance with wortmannin did not alter smooth muscle cell-phenotype thus, necessitating further investigation into the potential role of AKT pathway. It was successfully demonstrated that insulin exerts a pro-proliferative dedifferentiation of RASMCs to a relatively greater synthetic-state, as evidenced by reduced expression of contractile-state associated protein markers (αSM actin and SM22α) and conformity of current results with previous studies and clinical evidence of exaggerated restenosis in insulin requiring patients validate our diabetic model. Greater phenotypic modulation of VSMCs under these patient-specific conditions could serve as targets for

optimization of clinical treatment for diabetic patients. Future investigations should focus on exploring the exact mechanisms involved in mediating greater phenotypic modulation of VSMCs under these conditions. In addition, other patient-specific risk factors or complications can be combined on this platform to further understand cellular-response under complex clinical conditions. VSMCs acclimated to chronic high glucose (25 mM D-Glucose for 4-5 weeks) and subjected 0-7% cyclic strain with low wall-shear stress (~0.3 dynes cm^{-2}) under physiologically relevant insulin administration (10 ng/mL) demonstrated a more accurate and representative response as compared to conventional static cultures.

Chapter 4: "Development and characterization of hypertensive-diabetic cellular response evaluation model for restenosis"

Purpose: Current study explores the influence of hypertension-associated elevated mechanical loading combined with stent-associated low wall-shear stress on phenotypic modulation of RASMCs under diabetes specific chronic high-glucose and insulin administration to propose an in vitro diabetic-hypertensive cell-response model. As an application, efficacy of sirolimus in controlling dedifferentiation of RASMCs under hypertensive loading and insulin treatment was evaluated.

Methods: Passage 4 RASMCs cultured in high-glucose medium were subjected to physiological cyclic-tensile with low shear stress (NTS) and hypertensive-tensile with low shear stress (HTS) to evaluate the influence of elevated mechanical strain on vascular smooth muscle cell-phenotype. Cells were evaluated for their distribution within the cell-cycle, percentage of cells undergoing apoptosis, estimation of cellular hypertrophy by comparing cell-area and aspect ratio, comparison of protein expression – αSM actin and SM22α (contractile-state markers); p-ERK ½ (proliferation marker); Hsp47 (collagen marker). All measurements were compared using one-way ANOVA with Tukey's HSD as a post-hoc test.

Results: Subjecting cells to hypertension-associated elevated mechanical strain with low shear (HTS) resulted in significantly greater % cells in the G2/M ($p < 0.0001$) and S-phase ($p < 0.0001$) of the cell-cycle indicating a pro-proliferative effect in comparison to normotensive controls (NTS) for all treatments. This effect was augmented with insulin administration as demonstrated by significantly greater % cells in the G2/M phase for insulin ($p < 0.0001$ for HITS vs HTS). In addition, subjecting cells to elevated mechanical strain resulted in significantly greater induction of apoptosis for all treatments ($p < 0.0001$ for HTS vs NTS; HITS vs NITS) while insulin

administration did not influence apoptosis. Hypertensive loading also resulted in greater dedifferentiation of cells as indicated by significantly reduced expression of contractile-state associated proteins – αSM-actin and SM22α ($p < 0.0001$ for HTS vs NTS; HITS vs NITS) with lesser expression with insulin ($p < 0.0001$ for HITS vs NITS). Greater proliferation was further confirmed by significantly higher expression of p-ERK ½ in response to elevated mechanical loading ($p < 0.0001$ for HTS vs NTS; HITS vs NITS) which was significantly augmented by insulin administration ($p < 0.0001$ for HITS vs HTS). Treatment of cells under diseased associated conditions with 10 ng/mL sirolimus demonstrated a significantly regulated cellular-response however, insulin administration still demonstrated greater pro-proliferative response in conjunction with relatively greater phenotypic modulation in comparison to controls.

Conclusion:

In the current investigation, we successfully combined two clinically relevant patient-specific risk factors to subject chronic high-glucose acclimated rat aortic smooth muscle cells to complications-associated with diabetes and hypertension under altered hemodynamics associated with stent-implantation. This in vitro diabetic-hypertensive cellular-response evaluation concept model can be used in future, to investigate the efficacy of novel drugs and identification of novel therapeutic targets aimed at reducing in-stent restenosis in diabetic-hypertensive patients, prior to pre-clinical evaluation.

4.1: Introduction:

Clinically, hypertension is a known patient-specific risk associated with poorer prognosis of percutaneous coronary intervention (PCI) with studies indicating hypertension to be significantly associated with restenosis (156). In addition, higher rates of myocardial infarction have been reported in patients afflicted with diabetes and hypertension ultimately suggesting poorer prognosis of percutaneous coronary intervention (PCI) in these patients (213). A direct outcome of hypertension is elevated cyclic mechanical strain with almost two-fold increase (15-30%) in circumferential strain on the arterial wall (214,215).

Elevated mechanical strain has been shown to promote synthetic-phenotype in vascular smooth muscle cells (216–218) and have been previously documented to exhibit reduced expression of contractile-state markers alongside elevated cell-proliferation (219–221) and apoptosis (222–225). Animal models of hypertension have been reported to exhibit greater neointimal hyperplasia in response to PCI and hypertension is a clinical predictor of target vessel revascularization (226) and contributor to the development of neointimal hyperplasia (227). Cellular-response under hypertension associated conditions has been well characterized by others (222,228,229) however, characterization of cellular-response under elevated mechanical stain and diabetes-associated chronic high glucose and insulin administration have not been reported previously in addition to the non-availability to test platforms capable of combining all these patient-related complications.

In our previous investigations we have successfully demonstrated the influence of diabetes associated chronic high glucose alone (192) and in combination with insulin administration (previous chapter) on dedifferentiation of rat aortic smooth muscle cells (RASMCs) under dynamic loading of physiologically relevant circumferential strain and stent-implant associated low wall-shear-stress. At the clinical level, patients afflicted with diabetes also suffer from hypertension in

a majority of cases however, due to inability of clinical studies to discern individual effects of these complications, cellular-response during these patient-specific complications have not been evaluated.

In the current investigation, we combined diabetes-associated chronic high glucose and insulin administration with dynamic loading of hypertension-associated elevated mechanical strain and stent-associated low wall-shear stress to capture the cellular-response under these clinically relevant conditions more accurately and conceptualize an in vitro cell-response diabetic-hypertensive model. As an application of this model, we evaluated the efficacy of sirolimus, a commonly employed in drug-eluting stents, to investigate if these patient-specific complications altered sirolimus' capacity to regulate and control phenotypic modulation of VSMCs. We hypothesize that elevated mechanical strain with low-shear stress will result in greater dedifferentiation of RASMCs and insulin administration will augment this effect. In addition, due to greater proliferative effect of these patient-specific risk factors, equimolar concentration of sirolimus will result in poor regulation of VSMC phenotype.

For this investigation, we compared the results of hypertensive loading with previously reported results of insulin administration under normal circumferential loading with low shear stress and have been labeled as normotensive-tensile-shear (NTS) or normotensive-tensile-shear with insulin (NICTS) wherever required (previous chapter - DCTS and DICTS). In future, the currently proposed model will be extremely useful in exploring molecular mechanisms involved in regulating the cellular response under multiple patient-specific complications such as hypertension and diabetes and can serve as an In-vitro test platform to evaluate the efficacy of novel molecular therapies aimed at reducing In-stent restenosis in diabetic patients afflicted with hypertension and requiring insulin administration prior to pre-clinical investigations.

4.2: Materials and Methods:

4.2a. Isolation of rat aortic smooth muscle cells: Isolation of rat aortic smooth muscle cells: Rat aortas were harvested from 9-10 weeks old female Sprague-Dawley^{TM} rats using a modified version of a previously published protocol (193) and was approved by Clemson University Institutional Animal Care and Use Committee (IACUC). Briefly, aorta isolated from rat, was transferred back to the laboratory and immediately rinsed with 1x sterile Dulbecco's phosphate buffered solution (DPBS; Cellergo, 21-031-CV) at 37 ^{0}C for 1-2 minutes in order to remove blood clots and any unwanted tissue. Aorta were subsequently treated with Collagenase type-II (300U/mL, Worthington 4176) in sterile Dulbecco's modified essential medium (DMEM with 25 mM D-Glucose; Corning 10-013-CM) for 12-15 minutes to enable enzymatic degradation of the adventitial layer. Subsequently, using straight and angular forceps, tears in the adventitial layer were created to facilitate its easy removal. After successfully removing the adventitial layer, aorta was split open along its longitudinal axis thus, allowing easy scraping on the luminal side to remove the endothelial monolayer. Multiple 1x DPBS rinses were performed to ensure removal of any loose cells and tissue after which, aorta was chopped into small sections (about 1mm^2) and subjected to another enzymatic digestion containing type I collagenase - 10mg/mL, elastase (10 U/mL, Worthington 2292) treatment for 3-4 hours under gentle shaking conditions at 37 ^{0}C thus allowing complete dissolution of the extracellular matrix of the medial layer. At the end of enzymatic digestions, the suspension was centrifuged and cells were transferred to T-25 flasks in DMEM (containing 25 mM D-Glucose) supplemented with 10% fetal bovine serum (FBS; Corning 35-010-CV) and 1% Antibiotic-Antimycotic agent (Penicillin/Streptomycin; Cellgro 30-004-CI). The primary cell line was incubated for about a week before passaging and subsequent passaging was performed every two weeks until passage 4. Cells were recruited at passage 4 for all experiments, in order to remove any passage-associated variability.

4.2b. Preparation of silicone membranes and Cell seeding: *:* Two baseplates were used providing a total sample size of 6 test specimens per experiment, as described previously (192). Biomedical-grade silicone membrane of 0.015-inch thickness (0.15" NRV G/G 40D, Specialty Manufacturing Inc., MI) were cut to fit the custom cell-culture assembly (Figure 6a) which were coated with type 1 collagen using Teflon ring (2.75 cm^2 inner cross-sectional area and 1.2 cm height) centered on the silicone surface exactly above the loading post (Figure 6b). To minimize friction between the loading post and the silicone membrane, 0.2 ml of silicone lubricant (Loctite, 51360) was distributed evenly on the loading-post under aseptic conditions.

The simulator design enables user to accommodate three of such assemblies on each baseplate (3 loading stations per baseplate) and with two baseplates it provides a total sample size of 6 test specimens. System sterilization is performed by subjecting baseplate to an overnight UV treatment whereas all detachable parts are autoclaved. Each sandwich assembly was placed on a loading post with 0.2 cc of silicone lubricant (Loctite, 51360) distributed evenly in between. Sterile Teflon rings (2.75 cm^2 inner cross-sectional area and 1.2 cm height) were then centered on the silicone surface exactly above the loading post. The surface area confined by the Teflon ring was coated with collagen type-I (Advanced Biomatrix, 5005B) at a final concentration of 50 µg/mL using deionized water.

Passage 4 VSMCs cultured in media containing 25 mM D-Glucose were trypsinized (Corning, 25-050-CI) and counted using scepter cell-counter (Millipore, PHCC00000) and seeded at a density of 3.6 x 10^4 cells/cm^2 or 100,000 cells per well/loading station and allowed to attach and spread for 36 hours in cell culture media containing 10% FBS, 1% Ab/Am and 25 mM dimethyl sulfoxide (DMSO). After 36 hours, media was changed to DMEM containing 1% FBS, 1% Ab/m and 1%

Dextran (Sigma, 9004-54-0) to induce quiescence and adjust media viscosity respectively. Cells were subjected to media supplemented with 10 ng/mL insulin (Sigma, I0516) during induction of quiescence and mechanical loading to represent insulin administration and to represent sirolimus treatment, cells were subjected to mechanical loading in media supplemented with 10 ng/mL sirolimus dissolved in DMSO (Table 8). Exact concentration of sirolimus in the vasculature is not properly defined however, previous investigations with sirolimus-eluting stents have demonstrated sirolimus concentrations in the blood to fall within range after deployment in animal models (230). Final concentration of DMSO was 25 mM in all treatments to normalize any effect. Upon completion for every loading condition for each respective treatment, cells were rinsed with sterile 1x DPBS for 1-2 minutes and were subsequently detached using 1mL/well of trypsin-EDTA treatment and assayed.

Table 8 *– Treatments and loading conditions*

Treatment / ***Loading***	***Normotensive-strain Shear* (NTS)** *(0-7 % cyclic strain, 0.5 Hz for 24 hours with shear from flow ~ 0.3 dynes.cm^{-2})*	***Hypertensive-strain Shear* (HTS)** *(0-15 % cyclic strain, 0.5 Hz for 24 hours with shear from flow ~ 0.3 dynes.cm^{-2})*
DMSO Control (D)	**NTS:** Cells in media containing 25 mM DMSO during seeding (36 hours), induction of quiescence (24 hours) and normotensive-loading (24 hours) *(Previous chapter)*	**HTS:** Cells in media containing 25 mM DMSO during seeding (36 hours), induction of quiescence (24 hours) and hypertensive-loading (24 hours).

DMSO + 10 ng/mL Sirolimus (DS)	**NTSS:** Cells in media containing 25 mM DMSO during seeding (36 hours) and induction of quiescence (24 hours), 25 mM DMSO + 10 ng/mL sirolimus during normotensive-loading (24 hours).	**HTSS:** Cells in media containing 25 mM DMSO during seeding (36 hours) and induction of quiescence (24 hours), 25 mM DMSO + 10 ng/mL sirolimus during hypertensive-loading (24 hours).
DMSO + Insulin (10 ng/mL) (DI)	**NITS:** Cells in media containing 25 mM DMSO during seeding (36 hours), 25 mM DMSO + 10 ng/mL insulin during induction of quiescence (24 hours) and normotensive-loading (24 hours). *(Previous chapter)*	**HITS:** Cells in media containing 25 mM DMSO during seeding (36 hours), 25 mM DMSO + 10 ng/mL insulin during induction of quiescence (24 hours) and hypertensive-loading (24 hours).
DMSO + Insulin (10 ng/mL) + 10 ng/mL Sirolimus (DIS)	**NITSS:** Cells in media containing 25 mM DMSO during seeding (36 hours), 25 mM DMSO + 10 ng/mL insulin during induction of quiescence (24 hours); 25 mM DMSO + 10 ng/mL insulin + 10 ng/mL sirolimus during normotensive-loading (24 hours).	**HITSS:** Cells in media containing 25 mM DMSO during seeding (36 hours), 25 mM DMSO + 10 ng/mL insulin during induction of quiescence (24 hours); 25 mM DMSO + 10 ng/mL insulin + 10 ng/mL sirolimus during hypertensive-loading (24 hours).

4.2c. Mechanical Loading: Cells were subjected to either physiological tensile strain (0-7% at 0.5 Hz) and low wall-shear stress (NTS, ~0.30 dynes.cm^{-2}) or hypertensive tensile strain (0-15% at 0.5 Hz) and low wall-shear stress (HTS, ~0.30 dynes.cm^{-2}), with treatments and loadings summarized

in table 8. Cyclic strain was applied using FlexCell-3000^{TM} system (Flexcell International, NC) where shear stress was provided by externally supplied flow at 350 mL/min using a peristaltic pump (Cole-Parmer). All simulations were performed at 37 ^{0}C in an incubator (Fisher Scientific).

4.2d. Cell-cycle analysis: Cell cycle analysis was performed using propidium iodide staining method using the Guava cell-cycle flow cytometric assay (Millipore, 4500-0220). Briefly, cells were detached at the end of every simulation using trypsinized-EDTA and were centrifuged at 500x g for 5 minutes. Subsequently, cells were rinsed in 1x DPBS and re-centrifuged for 5 minutes at 500x g. Cells were redissolved in 200 µL of 1x DPBS and fixed in ice-cold 70% ethanol with gentle-intermittent shaking and stored at -20 ^{0}C for 48 hours at least. On the day of the assay, cells were removed from ethanol, rinsed in 1x DPBS and resuspended in 200 µL of guava cell-cycle reagent after which they were incubated in dark conditions for 30 minutes at room temperature. Finally, cells were assayed for their distribution within the cell cycle with Guava HT flow cytometer. For each sample, the threshold cellular count was set to 2000 events (195,196).

4.2e. Apoptosis analysis: Apoptotic analysis was performed using the TUNEL assay approach where cells undergoing apoptosis were incorporated with fluorescently labeled dUTP and subsequently assay for their intensity using Guava flow cytometer. Cells were detached and fixed in 70% ethanol similarly to cell-cycle analysis, for measuring apoptotic index for all treatments and on the day of the assay, cells were first incubated with a reaction mixture containing dUTP monomers for 1 hour and subsequently incubated with Anti-BrDU antibody, according to manufacturer's protocol (Millipore 4500-0121) (196).

4.2f. Cellular Hypertrophy: Measurement of cellular hypertrophy was performed as described previously (192). Briefly, cells after each treatment were fixed and permeabilized with 0.2% Triton X-100 in PBS following which cells were incubated with rhodamine-phalloidin (P1951, Sigma; 1:2000) and DAPI (1:2000) in PBS. Cells were imaged using fluorescent microscope (Digital inverted microscope, EVOS f1, AMG). For each sample, five to six random field-of-view were recorded and analyzed per sample, resulting in a total sample size of 180 per experimental group. Cell area (indicative of cellular hypertrophy) and aspect ratio (major axis length to minor axis length ratio) were measured using ImageJ software (NIH. Mean cell area (μm^2) & aspect ratio were measured and analyzed for a sample size of 180 per treatment (192).

4.2g. Protein extraction and Western blotting: Whole cell lysates were prepared from the cells at the end of each simulation using extraction buffer (20 mM Tris 1% SDS, 0.5% Triton and 10 µL/mL protease inhibitor cocktail, Sigma P 8340). Total protein concentration was calculated using BCA-assay kit (Life Technologies, 23225) using BSA know standards as described by manufacturer. SDS-PAGE was performed using Mini-PROTEAN TGX 10% precast-gels (BioRad 4561034). For each well, 10 µg of total protein was loaded using 5x loading buffer and electrophoresis was performed at 110 V for 90 minutes. Protein samples were subsequently transferred to PVDF membranes (BioRad 1620177) at 100V for 75 minutes under ice-cold conditions. Blots were blocked with 3% BSA in PBS and were probed with primary antibodies overnight at 4 ^{0}C (SM α-actin ab 119952, 1:500; SM-22α, ab10135 1:1500; α-tubulin, ab7291 1:1500; p-AKT 4060s Cell signaling technologies 1:1000; p-ERK ½ 4370s Cell signaling technologies 1:1000). Luminol was used as a chemiluminescence-substrate (Santa Cruz, SC-2048) reagent prior to blot-imaging. Densitometric analysis was performed using ImageJ software to quantify the amount of protein

expressed. Prior to analysis, all protein bands were normalized with α-tubulin, which was the loading control (192).

4.2h. Statistical analysis: Statistical Analysis was performed with One-way ANOVA and Tukey's HSD post hoc for all data sets with 0.05 level of significance ($\alpha = 0.05$). All tests were performed with JMP 12 pro and plots were created with OriginPro 2017.

4.3: Results:

4.3a. Cell-cycle analysis: In order to evaluate the effects of hypertensive mechanical loading and efficacy of sirolimus, cells were assayed using the Guava cell-cycle assay. Distribution of cells within the cell-cycle is shown in figure 20 with treatments in columns and mechanical loading in rows. Percentage of cells in all the cell-cycle phase are summarized in table 9.

Table 9: *Cell-cycle results for aim 2*

Loading	Treatment	% Cells in G1/G0-phase	% Cells in S-phase	% Cells in G2/M-phase	Sample
Normal	Control	78.41 ± 2.06	6.63 ± 1.07	11.95 ± 1.63	**NTS**
Hypertensive	Control	63.55 ± 3.62	5.46 ± 0.74	30.98 ± 4.08	**HTS**
Normal	Insulin	53.1 ± 3.560	9.43 ± 1.76	37.46 ± 2.25	**NITS**
Hypertensive	Insulin	45.95 ± 3.19	8.7 ± 1.94	35.35 ± 2.62	**HITS**
Normal	Control + Sirolimus	89.81 ± 5.11	7.05 ± 0.91	3.18 ± 0.69	**NTSS**
Hypertensive	Control + Sirolimus	77.45 ± 5.04	3.9 ± 0.94	18.64 ± 2.69	**HTSS**
Normal	Insulin + Sirolimus	69.67 ± 4.64	11.76 ± 2.58	28.56 ± 4.49	**NITSS**
Hypertensive	Insulin + Sirolimus	62.07 ± 4.56	7.15 ± 0.61	30.78 ± 1.20	**HITSS**

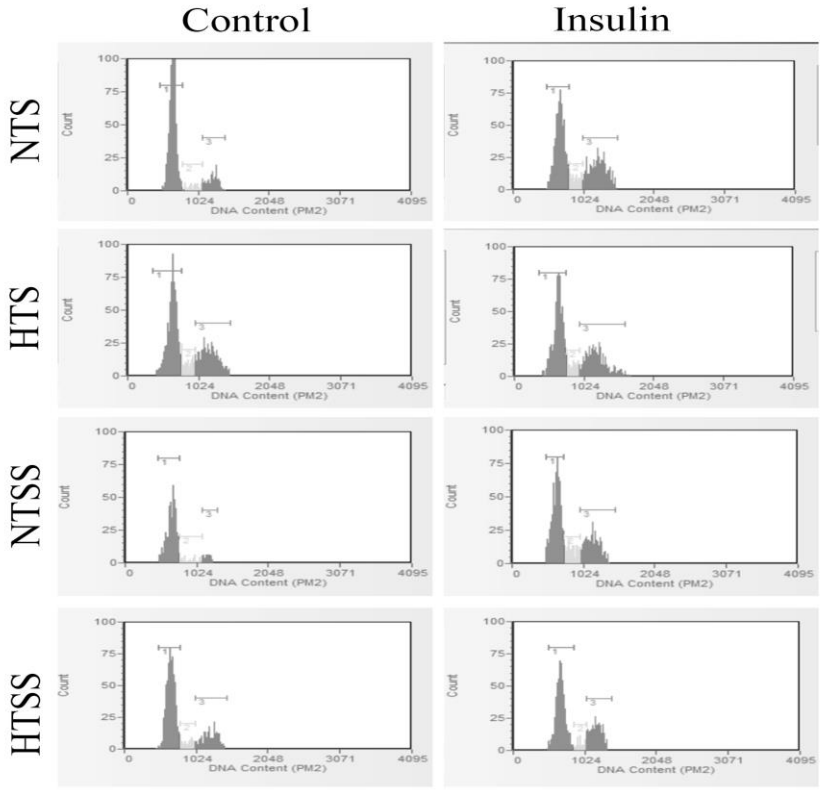

Figure 20: *Treatment and loading-wise cell-cycle distribution of cells. Each sample was assayed for 2000 cells. First peak represents % cells in the G1/G0 phase whereas second peak represents % cells in G2/M phase. All cells in between these two distinct peaks were categorized in the s-phase.*

From these results, it is evident that application of elevated mechanical strain (associated with hypertension) led to significantly reduced number of cells in the G1/G0 phase control (p-value <0.0001 for NTS vs HTS) as well as insulin (p-value <0.0001 for NITS vs HITS) whereas influence of insulin can be appreciated from even lower percentage of cells in the G1/G0 phase with insulin treatment under hypertensive loading (p-value < 0.0001 for NITS vs HITS). With administration of sirolimus, there was a significant increase in the percentage of cells in the G1/G0 phase across all treatments (p-value < 0.0001 for NTSS vs NTS; HTSS vs HTS; NITS vs NITSS; HITSS vs HITS) however, presence of insulin and application of elevated mechanical strain still resulted in significantly lower number of cells in the G1/G0 phase (p-value < 0.0001 for NTSS vs HTSS; NITSS vs HITSS) with insulin combined with hypertensive loading resulting in the lowest number of cells in the G1/G0 (Figure 21).

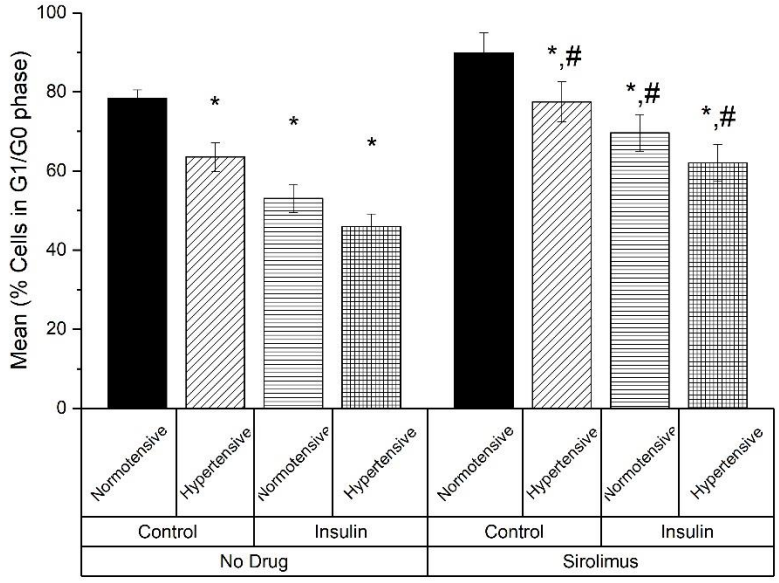

Figure 21: *Treatment-wise percentage of cells in the G1/G0 phase within each mechanical loading; Values represented as Mean ± SD for every treatment (n=6 for each). '*' represents statistical significance (p-value < 0.05) in comparison to respective normotensive control; '#' represents statistical significance (p-value < 0.05) in comparison to respective no-drug treatment.*

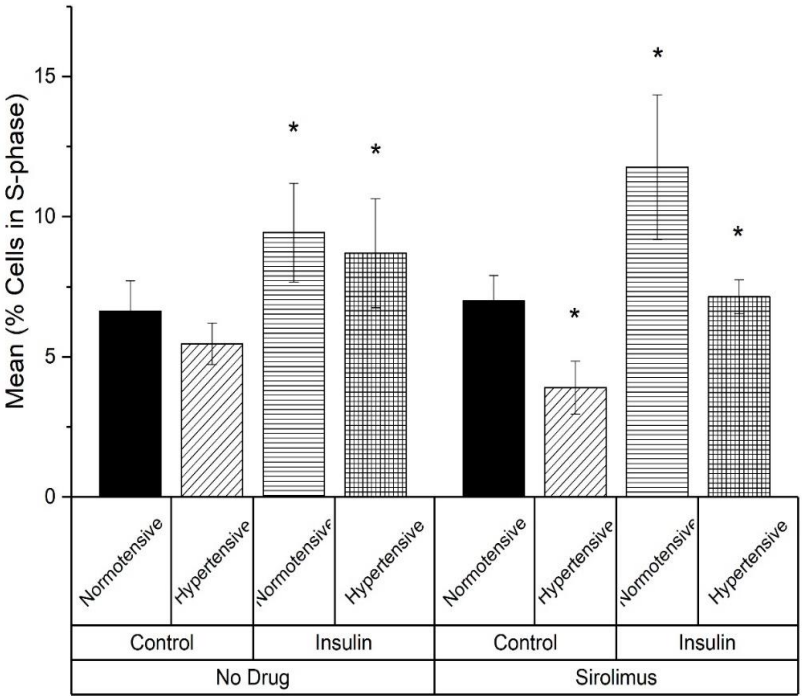

Figure 22*: Treatment-wise percentage of cells in the S-phase within each mechanical loading; Values represented as Mean ± SD for every treatment (n=6 for each). '*' represents statistical significance (p-value < 0.05) in comparison to respective normotensive control.*

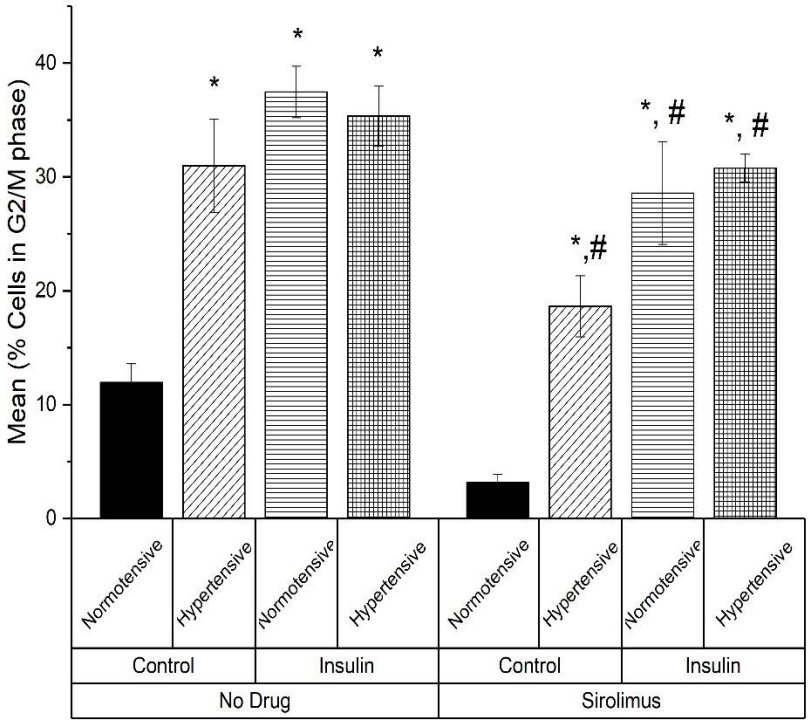

Figure 23: *Treatment-wise percentage of cells in the G2/M-phase within each mechanical loading; Values represented as Mean ± SD for every treatment (n=6 for each). '*' represents statistical significance (p-value < 0.05) in comparison to respective normotensive control; '#' represents statistical significance (p-value < 0.05) in comparison to respective no-drug treatment.*

Reduction in percentage of cells in the G1/G0 phase corresponded to increase in percentage of cells in the S (figure 22) and G2/M phases (figure 23). As evident from the results application of hypertensive mechanical strain resulted in significantly greater percentage of cells in the S-phase for both control (p-value < 0.0001 for NTS vs HTS) and insulin treatment (p-value < 0.0001 for NITS vs HITS) and significantly greater percentage of cells in the G2/M phase for both control (p-value < 0.0001 for NTS vs HTS) and insulin (p-value < 0.0001 for NITS vs HITS) treatment as well. Treatment of these groups with sirolimus markedly reduced the percentage of cells in the G2/M phase for all treatments and loadings (p-value < 0.0001 for NTSS vs NTS; NITSS vs NITS; HTSS vs HTS; HITSS vs HITS) however, differences in the S-phase were non-significant.

Collectively, these results indicate a pro-proliferative effect of elevated mechanical strain thus, indicating greater phenotypic modulation of RASMCs due to hypertension-associated mechanical forces. Further, in conformity with previously results (previous chapter), insulin treatment resulted

in greater percentage of cells in the G2/M phase. Combined with hypertensive-loading, insulin administration led to the lowest percentage of cells in the G1/G0 phase with corresponding increase in the G2/M phase consequently demonstrating a corroborating effect of both hypertensive-loading and insulin treatment.

4.3b. Apoptosis analysis: Cells undergoing apoptosis were estimated by measuring the percentage of cells stained positive for TUNEL staining with flow cytometric assay. Distribution of percentage of cells undergoing apoptosis is shown in figure 24. Percentage of cells undergoing apoptosis for each treatment are summarized in table 10. As evident from the results, (figure 25), insulin treatment resulted in significantly reduced number of cells undergoing apoptosis (p-value < 0.0001 for NITS vs NTS; HITS vs HTS). Hypertensive mechanical loading led to significantly greater number of cells undergoing apoptosis for both the control (p-value < 0.0001 for HTS vs NTS) and insulin (p-value < 0.0001 for HITS vs NITS). Supplementation of sirolimus reduced the overall number of cells undergoing apoptosis for both control (p-value < 0.0001 for NTSS vs NTS) and insulin (p-value < 0.0001 for NITSS vs NITS) under normotensive conditions as well as for both control (p-value < 0.0001 for HTSS vs HTS) and insulin (p-value < 0.0001 for HITSS vs HITS) treatments under hypertensive loading conditions.

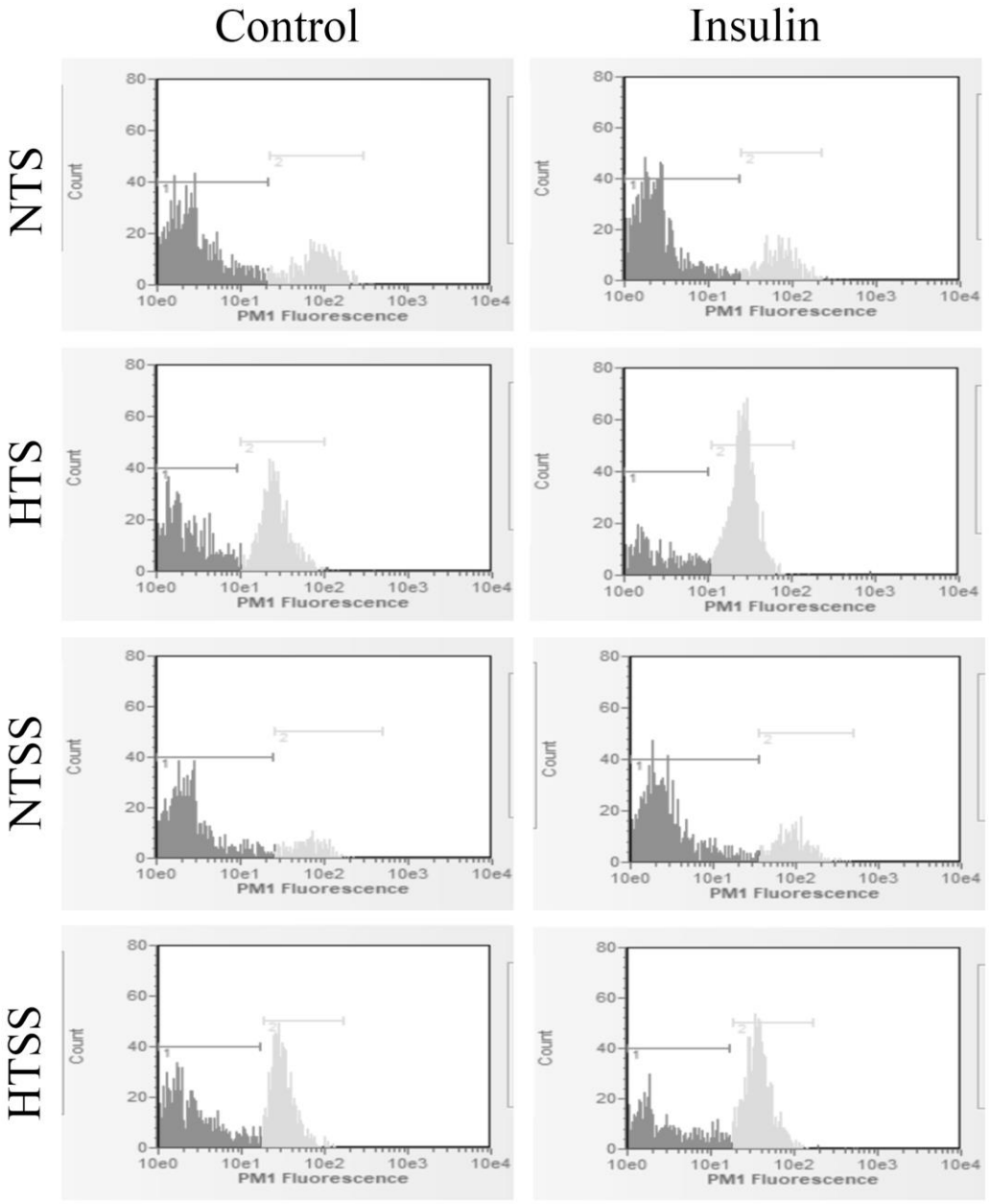

Figure 24: *Treatment and loading-wise TUNEL positive cell-distribution. Each sample was assayed for 2000 cells. First peak represents % cells in the negative for TUNEL statin whereas second peak represents % cells positive for TUNEL stain. All cells in between these two distinct peaks were categorized in the s-phase.*

Table 10: *TUNEL results for aim 2*

Loading	Treatment	% Apoptotic cells (Mean ± SD)	Sample
Normal	Control	29.12 ± 0.85	**NTS**
Hypertensive	Control	54.57 ± 1.01	**HTS**
Normal	Insulin	29.19 ± 2.49	**NITS**
Hypertensive	Insulin	77.49 ± 6.63	**HITS**
Normal	Control + Sirolimus	19.11 ± 3.40	**NTSS**
Hypertensive	Control + Sirolimus	46.56 ± 2.97	**HTSS**
Normal	Insulin + Sirolimus	22.07 ± 2.58	**NITSS**
Hypertensive	Insulin + Sirolimus	57.72 ± 2.56	**HITSS**

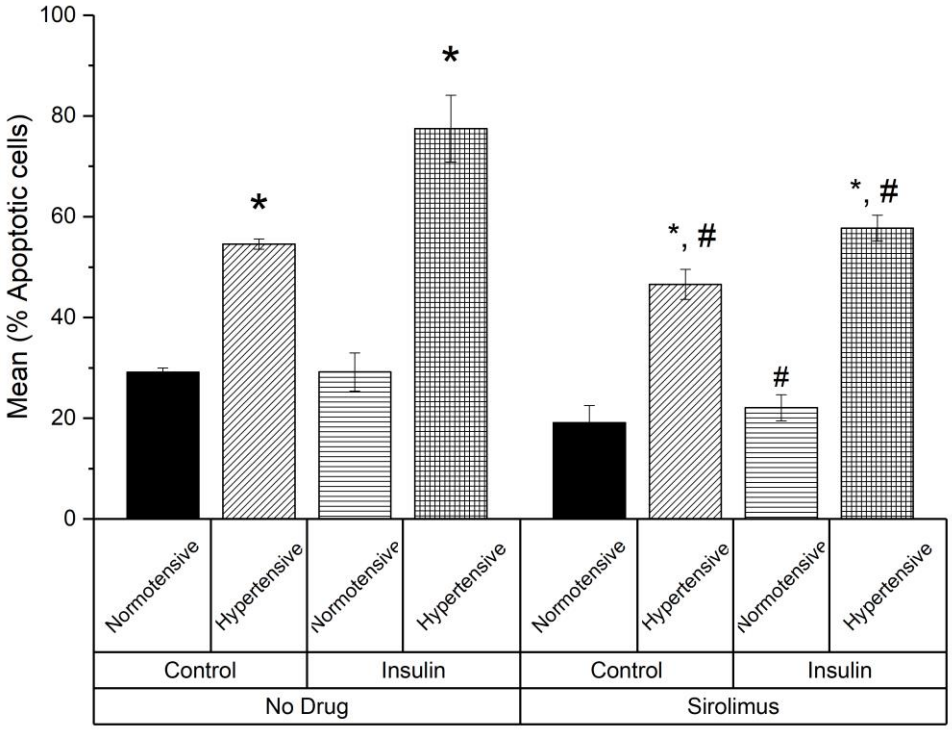

Figure 25: *Treatment-wise percentage of cells undergoing apoptosis within each mechanical loading; Values represented as Mean ± SD for every treatment (n=6 for each). '*' represents statistical significance (p-value < 0.05) in comparison to respective normotensive control; '#' represents statistical significance (p-value < 0.05) in comparison to respective no-drug treatment.*

4.3c. Hypertrophy analysis: RASMCs stained with rhodamine-phalloidin are shown in figure 26 and results for both cell-area and aspect-ratio are summarized in table 11. Cell area measurements were observed to be for NTS; for HTS; for NITS; for HITS; for NTSS; for HTSS; for NITSS; for HITSS.

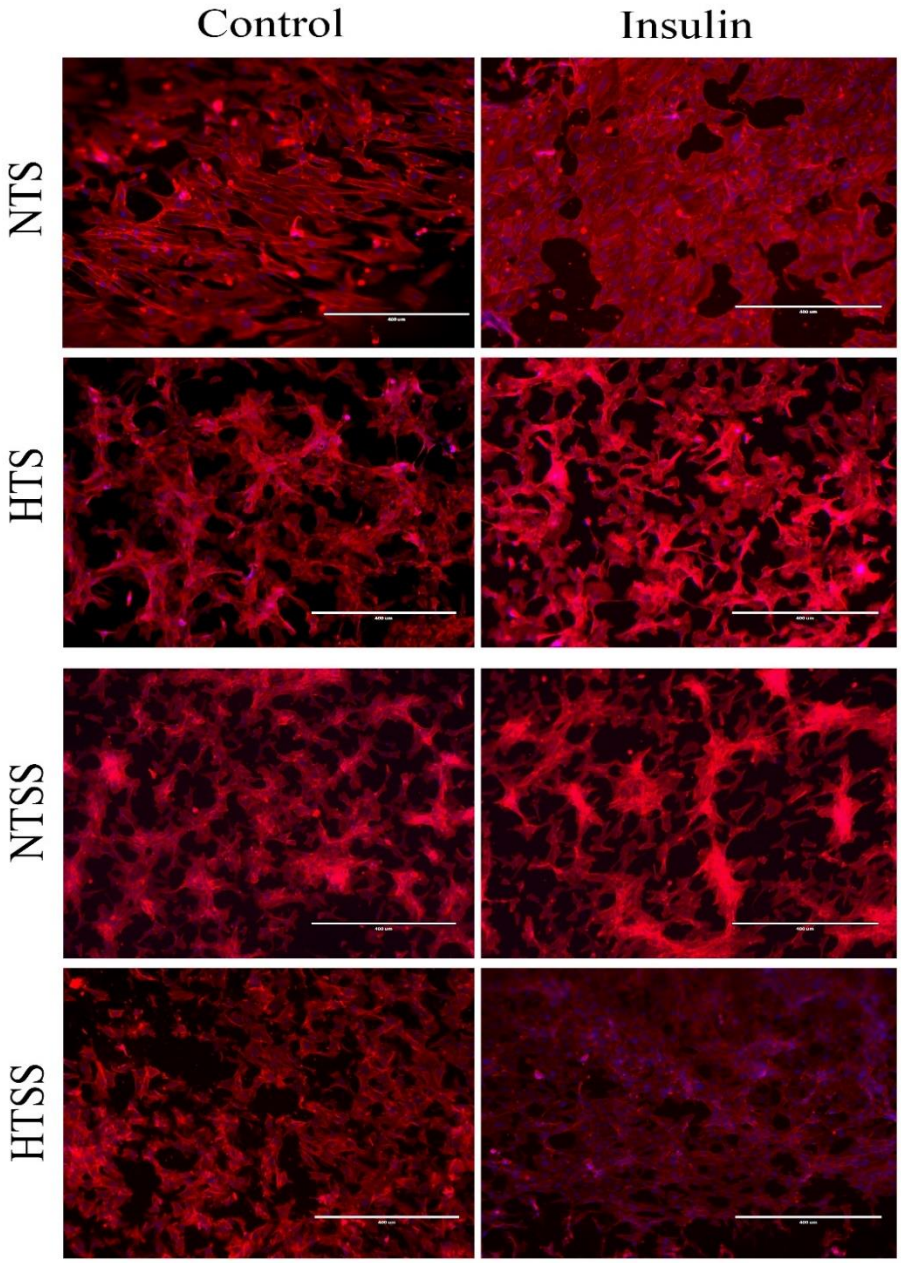

Figure 26: *Rhodamine-phalloidin stained images with treatments as rows and mechanical loadings as columns. Scale-bar 400 µm*

Table 11: *Cell-area and aspect-ratio results for aim 2*

Loading	Treatment	Cell Area (sq.µm) Mean ± SD	Aspect Ratio Mean ± SD	Sample
Normal	Control	2994.73 ± 65.75	2.31 ± 0.05	**NTS**
Hypertensive	Control	4356.92 ± 650.87	1.39 ± 0.14	**HTS**
Normal	Insulin	4362.94 ± 88.67	1.84 ± 0.23	**NITS**
Hypertensive	Insulin	6775.89 ± 450.05	0.99 ± 0.17	**HITS**
Normal	Control + Sirolimus	2690.06 ± 270.01	1.96 ± 0.26	**NTSS**
Hypertensive	Control + Sirolimus	3119.34 ± 289.04	1.46 ± 0.21	**HTSS**
Normal	Insulin + Sirolimus	3507.23 ± 287.65	1.58 ± 0.29	**NITSS**
Hypertensive	Insulin + Sirolimus	5520.31 ± 509.89	1.09 ± 0.13	**HITSS**

From figure 27, it can be appreciated that application of hypertensive mechanical strain led to significantly greater cell area (p-value < 0.0001 for HTS vs NTS) and insulin treatment further led to larger cell-area (p-value < 0.0001 for HITS vs NITS) thus, indicating that application of elevated mechanical strain leads to a relatively hypertrophic response which is further exaggerated by insulin treatment. Sirolimus treatment did reduce the cell-area across all treatments (p-value <0.0001 for NTSS vs NTS; HTSS vs HTS; NITSS vs NITS; HITSS vs HTS) however, cell area was greater for insulin treatment combined with hypertensive mechanical loading despite insulin treatment as compared to control during normotensive loading (p-value < 0.0001 for HITSS vs NTSS).

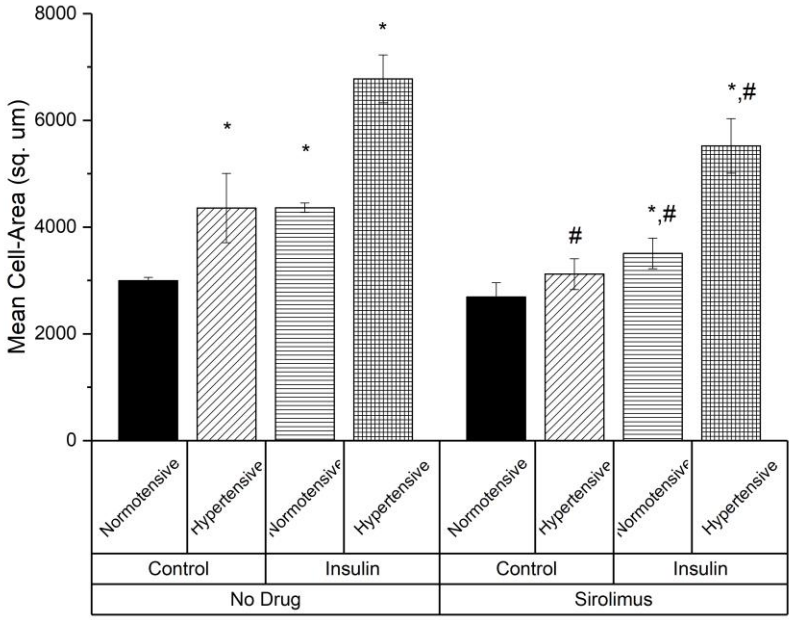

Figure 27: *Treatment-wise Cell area (sq. µm) within each mechanical loading; Values represented as Mean ± SD for every treatment (n=6 for each with 180 cells per sample). '*' represents statistical significance (p-value < 0.05) in comparison to respective normotensive control; '#' represents statistical significance (p-value < 0.05) in comparison to respective no-drug treatment.*

Corresponding aspect ratio measurements were observed to be Aspect ratio results (figure 28) were in accordance with cell-are measurements where application of hypertensive mechanical strain results in significantly reduced aspect ratio for control (p-value < 0.0001 for HTS vs NTS) and insulin treatment (p-value < 0.0001 for HITS vs NITS) with significantly lower aspect ratio for insulin treated samples under hypertensive loading as compared to hypertensive control treatment (p-value < 0.0001 for HITS vs HTS). Further, sirolimus treatment led to an overall increase in the mean aspect ratio for all treatments under normotensive (p-value < 0.0001 for NTSS vs NTS; NITSS vs NITS) and hypertensive loading (p-value < 0.0001 for HTSS vs HTS; HITSS vs HITS).

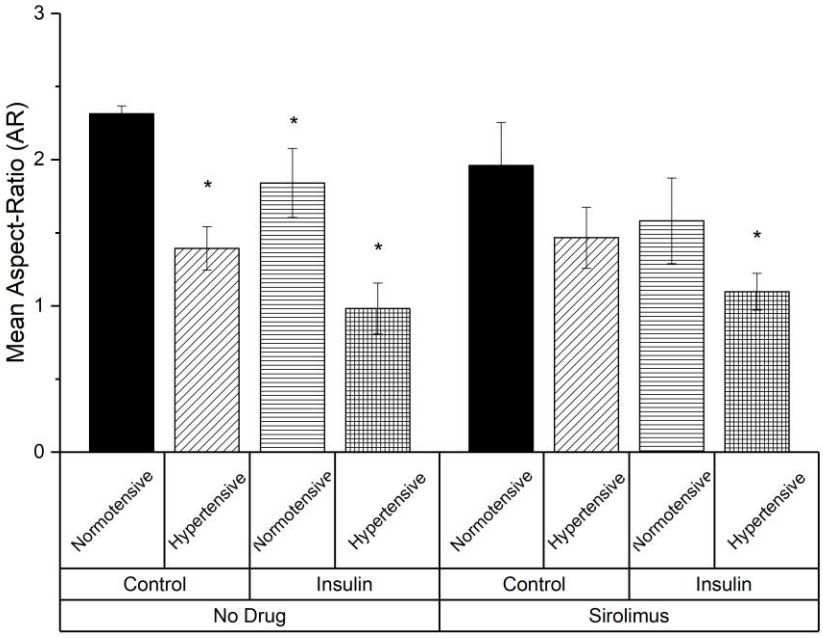

Figure 28: *Treatment-wise aspect-ratio within each mechanical loading; Values represented as Mean ± SD for every treatment (n=6 for each with 180 cells per sample). '*' represents statistical significance (p-value < 0.05) in comparison to 'control or DMSO' for every loading with one-way ANOVA and Tukey's HSD post-hoc comparison.*

In summary, these results demonstrate a relatively greater synthetic state of RASMCs subjected to hypertensive loading due to greater cellular hypertrophy as indicated by significantly greater cell area and reduced aspect ratio. Further, these results demonstrate the combined influence of insulin administration and hypertensive loading since this particular groups had the greatest cell area corresponding to lowest aspect ratio.

4.3d. Protein expression: Phenotypic dedifferentiation of RASMCs was evaluated by comparing α-SM actin and SM22α expression between different loadings and treatments. α-SM actin results (figure 29) reveal that subjecting cells to hypertensive loading to greater dedifferentiation of RASMCs as compared to normotensive loading for both control (p-value < 0.0001 for HTS vs NTS) and insulin treatment (p-value < 0.0001 for HITS vs NITS). In addition, effects of insulin can be appreciated from significantly reduced expression of α-SM actin under hypertensive loading in comparison to normotensive loading of insulin treated cells (p-value < 0.0001 for HITS vs NITS) and hypertensive loading of control treatment (p-value < 0.0001 for HITS vs HTS) thus, indicating

greater dedifferentiation of RASMCs with hypertensive loading which is further enhanced with insulin treatment.

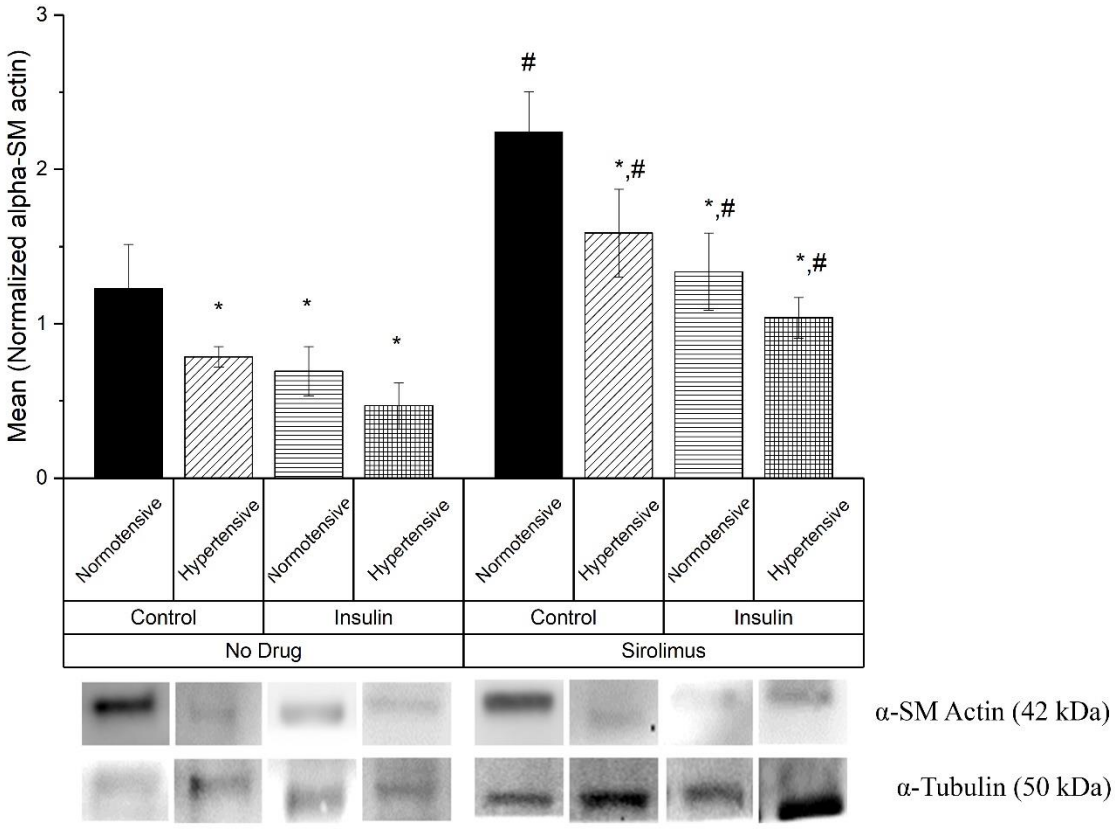

Figure 29: *Treatment-wise α-SM actin expression normalized to α-Tubulin expression within each mechanical loading; Values represented as Mean ± SD for every treatment (n=6 for each). '*' represents statistical significance (p-value < 0.05) in comparison to respective normotensive control; '#' represents statistical significance (p-value < 0.05) in comparison to respective no-drug treatment.*

SM22α was another protein marker employed to evaluate the effects of treatment and loading on phenotypic modulation of RASMCs. Consistent with actin expression, SM22α expression results (figure 30) indicate significantly reduced expression of SM22α with hypertensive loading in comparison to normotensive loading with control (p-value < 0.0001 for HTS vs NTS) and insulin treatment (p-value < 0.0001 for HITS vs NITS). Further, in the presence of insulin hypertensive

loading greatly reduced SM22α expression in comparison to normotensive insulin treated cells (p-value < 0.001 for HITS vs NITS). Sirolimus treatments resulted in significantly greater SM22α expression across all treatments under normotensive and hypertensive loading albeit, hypertensive loading did not result in significantly reduced expression of SM22α during insulin treatment with sirolimus. These results indicate significantly reduced expression of contractile-state associated proteins – α-SM actin and SM22α due to hypertensive loading and in combination with insulin treatment, hypertensive loading led to greater dedifferentiation of RASMCs as indicated by reduced expression of contractile-state associated proteins. Further, sirolimus treatment did improve the cellular outcome in control treatment under normotensive and hypertensive loading, it only controlled dedifferentiation for insulin treated cells under normotensive loading but not hypertensive loading.

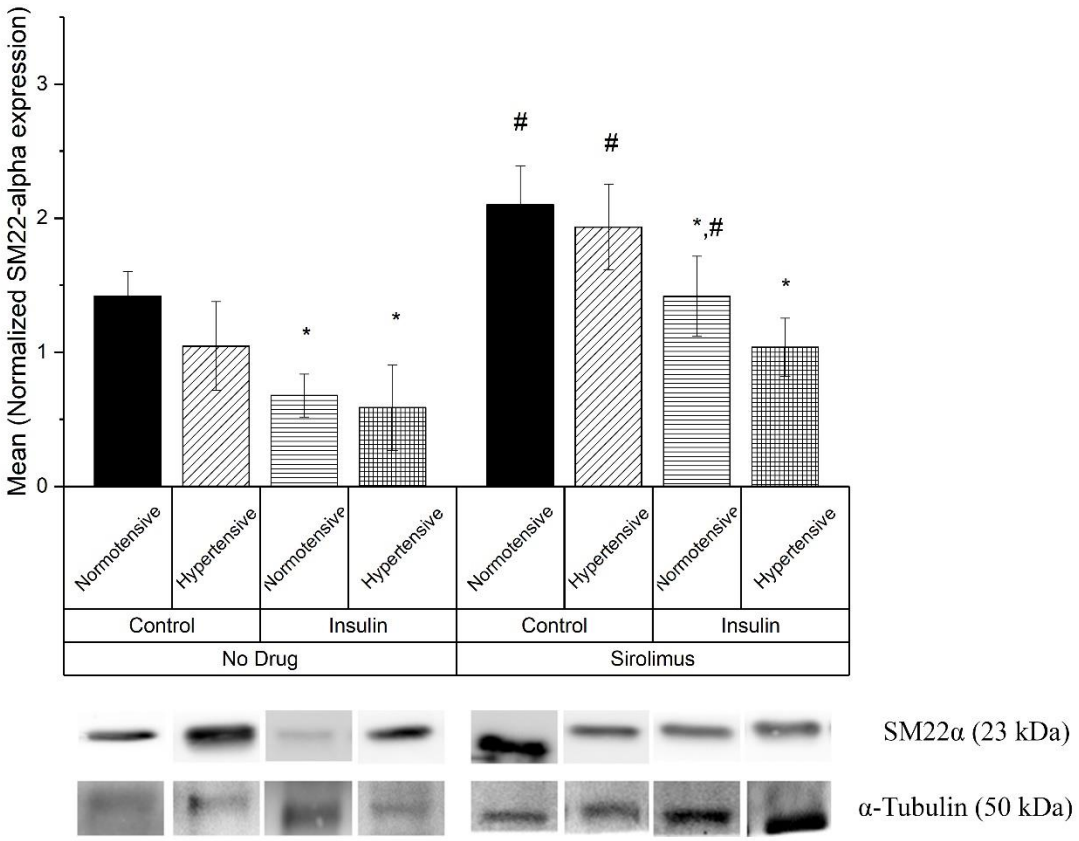

Figure 30: *Treatment-wise SM22α expression normalized to α-Tubulin expression within each mechanical loading; Values represented as Mean ± SD for every treatment (n=6 for each). '*' represents statistical significance (p-value < 0.05) in comparison to respective normotensive control; '#' represents statistical significance (p-value < 0.05) in comparison to respective no-drug treatment.*

Phosphorylation of ERK ½ is a known molecular effect during cellular proliferation and thus were compared for different loadings and treatments. Results of p-ERK ½ expression (figure 31) indicate that hypertensive loading led to significantly greater expression of p-ERK ½ for both control (p-value < 0.0001 HTS vs NTS) and insulin treatment (p-value < 0.0001 for HITS vs NITS) thus, indicating direct growth promoting effects of hypertensive loading. Further, insulin treatment led to significantly greater expression of p-ERK ½ normotensive (p-value < 0.0001 for NITS vs NTS) as well as hypertensive loading (p-value < 0.0001 for HITS vs HTS) in comparison to control treatment. Treatment with sirolimus resulted in reduced expression of p-ERK ½ for both control

and insulin treatment under normotensive (p-value < 0.0001 for NTSS vs NTS; NITSS vs NITS) as well as hypertensive (p-value < 0.0001 for HTSS vs HTS; HITSS vs HITS) loading.

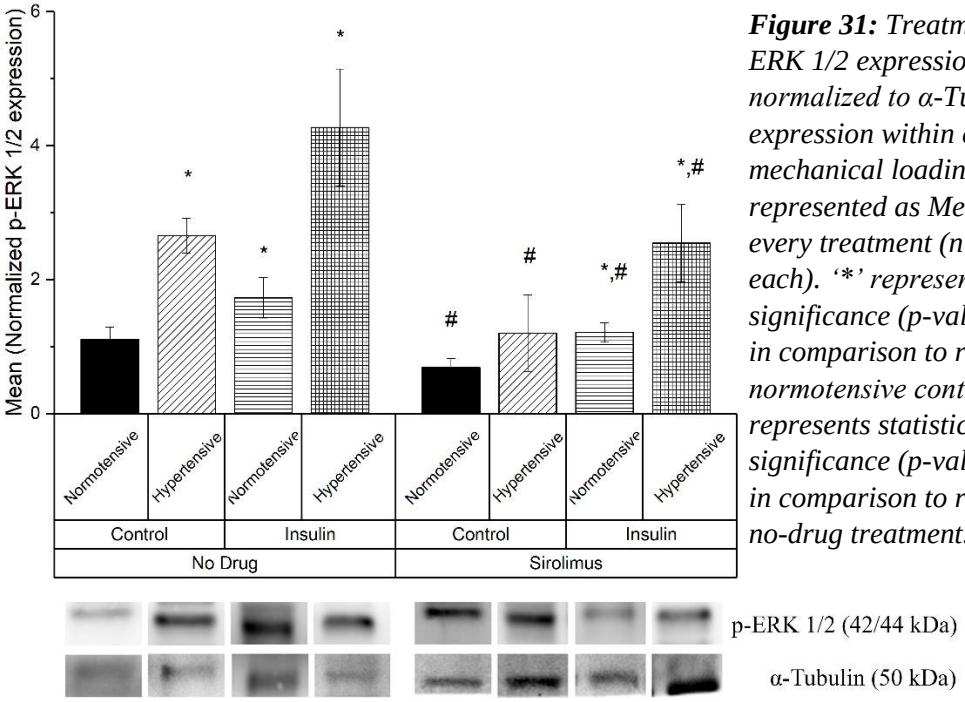

Figure 31: *Treatment-wise p-ERK 1/2 expression normalized to α-Tubulin expression within each mechanical loading; Values represented as Mean ± SD for every treatment (n=6 for each). '*' represents statistical significance (p-value < 0.05) in comparison to respective normotensive control; '#' represents statistical significance (p-value < 0.05) in comparison to respective no-drug treatment.*

Hsp47 has been identified as an indirect marker of collagen expression which in turn indicates the phenotypic modulation of RASMCs since synthetic phenotype is known to generate greater amount of collagen. Hsp47 expression was evaluated for hypertensive loading only and results (figure 32) demonstrate that insulin administration led to greater expression of Hsp47 as compared to control under hypertensive loading (p-value < 0.0001 for HITS vs HTS and sirolimus successfully controlled Hsp47 expression for both control (p-value < 0.0001 for HTSS vs HTS and insulin treatments (p-value < 0.0001 for HITSS vs HITS). Greater expression of Hsp47 with insulin treatment indicates greater dedifferentiation of RASMCs which in turn is reduced with sirolimus

administration however, was still significantly higher for insulin treated cells despite sirolimus treatment (p-value < 0.0001 for HITSS vs HITS).

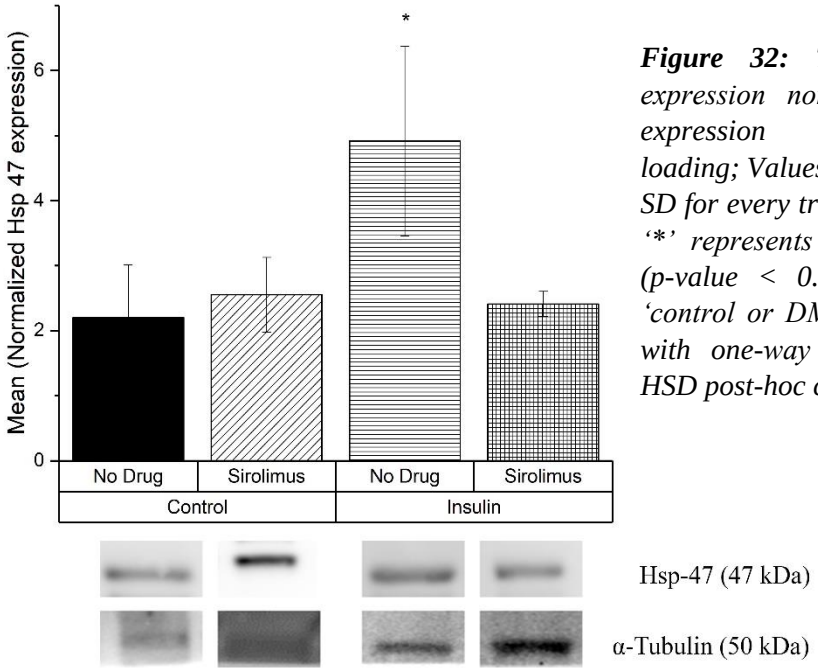

Figure 32: *Treatment-wise Hsp47 expression normalized to α-Tubulin expression within hypertensive loading; Values represented as Mean ± SD for every treatment (n=6 for each). '*' represents statistical significance (p-value < 0.05) in comparison to 'control or DMSO' for every loading with one-way ANOVA and Tukey's HSD post-hoc comparison.*

Overall results from this investigation are summarized in table 12 in comparison to NTS group where '*' represents significantly different in comparison to NTS. Expression of Hsp47 was evaluated for hypertensive loading only and hence '$' represents Hsp 47 expression in comparison to HTS loading. Results clearly indicate a significantly greater phenotypic modulation of RASMCs due to hypertension-associated elevated mechanical strain across all treatments and this effect was augmented by insulin administration as HITS demonstrated significant effect across all assays. In addition, sirolimus successfully reduced phenotypic modulation of RASMCs and also demonstrated significantly greater percentage of cells in the G1/G0 phase across all loadings however results were significantly poorer during insulin administration.

Table 12: *Summary of all treatment and loading-wise comparison. Each row represents treatment; each column represents assay performed; "Group" column represents loading condition. '*' indicates significantly different results in comparison to NTS*

Treatment	**Cell Cycle**	**TUNEL**	**Area**	**Aspect Ratio**	**Actin**	**SM22α**	**p-ERK 1/2**	**Hsp 47**	**Group**
Control	*	*	*	*	*		*		HTS
Control + Sirolimus (10 ng/mL)	*	*		*	*	*	*		NTSS
	*	*	*			*			HTSS
Insulin (10 ng/mL)	*		*	*	*	*	*		NITS
	*	*	*	*	*	*	*	$	HITS
Insulin (10 ng/mL) + Sirolimus (10 ng/mL)	*		*	*					NITSS
	*	*	*	*	*	*	*		HITSS

Discussion:

Hypertension continues to significantly influence the prognosis of PCI procedures even in the age of second generation drug eluting stents and patients afflicted with diabetes and hypertension continue to suffer from higher rates of revascularization procedures (156,213). A direct consequence of hypertension is elevated circumferential stress in the arterial wall and as a result, vascular cells experience significantly higher circumferential forces (214,215). Previous investigations have successfully explored the effects of hypertensive mechanical strain on phenotypic modulation of vascular smooth muscle cells (216,218) however, effects of these forces in patient-specific complications of chronic high glucose and insulin administration remains unexplored. In the current study, we investigated the effects of hypertension-associated elevated

mechanical strain and implant associated low wall-shear stress on chronic high glucose acclimated RASMCs with or without insulin to capture the clinically relevant cellular-response more accurately and conceptualize an in vitro diabetic-hypertensive model. As an application, we explored the ability of sirolimus (10 ng/mL), a drug commonly used for drug-eluting stents, to effectively regulate RASMC differentiation under the diseased conditions. Sirolimus was the drug of choice for this study since clinical investigations have demonstrated sirolimus eluting stents to be associated with lower late luminal loss and hence restenosis than paclitaxel (231). In addition, multiple clinical trials have shown poorer outcomes of DES in diabetic patients especially those requiring insulin administration and non-significant performance of second generation of DES in diabetic patients (105,232,233). This is further complicated by elevated blood pressure which has been clinically demonstrated to promote in-stent restenosis (69). Efficacy of sirolimus under these patient-specific complications has not been performed previously and successfully demonstrates the advantage of this model in comparison to conventional static approaches.

Results from the current investigation demonstrated that application of elevated mechanical strain significantly reduced % cells in the G1/G0 phase and subsequently increased % cells in the S and G2/M phase of the cell cycle for both control and insulin treatment (p-value < 0.0001 for HTS vs NTS and HITS vs NITS) thus, indicating a proliferative cellular-response associated with elevated mechanical strain. insulin administration led to significantly greater proliferative response in comparison to control under normotensive loading (previous study) and in the current investigation, hypertension-associated loading also resulted in significantly greater proliferative response of RASMCs with insulin administration in comparison to control (p-value < 0.0001 for HITS vs HTS). These results indicate a pro-proliferative response of hypertension-associated elevated mechanical strain which in turn, exerts a corroborating effect with insulin administration. These results are in

agreement with previous investigations where elevated mechanical strain was shown to enhance proliferation of VSMCs (219–221) and further supported by a greater proliferative response to PCI in spontaneously hypertensive rats (SHR) (227). Sirolimus is a commonly employed drug in stents with an anti-proliferative effect on VSMCs (234) and in the current study demonstrated too successfully reduce % cells in the S and G2/M phase of the cell cycle for both normal and hypertensive loading under control and insulin treatments (p-value < 0.0001 for all NTSS vs NTS; HTSS vs HTS; NITSS vs NITS; HITSS vs HITS) however, did not reduce proliferation of cells under insulin treatment to levels comparable to control under normal (p-value < 0.0001 for NITSS vs NTSS) and hypertensive loading (p-value < 0.0001 for HITSS vs HTSS). Thus, for equimolar drug concentrations, sirolimus treatment did not result in similar proliferative response for control and insulin treatment further underscoring the need to design and test novel anti-restenotic treatments at cellular level under disease-associated conditions.

Cells were evaluated for apoptosis with TUNEL-staining with flow cytometry and results from the current study indicate that hypertension-associated elevated mechanical strain resulted in significantly greater % cells undergoing apoptosis for both control (p-value < 0.0001 for HTS vs NTS) and insulin treatment (p-value < 0.0001 for HITS vs NITS). Previously, insulin administration resulted in an overall decrease in the % cells positive for TUNEL (previous study) and similar effects of insulin were observed under hypertensive loading as well where insulin administration resulted in reduced % cells undergoing apoptosis in comparison to control (p-value < 0.0001 for HITS vs HTS). These findings are in accordance with previous in vitro and animal model investigations where hypertensive mechanical strain (222–224) and systemic hypertension resulted in greater apoptosis of VSMCs in parallel to higher proliferation (235,236). Sirolimus is known for not inducing apoptosis in smooth muscle cells, with prior evidence showing its pro-survival effect in vitro (237). Under hypertension-associated elevated mechanical strain, sirolimus

treatment resulted in reduced % TUNEL-positive cells for both control (p-value < 0.0001 for HTSS vs NTSS; HITSS vs NITSS) and insulin treatment with significantly lower apoptotic cells observed for insulin (p-value < 0.0001 for HITSS vs HTSS). VSMC apoptosis is known to exaggerate the inflammatory response post PCI procedure owing to activation of multiple pathways (238), which may further increase the neointimal response while localized delivery of sirolimus, has been shown to result significantly lower apoptotic response in rats (237), in part due to lowered inflammatory response.

Cellular hypertrophy was estimated by indirect measures of comparing cell-area and aspect ratio with results indicating significantly greater cell-area and correspondingly recued aspect ratio for cells subjected to hypertension-associated elevated mechanical loading in comparison to normotensive loading reported previously with insulin treatment resulting in significantly greater hypertrophic response as compared to control treatment under hypertensive loading (p-value < 0.0001 for HITS vs HTS). Systemic hypertension is known to induce hypertrophy in various tissue and organs including vessel-wall (237) in addition to tissue hypertrophy observed in SHR animal model of hypertension (239) thus, validating results from the current study with previous findings. In addition, Sirolimus treatment successfully reduced overall hypertrophy significantly albeit, hypertrophy was significantly greater for insulin treated cells (p-value < 0.0001 for HITSS vs HTSS; NITSS vs NTSS) and hypertensive mechanical strain added to this effect (p-value < 0.0001 for HTSS vs NTSS) thus, demonstrating the combined effect of the two patient-specific complications.

Expression levels of contractile-state associated markers directly indicate phenotypic modulation in VSMCs and in the current study, expression levels of αSM-actin and SM22α were compared. Results indicate significantly reduced expression of αSM-actin with hypertensive mechanical loading for both the control and insulin treatment (p-value < 0.0001 for HTS vs NTS; HITS vs

NITS) with significantly lowered αSM-actin expression levels for insulin under hypertensive loading in comparison to control (p-value < 0.0001 for HITS vs HTS). Sirolimus treatment did not results an in overall increase in αSM-actin expression for both control and insulin treatment across all loadings however, insulin treated cells still expressed lower levels of αSM-actin in comparison to controls with lowest levels for insulin treated hypertensive-loaded group. SM22α demonstrated similar results with insulin treatment exhibiting significantly reduced SM22α levels in comparison to control (p-value < 0.0001 for NITS vs NTS; reported previously) which were further lowered with hypertensive mechanical loading (p-value < 0.0001 for HITS vs NITS). These results demonstrate that application of hypertension-associated elevated mechanical strain results in significant phenotypic modulation of chronic high glucose acclimated RASMC which in turn results in greater dedifferentiation with insulin administration under these conditions. Consistent with our results, previous investigations have also demonstrated recued expression of contractile-state associated markers in VSMCs subjected to elevated mechanical strain (216,218). Sirolimus treatment did cause greater expression of SM22α across all treatments under hypertensive loading however, results were still significantly lower for insulin treated cells in agreement with previous investigations demonstrating induction of contractile phenotype with sirolimus treatment (237).

Expression levels of p-ERK ½ were compared to evaluate if proliferative effects of hypertension-associated elevated mechanical strain is observable at a proteins level. Results indicate that application of elevated mechanical strain resulted in significantly greater expression of p-ERK ½ for both control (p-value < 0.0001 for HTS vs NTS) and insulin (p-value < 0.0001 for HITS vs NITS) under hypertensive loading and were consistent with normotensive results. insulin treatment resulted in significantly greater expression of p-ERK ½ in comparison to control, for hypertensive loading (p-value < 0.0001 for HITS vs HTS). With sirolimus treatments, there was an overall decrease in the expression of p-ERK ½ for both control (p-value < 0.0001 for NTSS vs NTS; HTSS

vs HTS) and insulin treatments (p-value < 0.0001 for NITSS vs NITS; HITSS vs HITS) under normotensive and hypertensive loadings however, levels were significantly greater for insulin treatment in comparison to control with hypertensive-mechanical loading adding to the effect (p-value < 0.0001 for HITSS vs HTSS). These results indicate an overall pro-proliferative effect of hypertension-associated elevated mechanical loading on chronic high glucose acclimated RASMCs with insulin treatment further contributing to proliferation. Historically, investigations have demonstrated significantly higher expression of p-ERK ½ in VSMCs subjected to elevated mechanical strain and co-associated with proliferation (240–242).

Collagen expression is increased during VSMC dedifferentiation and elevated collagen a characteristic marker of synthetic-state phenotype (243). Expression of Hsp47 was evaluated as indirect estimator of collagen production under hypertension-associated elevated mechanical strain, as previously it has been demonstrated to be associated with increased collagen production (243). Results indicate that insulin treatment led to significantly greater expression of Hsp47 as compared to control under hypertensive mechanical strain (p-value < 0.0001 for HITS vs HTS) which were subsequently reduced with sirolimus treatment to level similar to control treatment hence demonstrating the efficacy of sirolimus in controlling Hsp 47 expression and thus, collagen expression under disease-associated conditions. Clinically, patients requiring insulin administration have been reported to have restenotic lesions rich in extracellular-matrix primarily composing of collagen (243) with in vitro evidence of synthetic-state of VSMCs reported to secrete higher amounts of collagen.

Overall, results from the current study demonstrate the significance of combining multiple patient-specific complications such chronic high glucose, insulin treatment and hypertension-associated elevated mechanical strain with implant associated low wall-shear stress where, disease specific conditions resulted in significantly higher proliferative behavior and relatively greater phenotypic

modulation. Cells subjected to these conditions capture the clinically relevant cellular-response of diabetic patients afflicted with hypertension and implanted with stents more accurately.

Conclusion:

In the current study, we hypothesized that application of hypertension-associated elevated mechanical strain will result significantly greater phenotypic modulation and pro-proliferative behavior of RASMCs with additive effect of inulin treatment. Current results support our hypothesis since hypertensive-mechanical strain resulted significantly greater % cells in the S and G2/M phase of the cell cycle, greater apoptosis, higher cellular hypertrophy estimated by cell-area and aspect ratio, reduced expression of contractile-state associated markers αSM actin and SM22α with concomitant increase in expression levels of p-ERK ½. Dedifferentiation was more pronounced with insulin administration thus, illustrating the combined effects of mechanical loading, diabetes associated chronic high glucose and insulin administration, and hypertensive mechanical loading altogether on phenotypic modulation of RASMCs. As an application of the model, we evaluated the efficacy of sirolimus (10 ng/mL) in controlling proliferation and phenotypic modulation of RASMCs which indicated that equimolar drug concertation may not be sufficient to control a greater proliferative response associated with these patient-specific complications and necessitates a more targeted approach. In future, this model can be utilized to explore the complex and intricate cellular pathway involved in executing these responses and molecular targets can be tested in regulating VSMC phenotype for novel clinical solutions aimed at improving outcomes of PCI in these patients.

Chapter 5: Project conclusions and recommendations

5.1 Project Conclusions:

In the current dissertation project, patient-specific complication of insulin administration and selective insulin resistance were combined with physiologically relevant circumferential strain and stem-implantation associated low wall-shear stress to evaluate their effect on proliferation and phenotypic modulation of RASMCs in order to propose an in vitro diabetic model which captures the clinically relevant cellular-response more accurately than conventional unloaded/static studies. With this model, it was successfully demonstrated that administration of insulin contributed to the dedifferentiation of RASMCs as they demonstrated greater proliferative response under these conditions combined with reduced expression levels of contractile-state associated proteins. Selective insulin resistance with wortmannin was incorporated to represent experimental diabetes in vitro however, current results indicate that selective inhibition of AKT phosphorylation did not result in significantly different proliferative behavior which was subordinated with similar expression levels of αSM actin and SM22α thus, necessitating further investigations into the involvement of AKT pathway in mediating insulin resistance in vascular smooth muscle cells. However, similarity of cellular response with insulin treatment with prior in vitro investigations and animal studies validate our results and are in accordance with clinical observation of exaggerated progression of neointimal lesions in diabetic patients requiring insulin administration (Chapter 3).

In the second phase of this project, hypertension-associated elevated mechanical strain was incorporated to combine another clinically significant risk factor of developing in-stent restenosis with previously explored diabetes-associated insulin administration to evaluate proliferation and phenotypic modulation of RASMCs under diabetic-hypertension associated conditions. Results

successfully demonstrated that elevated mechanical strain associated with hypertension results significantly greater dedifferentiation of chronic high glucose acclimated RASMCs and these effects were further advanced with insulin administration thus, illustrating that insulin administration under hypertension-associated elevated mechanical strain results in the highest level of VSMC proliferation and dedifferentiation. Thus, with this experimental approach we were able to successfully combine two of the most significant patient-specific risk factors with implant specific mechanical forces and evaluate their influence on cellular-response (Chapter 4).

Clinically, sirolimus eluting stents are the preferred choice for high-risk patients in comparison to paclitaxel stents however, studies have indicated that while SES performed better than paclitaxel eluting stents – this performance benefit is not extended to diabetic patients. As an application, the current diabetic-hypertensive model was applied to test the efficacy of equimolar sirolimus in controlling and reducing RASMC-proliferation and phenotypic modulation. We successfully demonstrated that under insulin administration, cells demonstrated a greater proliferative response with reduced expression of contractile-state associated proteins even with sirolimus treatment and hypertension-associated elevated mechanical strain further added to dedifferentiation of RASMCs hence, providing a cellular-response based evidence which may be responsible for the clinical differences in efficacy of sirolimus eluting stents in controlling neointimal hyperplasia for diabetic and hypertensive patients (Chapter 4).

Future investigations with the current model can be performed to explore the molecular basis of the cellular-response thus divulging greater molecular intricacies and can be utilized a test platform for novel anti-restenotic drugs/molecular targets aimed at reducing in-stent restenosis in diabetic patients requiring insulin administration with comorbidity of hypertension. Our proposed cellular-response model is designed to capture the patient-associated complications and combine them with stent-implant associated altered hemodynamics at an in vitro level thus, providing a robust test

platform to evaluate novel drugs aimed at reducing in-stent restenosis in diabetic-hypertensive patients implanted with stents and in the long-term will serve as a tool to reduce the overall time required to test novel technologies by bridging the gap between in vitro and pre-clinical models (figure 33).

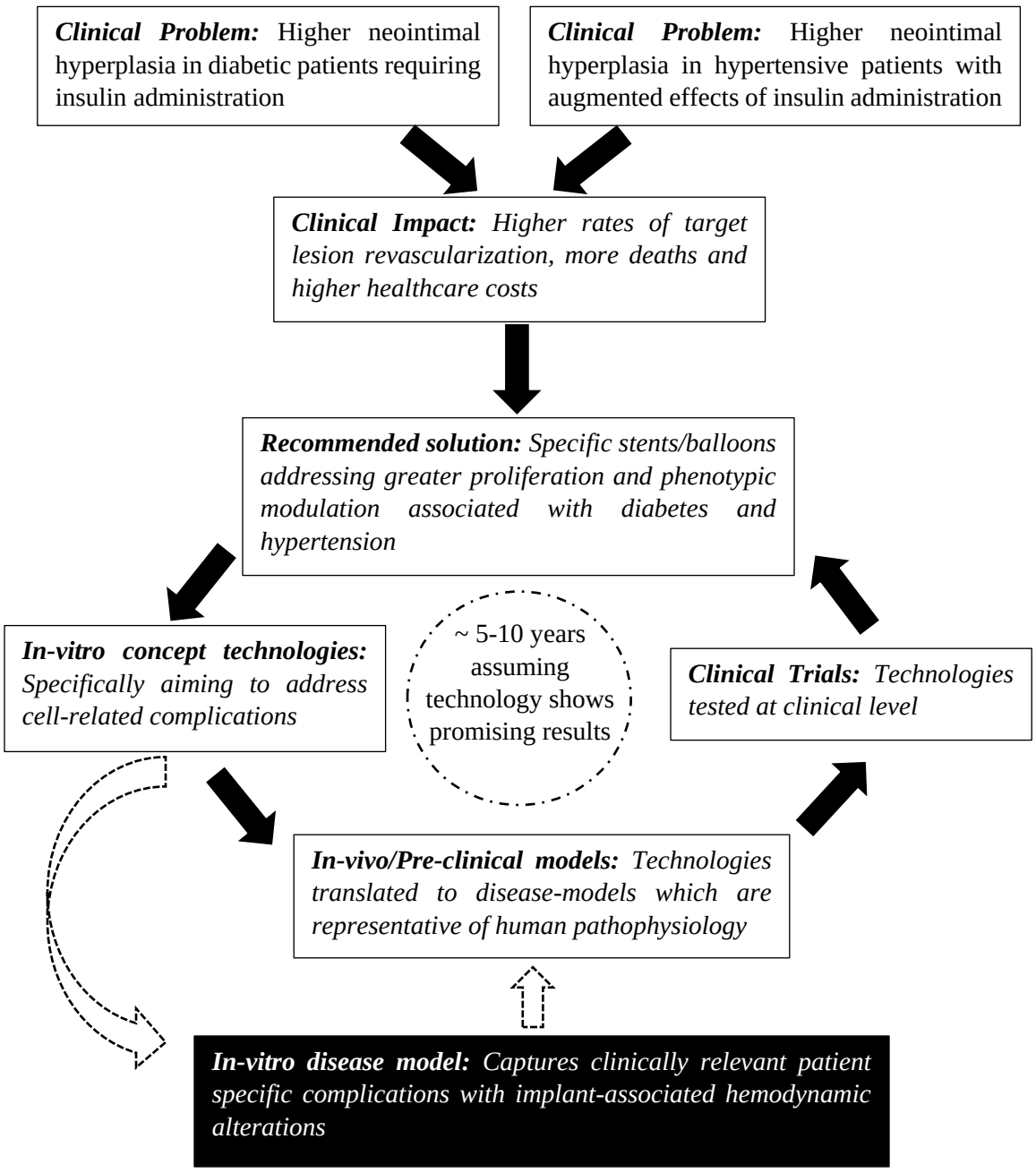

Figure 33: Project conclusion flow chart

5.2 Project Recommendations:

The dissertation project has successfully developed the relationship between cellular-response and clinically relevant pathological stimuli in diabetic-hypertensive patients with effects of these conditions on efficacy of sirolimus in controlling proliferation and phenotypic modulation of vascular smooth muscle cells. The overall approach of modeling diabetes-hypertension associated complications can be utilized for the following research areas:

1. *Response evaluation with human vascular smooth muscle cells:* Disease related conditions may be impacted by the source of cells incorporated for in vitro response evaluation. Patient-specific response accuracy can be significantly increased by isolating VSMCs from human arteries and utilizing them for the in vitro diabetic-hypertensive model. Further, this design can also be used for comparing the efficacy of various anti-restenotic drugs in controlling VSMC-response towards improvement and optimization of novel drug-eluting stents.

2. *Extension to 3-dimensional cell culturing approach*: Currently, various studies have been conducted which have demonstrated a variable response between 2-dimensional and 3-dimensional cell culturing approach. Using the approach utilized in our design, 3D cultures can be subjected to the diabetic-hypertensive conditions and hence, cellular response between our results and 3D investigations can be compared to reduce the current knowledge gaps associated with these approaches.

3. *Application to tissue engineering*: The future of cardiovascular intervention research is driven by bench-to-bedside technological approaches with tissue engineering being

the most useful approach for treating cardiovascular complications. Our modeling approach of combining diabetes and hypertension can be utilized in evaluating the response of stem cells with direct evidence of correlation between these complications and cellular-differentiation. Further, scaffold characterization under these conditions will improve the current understanding and will further optimize scaffolds for diabetic-hypertensive patients.

4. *Mathematical modeling*: Results from our research will be useful for investigators working towards developing mathematical models of VSMC-response to pathological stimuli and clinically relevant mechanical forces. Since current mathematical approaches are currently confined to modeling without considering the biochemical/biological aspects of components, these mathematical models may be significantly improved by incorporating our cause-effect results and hence will further design-optimization of novel stents and other interventional approaches such as bypass grafts.

Appendix A: Vascular smooth muscle cell isolation, passaging, characterization and maintenance of chronic high glucose conditions.

Thoracic aorta from 8-10 weeks old female Sprague-Dawley™ rats were isolated according to the Institutional Animal Care and Use Committee (IACUC) at Clemson University. Aorta was transferred back to the lab in sterile Dulbecco's minimal essential medium containing 1% Antibiotic/Antimycotic agent under ice-cold conditions. Next, the aorta was dissected under sterile condition in 1x DPBS (at 37 ^{0}C) in order to successfully remove all the waste tissue attached to the vessel and subsequently the vessel was subjected to enzymatic treatment with collagenase type I for 15 minutes at 37 ^{0}C. This step ensures easier removal of the adventitia where it comes off like a sock and does not damage the medial layer. Subsequently, the medial layer was scrapped on the inside with the blunt side of a sterile scalpel to denude the endothelial monolayer and gently scrapping was also performed on the outer side of the vessel to remove any remains of the adventitial layer following which, blood vessel was chopped into square pieces of approximately 1 mm^2 in size. Chopped tissue was then rinsed in fresh sterile 1x DPBS to remove any residual cells and consequently was transferred to enzymatic solution 2 (Type I collagenase – 1 mg/mL, Elastase – 0.25 mg/mL and Soybean trypsin inhibitor – 0.15 mg/mL) and incubated at 37 ^{0}C for 4-5 hours with gentle shaking. After 4-5 hours, when the tissue pieces have been dissolved in the enzymatic solution, the cell suspension was filtered through a cell strainer (100 µm pore size) following which the cell suspension was centrifuged. After aspirating enzymatic solution, the pelleted cells were re-dissolved in the fresh media (DMEM + 10% FBS + 1% Ab/Am) and transferred to a T-25 cm^2 flask. Cells were then incubated for 10-15 days with special attention to make sure that the flask is not disturbed. Cells were passaged to bigger vessels as soon as confluence was achieved. Typically, passaging was performed after 10-15 days for T-75 cm^2 flasks and 20-25 days for T-175 cm^2 flasks. Passage 4 cells were eventually incorporated for all the experiments in order to ensure that any

changes in phenotypic modulation are only associated with the treatment conditions and not due to passaging. For all experiments and passaging cell culture media contained 4.5 g/L of D-Glucose in order to replicate chronic high glucose exposure.

Appendix B: Flexcell frequency-dependent stretch characterization.

In order to model the hypertension-associated cyclic stretch in vitro, the stretch profile was altered to apply higher and clinically relevant levels of strain (~15%). To verify if the theoretical and applied strain are within acceptable range, strain profiles were measured at different strains and frequencies. Three rings were drawn on the silicone membrane where the first ring represented the out periphery of the cell-seeded area (diameter = 19.05 mm; Black), the second ring represented the middle cell-seeded area (diameter = 12.7 mm; Red) and finally the inner ring (diameter = 6.35 mm; Blue) as shown in Figure 34. Different strain regimes were applied to check if there were differences in applied strain and theoretical values. Membrane behavior was recorded using two camcorders and images were captured from the videos to measure circumferential strain and radial distance.

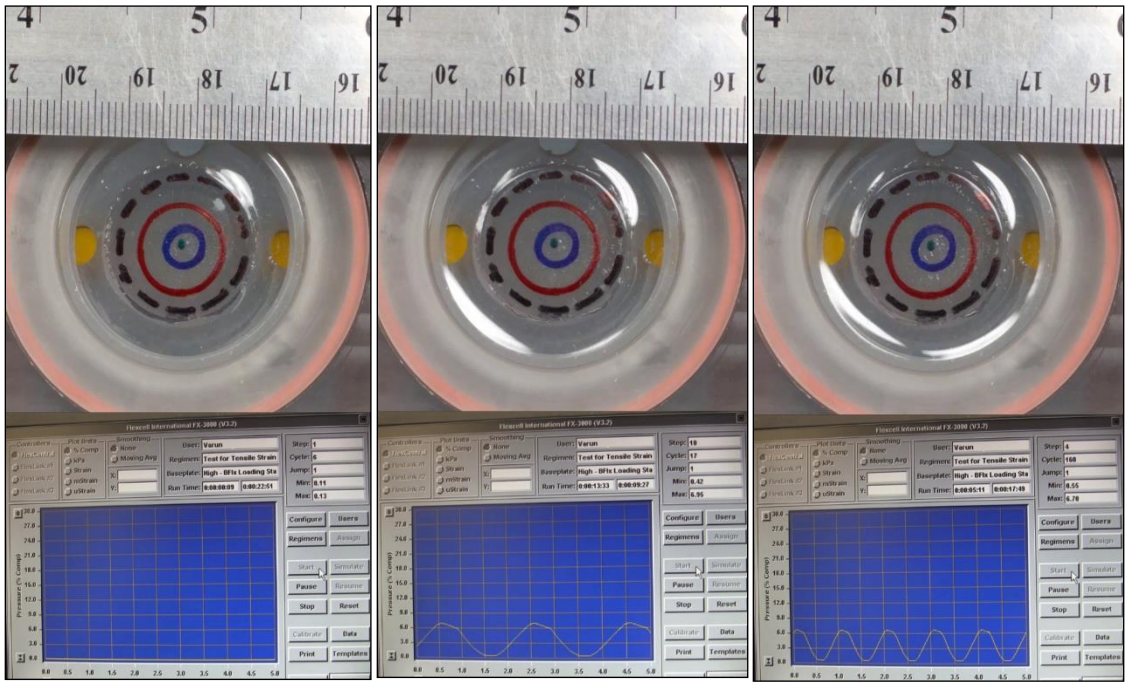

A B C

Figure 34: PIP images for strain calibration experiment. **A.** relaxed/no-strain; **B.** 0-7% at 0.5 Hz; **C.** 0-7% 1 Hz

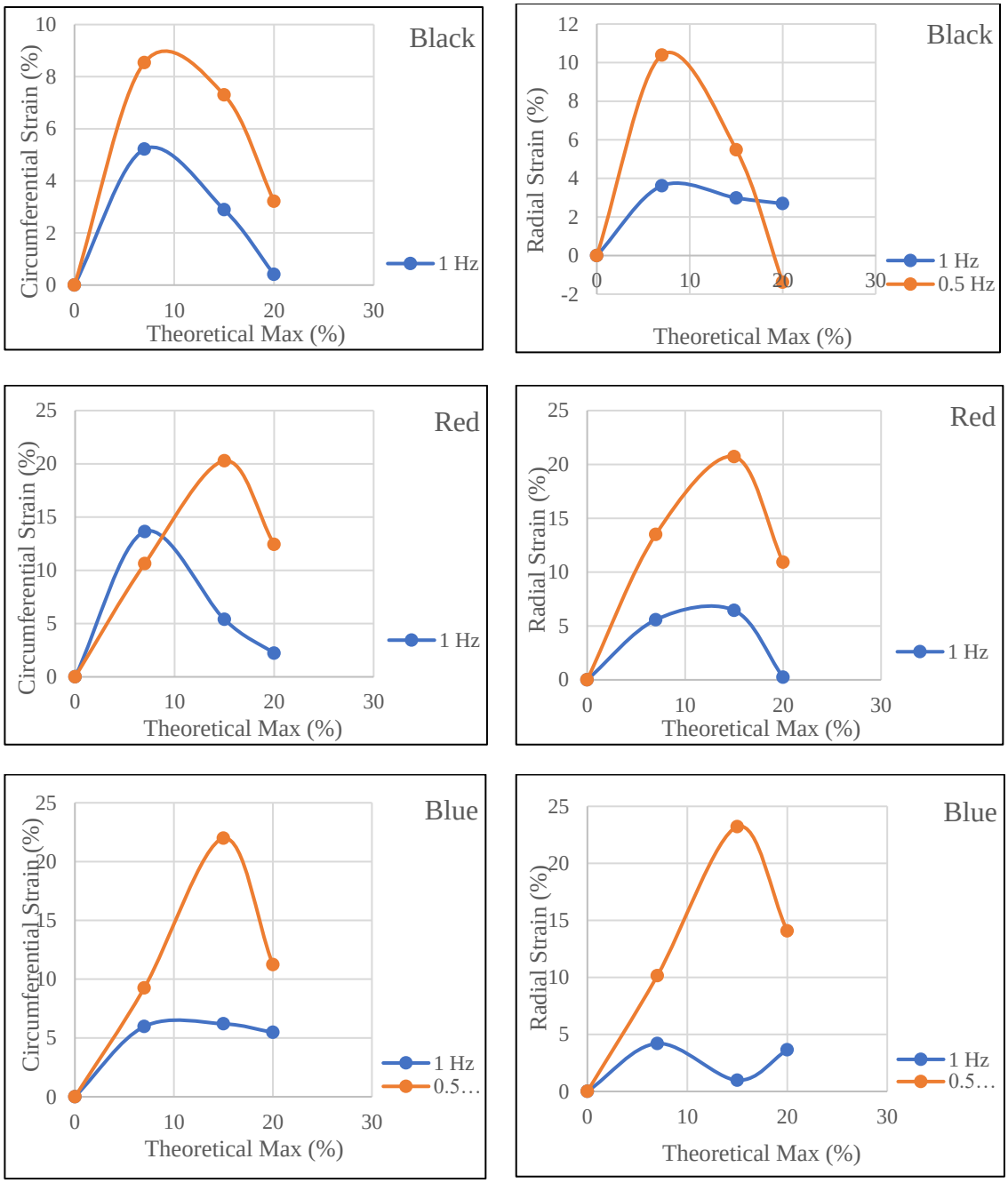

Figure 35: Measured circumferential strain correlation with theoretical strain for three different regions – black, red, blue.

Values were measured for each respective zone (black, blue or red) for circumferential strain and radial distance (figure 35) whereas compiled plots of individual region (blue, red or black) for circumferential strain vs theoretical strain are in figure 36a and circumferential strain vs radial distance in figure 36bIn order to estimate the averaged strain over the zone starting at the center of the membrane extending until the black ring, measured values were averaged for all zones and compiled separately for 0.5 Hz and 1 Hz (figure 36). Values for data points are enlisted in the table 13.

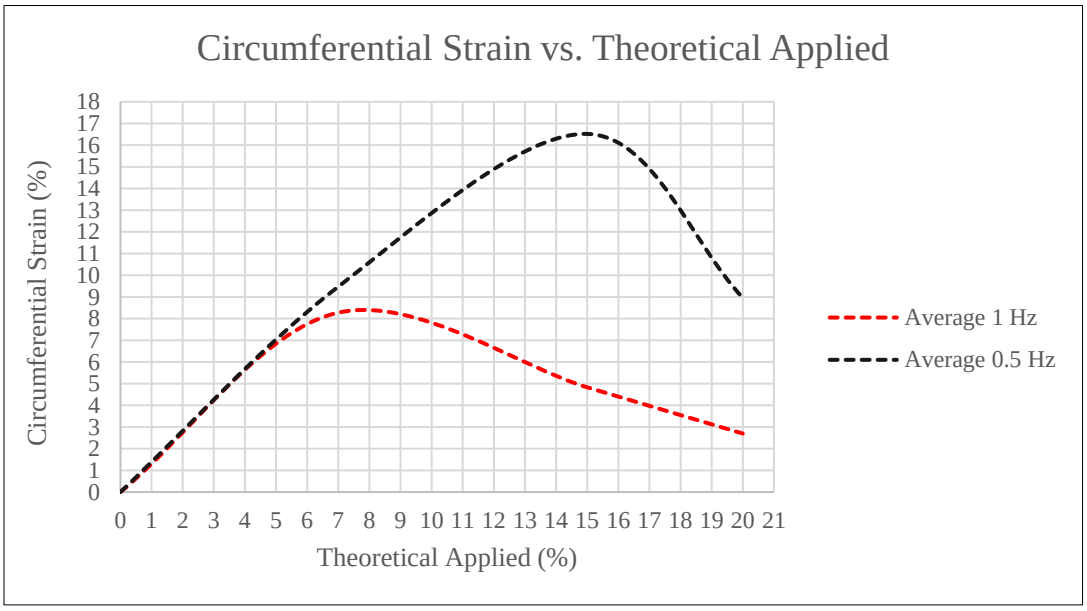

Figure 36: Averaged (measured circumferential strain) correlation with theoretical strain averaged for the entire membrane and plotted for 1 Hz (red) and 0.5 Hz (black).

Table 12: Tabular values for circumferential strain for three different regions – black, red, blue under 1 Hz and 0.5 Hz loading.

Frequency	Theoretical Strain	Circumferential Strain			Radial Strain		
		Black	Red	Blue	Black	Red	Blue
1 Hz	0	0	0	0	0	0	0
	7	5.21	13.63	5.96	3.61	5.57	4.19
	15	2.89	5.39	6.20	2.98	6.44	0.98
	20	0.41	2.21	5.47	2.69	0.23	3.64
0.5 Hz	0	0	0	0	0	0	0
	7	8.53	10.63	9.24	10.39	13.49	10.14
	15	7.29	20.28	21.97	5.48	20.72	23.21
	20	3.21	12.43	11.23	-1.38	10.91	14.07

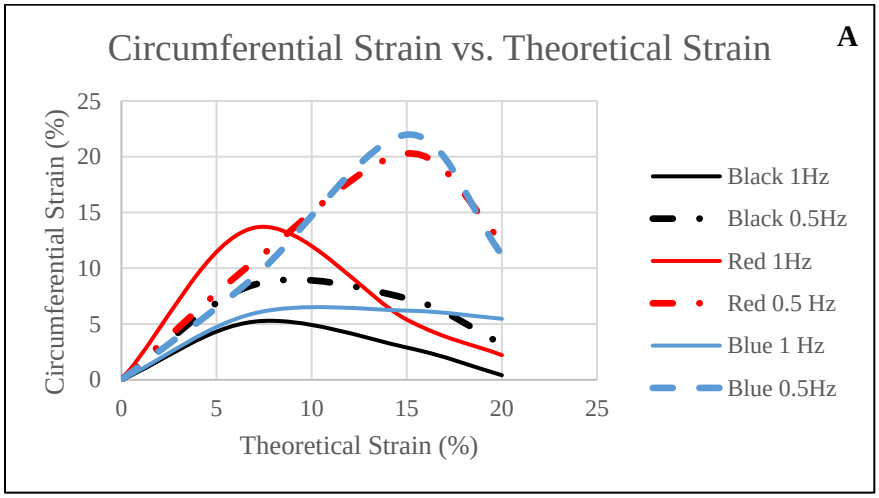

Figure 37: A- Compiled plots for measured strain vs theoretical strain of all three zones.

Figure 37: B - Compiled plots for measured strain vs radial distance of all three zones.

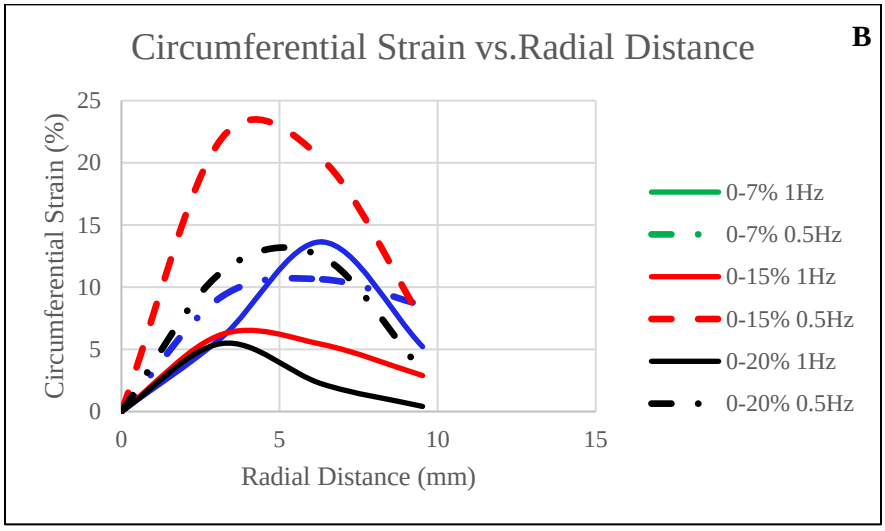

Both strain application frequencies demonstrated linear behavior in the physiologically relevant range of 0-7 % strain however, beyond this point – applied strain was only linear for 0.5 Hz frequency and not with 1 Hz in our custom vascular simulator. All measurements were recorded under true-experiment like conditions, including using silicone lubricant. Thus, a theoretical 15% strain would have resulted in ~ 5% applied strain with the current design and hence, would have not represented hypertension-associated elevated mechanical strain. Subsequently, all experiments were performed using 0.5 Hz frequency instead of 1 Hz.

Appendix C: CAD drawings of modified cell-culture rings

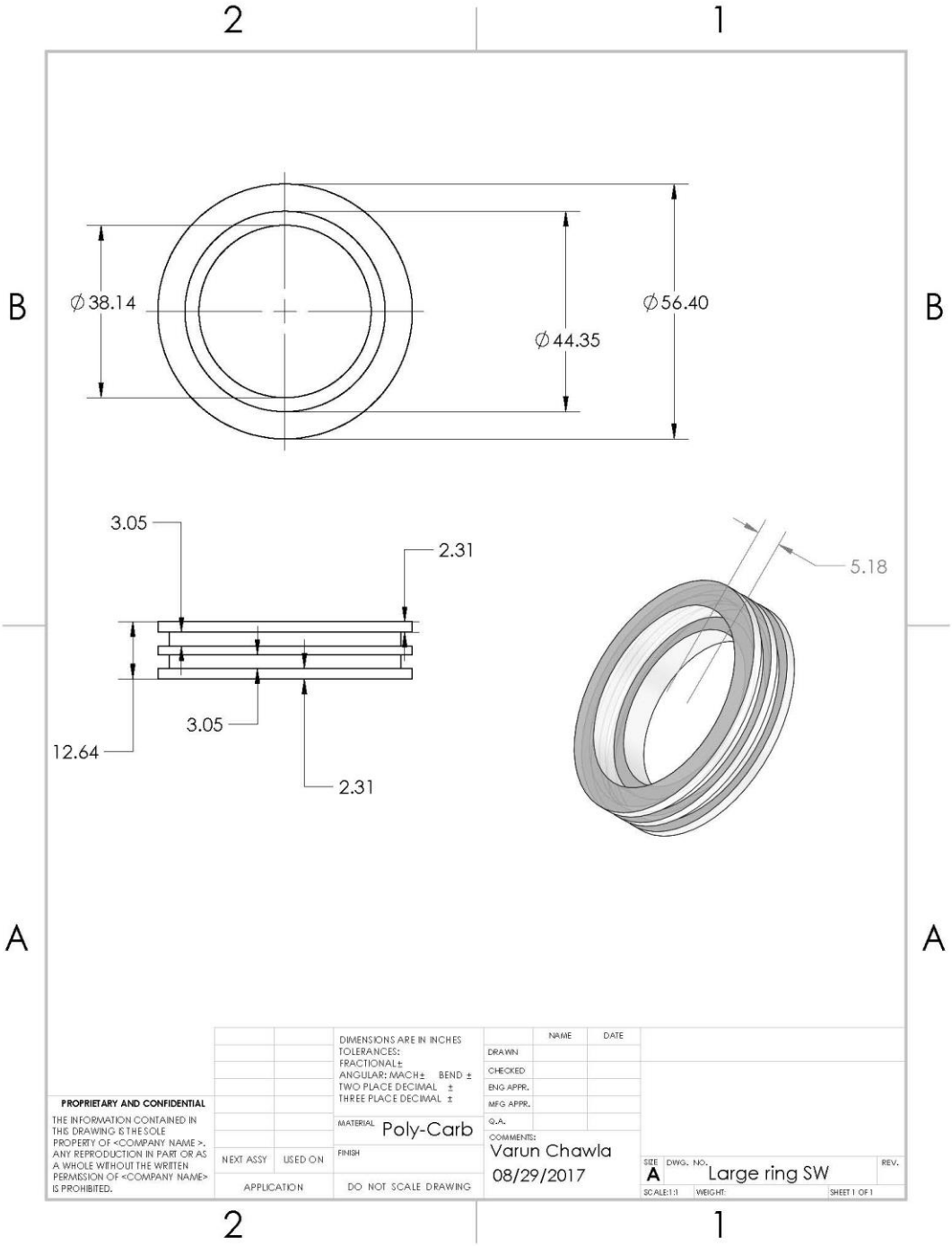

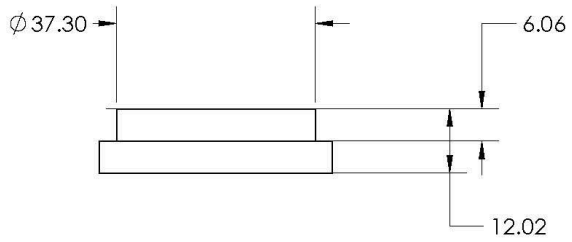

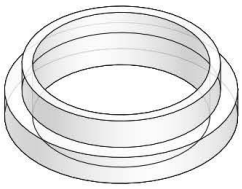

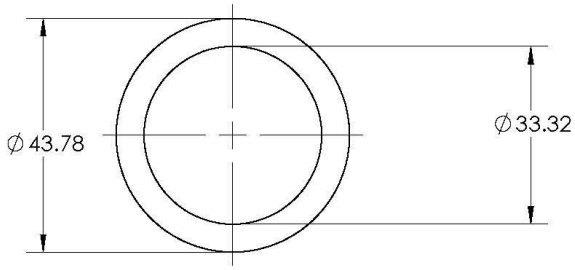

		DIMENSIONS ARE IN INCHES TOLERANCES: FRACTIONAL ± ANGULAR: MACH ± BEND ± TWO PLACE DECIMAL ± THREE PLACE DECIMAL ±		NAME	DATE
			DRAWN		
			CHECKED		
			ENG APPR.		
			MFG APPR.		
			Q.A.		
		MATERIAL Poly-Carb	COMMENTS: Varun Chawla 08/27/2017		
NEXT ASSY	USED ON	FINISH			
APPLICATION		DO NOT SCALE DRAWING			

PROPRIETARY AND CONFIDENTIAL

THE INFORMATION CONTAINED IN THIS DRAWING IS THE SOLE PROPERTY OF <COMPANY NAME >. ANY REPRODUCTION IN PART OR AS A WHOLE WITHOUT THE WRITTEN PERMISSION OF <COMPANY NAME> IS PROHIBITED.

SIZE	DWG. NO.	REV.
A	Small ring	
SCALE:1:1	WEIGHT:	SHEET 1 OF 1

References

1. Betts JG (Tyler JC, Desaix, Peter (UNC CH, Johnson E (Central OCC. Anatomy & Physiology. 2013. 1420 p.
2. Humphrey JD. Cardiovascular Solid Mechanics . Vol. 1, Springer. 2002. 757 p.
3. Lee RT, Kamm RD. Vascular mechanics for the cardiologist. J Am Coll Cardiol. 1994;23(6):1289–95.
4. Levy MN. Circulation Research. Circ Res. 1971;XIII(2):437–45.
5. Friedman MH, Hutchins GM, Bargeron CB, Deters OJ, Mark FF. Correlation between intimal thickness and fluid shear in human arteries. Atherosclerosis . 1981 Jun;39(3):425–36.
6. Munson BR, Okiishi TH, Huebsch WW, Rothmayer AP. Fundamentals of fluid mechanics 7th Edition. J Mech Work Technol. 2013;1–196.
7. Yoganathan AP, Cape EG, Sung HW, Williams FP, Jimoh A. Review of hydrodynamic principles for the cardiologist: Applications to the study of blood flow and jets by imaging techniques. J Am Coll Cardiol . 1988;12(5):1344–53.
8. Conway DE, Eskin SG, McIntire L V. Chapter II.1.6 – Effects of Mechanical Forces on Cells and Tissues (The Liquid–Cell Interface). In: Biomaterials Science. 2013. p. 474–87.
9. Dobrin PB, Littooy FN, Endean ED. Mechanical factors predisposing to intimal hyperplasia and medial thickening in autogenous vein grafts. Surgery . 1989;105(3):393–400.
10. Giddens DP, Zarins CK, Glagov S. The role of fluid mechanics in the localization and detection of atherosclerosis. J Biomech Eng . 1993 Nov;115(4B):588–94.
11. Stary H, Chandler A, Glagov S, Jr G, Insull W, Rosenfeld MJ, et al. AHA Medical / Scientific Statement Special Report A Definition of Initial , Fatty Streak , and Intermediate Lesions of Atherosclerosis. Circulation. 1994;89:2462–78.
12. Hansson GK. Inflammation, atherosclerosis and coronary artery disease. N Engl J Med . 2005;352(16):1685–95.
13. Siracuse JJ, Chaikof EL. The Pathogenesis of Diabetic Atherosclerosis. In: Shrikhande G V, McKinsey JF, editors. Diabetes and Peripheral Vascular Disease: Diagnosis and Management . Totowa, NJ: Humana Press; 2012. p. 13–26.
14. Ross R. Atherosclerosis--an inflammatory disease. N Engl J Med . 1999;340(2):115–26.
15. Gu L, Okada Y, Clinton SK, Gerard C, Sukhova GK, Libby P, et al. Absence of monocyte chemoattractant protein-1 reduces atherosclerosis in low density lipoprotein receptor-deficient mice. Mol Cell. 1998;2(2):275–81.
16. Rudijanto A. The role of vascular smooth muscle cells on the pathogenesis of atherosclerosis. Acta Med Indones . 2007;39(2):86–93.
17. Fersht AR. Catalysis, Binding and Enzyme-Substrate Complementarity. Proc R Soc B Biol

Sci . 1974;187(1089):397–407.

18. Jou LD, van Tyen R, Berger SA, Saloner D. Calculation of the magnetization distribution for fluid flow in curved vessels. Magn Reson Med. 1996;35(4):577–84.

19. Zarins CK, Giddens DP, Bharadvaj BK, Sottiurai VS, Mabon RF, Gladov S, et al. Carotid Bifurcation Atherosclerosis: Quantative Correlation of Plaque Localization with Flow Velocity Profiles and Wall Shear Stress. Circ Res . 1983;53(4):502–14.

20. Zatina M a, Ku DN. Shear stress regulation of arte U lumen diameter in experimental atherogenesis. Animals. :413–20.

21. Berthiaume F, Frangos JA. Flow-induced prostacyclin production is mediated by a pretussis toxin-sensitive G protein. FEBS Lett. 1992;308(August):277–9.

22. Furchgott RF, Zawadzki J V. The obligatory role of endothelial cells in the relaxation of arterial smooth muscle by acetylcholine. Nature. 1980;288(5789):373–6.

23. Palmer RM, Ashton DS, Moncada S. Vascular endothelial cells synthesize nitric oxide from L-arginine. Vol. 333, Nature. 1988. p. 664–6.

24. Busse R, Hecker M, Fleming I. Control of nitric oxide and prostacyclin synthesis in endothelial cells. Arzneimittelforschung . 1994 Mar;44(3A):392–6.

25. Garg UC, Hassid A. Nitric oxide-generating vasodilators and 8-bromo-cyclic guanosine monophosphate inhibit mitogenesis and proliferation of cultured rat vascular smooth muscle cells. J Clin Invest . 1989 May;83(5):1774–7.

26. Levesque MJ, Nerem RM, Sprague E a. Vascular endothelial cell proliferation in culture and the influence of flow. Biomaterials. 1990;11:702–7.

27. DePaola N, \mboxGimbrone Jr MA, Davies PF, \mboxDewey Jr CF. Vascular endothelium responds to fluid shear stress gradients. Arterioscler Thromb Vasc Biol. 1992;12:1254–7.

28. Kaiser D, Freyberg MA, Friedl P. Lack of hemodynamic forces triggers apoptosis in vascular endothelial cells. Biochem Biophys Res Commun . 1997;231(3):586–90.

29. Malek AM, Alper SL. and Its Role in Atherosclerosis. 2010;282(21):2035–42.

30. Korenaga R, Ando J, Kosaki K, Isshiki M, Takada Y, Kamiya a. Negative transcriptional regulation of the VCAM-1 gene by fluid shear stress in murine endothelial cells. Am J Physiol. 1997;273:C1506–15.

31. LaRosa JC, Hunninghake D, Bush D, Criqui MH, Getz GS, Gotto AM, et al. AHA Medical/Scientific Statement. Circulation . 1990;81(5):840–57.

32. Stary, Herbert C.; Chandler, A.; Bleakley MD; Dinsmore RE et al. A definition of Advanced Types of Atheroslcerotic Lesions and a Histological Classification of Atherosclerosis: A report form the committee on vascular lesions of the council on arteriosclerosis, Amercian Heart Association. 1995. p. 1355–74.

33. Tarkin JM, Dweck MR, Evans NR, Takx RAP, Brown AJ, Tawakol A, et al. Imaging Atherosclerosis. Circ Res. 2016;118(4):750–69.

34. Garcia JA, Chen SYJ, Messenger JC, Casserly IP, Hansgen A, Wink O, et al. Initial clinical experience of selective coronary angiography using one prolonged injection and a 180° rotational trajectory. Catheter Cardiovasc Interv. 2007;70(2):190–6.

35. van Velzen JE, Schuijf JD, de Graaf FR, Jukema W, de Roos A, Kroft LJ, et al. Imaging of Atherosclerosis : Invasive and Noninvasive Techniques. Hell J Cardiol. 2009;50:245–63.

36. Agatston AS, Janowitz WR, Hildner FJ, Zusmer NR, Viamonte M, Detrano R. Quantification of coronary artery calcium using ultrafast computed tomography. J Am Coll Cardiol. 1990;15(4):827–32.

37. Hecht HS. Coronary artery calcium scanning: Past, present, and future. JACC Cardiovasc Imaging. 2015;8(5):579–96.

38. Singh NH, Schneider PA. Chapter 8 – Balloon Angioplasty Catheters. In: Endovascular Surgery . 2011. p. 71–80.

39. Van Der Hoeven BL, Pires NMM, Warda HM, Oemrawsingh P V., Van Vlijmen BJM, Quax PHA, et al. Drug-eluting stents: Results, promises and problems. Vol. 99, International Journal of Cardiology. 2005. p. 9–17.

40. Akin I, Schneider H, Ince H, Kische S, Rehders TC, Chatterjee T, et al. Second- and third-generation drug-eluting coronary stents: Progress and safety. Vol. 36, Herz. 2011. p. 190–7.

41. Jukema JW, Verschuren JJW, Ahmed T a. N, Quax PH a. Restenosis after PCI. Part 1: pathophysiology and risk factors. Nat Rev Cardiol . 2011;9(1):53–62.

42. Serruys PW, Jaegere PD, Kiemeneji F, Macaya C, Rutsch W, Heyndrickx G, et al. N Engl J Med. 1994;331(8):481.

43. Roiron C, Sanchez P, Bouzamondo A, Lechat P, Montalescot G. Drug eluting stents: an updated meta-analysis of randomised controlled trials. Heart . 2006;92(5):641–9.

44. Weintraub WS. The Pathophysiology and Burden of Restenosis. Am J Cardiol. 2007;100(5 SUPPL.).

45. Rajagopal V, Rockson SG. Coronary restenosis: a review of mechanisms and management. Am J Med . 2003 Nov;115(7):547–53.

46. Caixeta AM, Arie S, Sândoli de Brito F, Piva de Albuquerque C, Fukushima JT, Garcia DP, et al. [Analysis of elastic retraction in the 1st 15 minutes after coronary balloon angioplasty]. Arq Bras Cardiol . 1996 Jan;66(1):5–9.

47. Rozenman Y, Gilon D, Welber S, Sapoznikov D, Gotsman MS. Clinical and angiographic predictors of immediate recoil after successful coronary angioplasty and relation to late restenosis. Am J Cardiol . 1993 Nov;72(14):1020–5.

48. Virmani R. Drug eluting stents: are human and animal studies comparable? Heart . 2003;89(2):133–8.

49. Dzavik V. New frontiers and unresolved controversies in percutaneous coronary intervention. In: American Journal of Cardiology. 2003.

50. Tanabe K, Hoye A, Lemos PA, Aoki J, Arampatzis CA, Saia F, et al. Restenosis rates following bifurcation stenting with sirolimus-eluting stents for de novo narrowings. Am J Cardiol. 2004;94(1):115–8.

51. Kim MS, Dean LS. In-Stent Restenosis. Cardiovasc Ther. 2011;29(3):190–8.

52. Lee MS, Pessegueiro A, Zimmer R, Jurewitz D, Tobis J. Clinical presentation of patients with in-stent restenosis in the drug-eluting stent era. J Invasive Cardiol . 2008 Aug;20(8):401–3.

53. Farooq V, Gogas BD, Serruys PW. Restenosis. Circ Cardiovasc Interv . 2011;4(2).

54. Chieffo A, Foglieni C, Nodari RL, Briguori C, Sangiorgi G, Latib A, et al. Histopathology of Clinical Coronary Restenosis in Drug-Eluting Versus Bare Metal Stents. Am J Cardiol. 2009;104(12):1660–7.

55. Meurice T, Vallet B, Bauters C, Dupuis B, Lablanche JM, Bertrand ME. Role of endothelial cells in restenosis after coronary angioplasty. Fundam Clin Pharmacol. 1996;10(3):234–42.

56. Liu MW, Roubin GS, King SB. Restenosis after coronary angioplasty. Potential biologic determinants and role of intimal hyperplasia. Circulation . 1989;79(6):1374–87.

57. Garcia J, Crespo A, Goicolea J, Sanmartin M, Garcia C. Study of the evolution of the shear stress on the restenosis after coronary angioplasty. J Biomech. 2006;39(5):799–805.

58. Larsen K, Cheng C, Tempel D, Parker S, Yazdani S, Den Dekker WK, et al. Capture of circulatory endothelial progenitor cells and accelerated re-endothelialization of a bio-engineered stent in human ex vivo shunt and rabbit denudation model. Eur Heart J. 2012;33(1):120–8.

59. Wentzel JJ, Krams R, Schuurbiers JCH, Oomen JA, Kloet J, van der Giessen WJ, et al. Relationship Between Neointimal Thickness and Shear Stress After Wallstent Implantation in Human Coronary Arteries. Circulation . 2001;103(13):1740–5.

60. Heise M, Krüger U, Rückert R, Pfitzman R, Neuhaus P, Settmacher U. Correlation of intimal hyperplasia development and shear stress distribution at the distal end-side-anastomosis, in vitro study using particle image velocimetry. Eur J Vasc Endovasc Surg. 2003;26(4):357–66.

61. Koskinas KC, Chatzizisis YS, Antoniadis AP, Giannoglou GD. Role of endothelial shear stress in stent restenosis and thrombosis: Pathophysiologic mechanisms and implications for clinical translation. Vol. 59, Journal of the American College of Cardiology. 2012. p. 1337–49.

62. Mehran R, Dangas G, Abizaid AS, Mintz GS, Lansky AJ, Satler LF, et al. Classification and Implications for Long-Term Outcome. Circulation. 1999;100:1872–8.

63. Kastrati A, Mehilli J, Dirschinger J, Pache J, Ulm K, Schühlen H, et al. Restenosis after coronary placement of various stent types. Am J Cardiol. 2001;87(1):34–9.

64. Kobayashi Y, De Gregorio J, Kobayashi N, Akiyama T, Reimers B, Finci L, et al. Stented segment length as an independent predictor of restenosis. J Am Coll Cardiol. 1999;34(3):651–9.

65. Cassese S, Byrne RA, Tada T, Pinieck S, Joner M, Ibrahim T, et al. Incidence and predictors of restenosis after coronary stenting in 10 004 patients with surveillance angiography. Heart. 2014 Jan;100(2):153–9.

66. Dangas GD, Claessen BE, Caixeta A, Sanidas EA, Mintz GS, Mehran R. In-stent restenosis in the drug-eluting stent era. J Am Coll Cardiol . 2010;56(23):1897–907.

67. Levine GN, Bates ER, Blankenship JC, Bailey SR, Bittl JA, Cercek B, et al. 2011 ACCF/AHA/SCAI Guideline for Percutaneous Coronary Intervention. A report of the American College of Cardiology Foundation/American Heart Association Task Force on Practice Guidelines and the Society for Cardiovascular Angiography and Interventions. J Am Coll Cardiol. 2011 Dec;58(24):e44-122.

68. Windecker S, Kolh P, Alfonso F, Collet J-P, Cremer J, Falk V, et al. 2014 ESC/EACTS Guidelines on myocardial revascularization: The Task Force on Myocardial Revascularization of the European Society of Cardiology (ESC) and the European Association for Cardio-Thoracic Surgery (EACTS)Developed with the special contribution o. Eur Heart J. 2014 Oct;35(37):2541–619.

69. Tocci G, Barbato E, Coluccia R, Modestino A, Pagliaro B, Mastromarino V, et al. Blood Pressure Levels at the Time of Percutaneous Coronary Revascularization and Risk of Coronary In-Stent Restenosis. Am J Hypertens . 2016 Apr;29(4):509–18.

70. Armstrong EJ, Waltenberger J, Rogers JH. Percutaneous Coronary Intervention in Patients With Diabetes. J Diabetes Sci Technol . 2014;8(3):581–9.

71. Costa MA, Simon DI. Molecular basis of restenosis and drug-eluting stents. Circulation. 2005 May;111(17):2257–73.

72. Yusuf RZ, Duan Z, Lamendola DE, Penson RT, Seiden M V. Paclitaxel resistance: molecular mechanisms and pharmacologic manipulation. Curr Cancer Drug Targets. 2003 Feb;3(1):1–19.

73. Huang S, Houghton PJ. Mechanisms of resistance to rapamycins. Drug Resist Updat. 2001 Dec;4(6):378–91.

74. Koster R, Vieluf D, Kiehn M, Sommerauer M, Kahler J, Baldus S, et al. Nickel and molybdenum contact allergies in patients with coronary in-stent restenosis. Lancet (London, England). 2000 Dec;356(9245):1895–7.

75. Nebeker JR, Virmani R, Bennett CL, Hoffman JM, Samore MH, Alvarez J, et al. Hypersensitivity cases associated with drug-eluting coronary stents: A review of available cases from the Research on Adverse Drug Events and Reports (RADAR) project. J Am Coll Cardiol . 2006;47(1):175–81.

76. Rathore S, Kinoshita Y, Terashima M, Katoh O, Matsuo H, Tanaka N, et al. A comparison of clinical presentations, angiographic patterns and outcomes of in-stent restenosis between bare metal stents and drug eluting stents. EuroIntervention J Eur Collab with Work Gr Interv Cardiol Eur Soc Cardiol. 2010 Feb;5(7):841–6.

77. de Jaegere P, Mudra H, Figulla H, Almagor Y, Doucet S, Penn I, et al. Intravascular ultrasound-guided optimized stent deployment. Immediate and 6 months clinical and

angiographic results from the Multicenter Ultrasound Stenting in Coronaries Study (MUSIC Study). Eur Heart J. 1998 Aug;19(8):1214–23.

78. Cook S, Wenaweser P, Togni M, Billinger M, Morger C, Seiler C, et al. Incomplete stent apposition and very late stent thrombosis after drug-eluting stent implantation. Circulation. 2007 May;115(18):2426–34.

79. Balakrishnan B, Tzafriri AR, Seifert P, Groothuis A, Rogers C, Edelman ER. Strut position, blood flow, and drug deposition: implications for single and overlapping drug-eluting stents. Circulation. 2005 Jun;111(22):2958–65.

80. Hong M-K, Mintz GS, Lee CW, Park D-W, Choi B-R, Park K-H, et al. Intravascular ultrasound predictors of angiographic restenosis after sirolimus-eluting stent implantation. Eur Heart J. 2006 Jun;27(11):1305–10.

81. Moses JW, Leon MB, Popma JJ, Fitzgerald PJ, Holmes DR, O'Shaughnessy C, et al. Sirolimus-eluting stents versus standard stents in patients with stenosis in a native coronary artery. N Engl J Med. 2003 Oct;349(14):1315–23.

82. Nakazawa G, Otsuka F, Nakano M, Vorpahl M, Yazdani SK, Ladich E, et al. The pathology of neoatherosclerosis in human coronary implants: Bare-metal and drug-eluting stents. J Am Coll Cardiol . 2011;57(11):1314–22.

83. for Disease Control C, Prevention, others. National Diabetes Statistics Report: Estimates of Diabetes and Its Burden in the United States. Atlanta, GA: Centers for Disease Control and Prevention; 2014. US Dep Heal Hum Serv. 2017;(Cdc):2009–12.

84. Waller BF, Palumbo PJ, Lie JT, Roberts WC. Status of the coronary arteries at necropsy in diabetes mellitus with onset after age 30 years. Analysis of 229 diabetic patients with and without clinical evidence of coronary heart disease and comparison to 183 control subjects. Am J Med. 1980 Oct;69(4):498–506.

85. Weber, M.B.N;Venalat KM. Chpater 1 Definition and Epidemiology of type 2 diabetes; In: McGuire DKM, editor. Diabetes in Cardiovascular disease: A companion to braunwald's heart disease. Elsevier; 2015. p. 1–10.

86. Van Belle E, Bauters C, Hubert E, Bodart J-CC, Abolmaali K, Meurice T, et al. Restenosis Rates in Diabetic Patients: A Comparison of Coronary Stenting and Balloon Angioplasty in Native Coronary Vessels . Circ . 1997 Sep 2;96(5):1454–60.

87. Carrozza JP, Kuntz RE, Fishman RF, Baim DS. Restenosis after arterial injury caused by coronary stenting in patients with diabetes mellitus. Ann Intern Med . 1993 Mar 1;118(5):344–9.

88. Elezi S, Kastrati A, Pache J, Wehinger A, Hadamitzky M, Dirschinger J, et al. Diabetes mellitus and the clinical and angiographic outcome after coronary stent placement. J Am Coll Cardiol. 1998;32(7):1866–73.

89. Lau KW, Ding ZP, Johan A, Lim YL. Midterm angiographic outcome of single-vessel intracoronary stent placement in diabetic versus nondiabetic patients: a matched comparative study. Am Heart J. 1998 Jul;136(1):150–5.

90. Schofer J, Schlüter M, Rau T, Hammer F, Haag N, Mathey DG. Influence of treatment

modality on angiographic outcome after coronary stenting in diabetic patients: a controlled study. J Am Coll Cardiol . 2000 May;35(6):1554–9.

91. Abizaid A, Kornowski R, Mintz GS, Hong MK, Abizaid AS, Mehran R, et al. The influence of diabetes mellitus on acute and late clinical outcomes following coronary stent implantation. J Am Coll Cardiol . 1998 Sep;32(3):584–9.

92. Marso SP, Lincoff a M, Ellis SG, Bhatt DL, Tanguay JF, Kleiman NS, et al. Optimizing the percutaneous interventional outcomes for patients with diabetes mellitus: results of the EPISTENT (Evaluation of platelet IIb/IIIa inhibitor for stenting trial) diabetic substudy. Circulation. 1999;100(25):2477–84.

93. Kornowski R, Mintz GS, Kent KM, Pichard AD, Satler LF, Bucher TA, et al. Increased restenosis in diabetes mellitus after coronary interventions is due to exaggerated intimal hyperplasia. A serial intravascular ultrasound study. Circulation . 1997 Mar 18;95(6):1366–9.

94. Pansuria M, Xi H, Li L, Yang X-F, Wang H. Insulin resistance, metabolic stress, and atherosclerosis. Front Biosci (Schol Ed) . 2012;4:916–31.

95. Spaulding C, Daemen J, Boersma E, Cutlip DE, Serruys PW. A pooled analysis of data comparing sirolimus-eluting stents with bare-metal stents. N Engl J Med. 2007 Mar;356(10):989–97.

96. Caixeta A, Leon MB, Lansky AJ, Nikolsky E, Aoki J, Moses JW, et al. 5-year clinical outcomes after sirolimus-eluting stent implantation insights from a patient-level pooled analysis of 4 randomized trials comparing sirolimus-eluting stents with bare-metal stents. J Am Coll Cardiol. 2009 Sep;54(10):894–902.

97. Bangalore S, Bhagwat A, Pinto B, Goel PK, Jagtap P, Sathe S, et al. Percutaneous Coronary Intervention in Patients With Insulin-Treated and Non–Insulin-Treated Diabetes Mellitus. JAMA Cardiol . 2016;10016(3):1–8.

98. Tian F, Chen Y, Liu H, Zhang T, Guo J, Jin Q. Assessment of characteristics of neointimal hyperplasia after drug-eluting stent implantation in patients with diabetes mellitus: an optical coherence tomography analysis. Cardiology . 2014 Jan;128(1):34–40.

99. Serruys PW, Morice M-C, Kappetein AP, Colombo A, Holmes DR, Mack MJ, et al. Percutaneous coronary intervention versus coronary-artery bypass grafting for severe coronary artery disease. N Engl J Med . 2009;360(10):961–72.

100. Goel SS, Shishehbor MH. Strategies for multivessel revascularization in patients with diabetes. Cardiol Rev. 2013;29(1):2375–84.

101. Grube E, Chevalier B, Guagliumi G, Smits PC, Stuteville M, Dorange C, et al. The SPIRIT v Diabetic Study: A randomized clinical evaluation of the XIENCE v everolimus-eluting stent vs the TAXUS Liberté paclitaxel-eluting stent in diabetic patients with de novo coronary artery lesions. Am Heart J. 2012;163(5).

102. Stone GW, Kedhi E, Kereiakes DJ, Parise H, Fahy M, Serruys PW, et al. Differential Clinical Responses to Everolimus-Eluting and Paclitaxel-Eluting Coronary Stents in Patients With and Without Diabetes Mellitus. Circulation . 2011 Aug 23;124(8):893–900.

103. Leon MB, Mauri L, Popma JJ, Cutlip DE, Nikolsky E, O'Shaughnessy C, et al. A Randomized Comparison of the Endeavor Zotarolimus-Eluting Stent Versus the TAXUS Paclitaxel-Eluting Stent in De Novo Native Coronary Lesions. 12-Month Outcomes From the ENDEAVOR IV Trial. J Am Coll Cardiol . 2010;55(6):543–54.

104. Jain AK, Lotan C, Meredith IT, Feres F, Zambahari R, Sinha N, et al. Twelve-month outcomes in patients with diabetes implanted with a zotarolimus-eluting stent: results from the E-Five Registry. Heart . 2010 Jun;96(11):848–53.

105. Briguori C, Airoldi F, Visconti G, Focaccio A, Caiazzo G, Golia B, et al. Novel approaches for preventing or limiting events in diabetic patients (naples-diabetes) trial: A randomized comparison of 3 drug-eluting stents in diabetic patients. Circ Cardiovasc Interv. 2011;4(2):121–9.

106. Silber S, Serruys PW, Leon MB, Meredith IT, Windecker S, Neumann F-J, et al. Clinical outcome of patients with and without diabetes mellitus after percutaneous coronary intervention with the resolute zotarolimus-eluting stent: 2-year results from the prospectively pooled analysis of the international global RESOLUTE program. JACC Cardiovasc Interv . 2013 Apr;6(4):357–68.

107. Armstrong EJ, Rutledge JC, Rogers JH, Wild S, Roglic G, Green A, et al. Coronary Artery Revascularization in Patients With Diabetes Mellitus. Circulation. 2013;128(15):1047–53.

108. Hage C, Norhammar A, Grip L, Malmberg K, Sarkar N, Svane B, et al. Glycaemic control and restenosis after percutaneous coronary interventions in patients with diabetes mellitus: a report from the Insulin Diabetes Angioplasty study. Diabetes Vasc Dis Res. 2009 Apr;6(2):71–9.

109. Corpus RA, George PB, House JA, Dixon SR, Ajluni SC, Devlin WH, et al. Optimal glycemic control is associated with a lower rate of target vessel revascularization in treated type II diabetic patients undergoing elective percutaneous coronary intervention. J Am Coll Cardiol. 2004 Jan;43(1):8–14.

110. Lindsay J, Sharma AK, Canos D, Nandalur M, Pinnow E, Apple S, et al. Preprocedure hyperglycemia is more strongly associated with restenosis in diabetic patients after percutaneous coronary intervention than is hemoglobin A1C. Cardiovasc Revascularization Med. 2007;8(1):15–20.

111. Nusca A, Patti G, Marino F, Mangiacapra F, D'Ambrosio A, Di Sciascio G. Prognostic role of preprocedural glucose levels on short- and long-term outcome in patients undergoing percutaneous coronary revascularization. Catheter Cardiovasc Interv. 2012 Sep;80(3):377–84.

112. Assert R, Scherk G, Bumbure A, Pirags V, Schatz H, Pfeiffer AF. Regulation of protein kinase C by short term hyperglycaemia in human platelets in vivo and in vitro. Diabetologia. 2001 Feb;44(2):188–95.

113. Keating FK, Sobel BE, Schneider DJ. Effects of increased concentrations of glucose on platelet reactivity in healthy subjects and in patients with and without diabetes mellitus. Am J Cardiol. 2003 Dec;92(11):1362–5.

114. Undas A, Wiek I, Stepien E, Zmudka K, Tracz W. Hyperglycemia is associated with

enhanced thrombin formation, platelet activation, and fibrin clot resistance to lysis in patients with acute coronary syndrome. Diabetes Care. 2008 Aug;31(8):1590–5.

115. Yngen M, Ostenson CG, Li N, Hjemdahl P, Wallen NH. Acute hyperglycemia increases soluble P-selectin in male patients with mild diabetes mellitus. Blood Coagul Fibrinolysis. 2001 Mar;12(2):109–16.

116. Barlovic DP, Soro-Paavonen A, Jandeleit-Dahm KAM. RAGE biology, atherosclerosis and diabetes. Clin Sci (Lond). 2011 Jul;121(2):43–55.

117. Cefalu WT, Schneider DJ, Carlson HE, Migdal P, Gan Lim L, Izon MP, et al. Effect of combination glipizide GITS/metformin on fibrinolytic and metabolic parameters in poorly controlled type 2 diabetic subjects. Diabetes Care. 2002 Dec;25(12):2123–8.

118. Kuki S, Imanishi T, Kobayashi K, Matsuo Y, Obana M, Akasaka T. Hyperglycemia accelerated endothelial progenitor cell senescence via the activation of p38 mitogen-activated protein kinase. Circ J. 2006 Aug;70(8):1076–81.

119. Lindner V, Reidy MA. Proliferation of smooth muscle cells after vascular injury is inhibited by an antibody against basic fibroblast growth factor. Proc Natl Acad Sci U S A. 1991 May;88(9):3739–43.

120. McClain DA, Paterson AJ, Roos MD, Wei X, Kudlow JE. Glucose and glucosamine regulate growth factor gene expression in vascular smooth muscle cells. Proc Natl Acad Sci U S A. 1992 Sep;89(17):8150–4.

121. Mori S, Takemoto M, Yokote K, Asaumi S, Saito Y. Hyperglycemia-induced alteration of vascular smooth muscle phenotype. J Diabetes Complications. 2002;16(1):65–8.

122. Srivastava S, Ramana K V, Tammali R, Srivastava SK, Bhatnagar A. Contribution of aldose reductase to diabetic hyperproliferation of vascular smooth muscle cells. Diabetes. 2006 Apr;55(4):901–10.

123. Natarajan R, Gonzales N, Xu L, Nadler JL. Vascular smooth muscle cells exhibit increased growth in response to elevated glucose. Biochem Biophys Res Commun. 1992 Aug;187(1):552–60.

124. Hiroishi G, Kobayashi S, Nishimura J, Inomata H, Kanaide H. High D-glucose stimulates the cell cycle from the G1 to the S and M phases, but has no competent effect on the G0 phase, in vascular smooth muscle cells. Biochem Biophys Res Commun. 1995 Jun;211(2):619–26.

125. Radhakrishnan Y, Maile LA, Ling Y, Graves LM, Clemmons DR. Insulin-like growth factor-I stimulates Shc-dependent phosphatidylinositol 3-kinase activation via Grb2-associated p85 in vascular smooth muscle cells. J Biol Chem. 2008 Jun;283(24):16320–31.

126. Igata M, Motoshima H, Tsuruzoe K, Kojima K, Matsumura T, Kondo T, et al. Adenosine monophosphate-activated protein kinase suppresses vascular smooth muscle cell proliferation through the inhibition of cell cycle progression. Circ Res. 2005 Oct;97(8):837–44.

127. Wu W, Yan H, Wang X, Gui Y, Gao F, Tang X, et al. Sodium tanshinone IIA silate inhibits high glucose-induced vascular smooth muscle cell proliferation and migration through

activation of AMP-activated protein kinase. PLoS One. 2014;9(4):e94957.

128. Li H, Peng W, Zhuang J, Lu Y, Jian W, Wei Y, et al. Vaspin attenuates high glucose-induced vascular smooth muscle cells proliferation and chemokinesis by inhibiting the MAPK, PI3K/Akt, and NF-kappaB signaling pathways. Atherosclerosis. 2013 May;228(1):61–8.

129. Park SH, Marso SP, Zhou Z, Foroudi F, Topol EJ, Lincoff AM. Neointimal hyperplasia after arterial injury is increased in a rat model of non-insulin-dependent diabetes mellitus. Circulation . 2001 Aug 14;104(7):815–9.

130. Centers for Diesease Control and Prevention. 2014 National Diabetes Statistics Report. National Diabetes Statistics Report. 2014.

131. Janka HU, Ziegler AG, Standl E, Mehnert H. Daily insulin dose as a predictor of macrovascular disease in insulin treated non-insulin-dependent diabetics. Diabete Metab. 1987 Jul;13(3 Pt 2):359–64.

132. Kronmal RA, Barzilay JI, Tracy RP, Savage PJ, Orchard TJ, Burke GL. The relationship of fasting serum radioimmune insulin levels to incident coronary heart disease in an insulin-treated diabetic cohort. J Clin Endocrinol Metab. 2004 Jun;89(6):2852–8.

133. Wang M-Y, Yu X, Lee Y, McCorkle SK, Clark GO, Strowig S, et al. Iatrogenic hyperinsulinemia in type 1 diabetes: its effect on atherogenic risk markers. J Diabetes Complications. 2013;27(1):70–4.

134. Barazzoni R, Kiwanuka E, Zanetti M, Cristini M, Vettore M, Tessari P. Insulin acutely increases fibrinogen production in individuals with type 2 diabetes but not in individuals without diabetes. Diabetes. 2003 Jul;52(7):1851–6.

135. Emanuele N, Azad N, Abraira C, Henderson W, Colwell J, Levin S, et al. Effect of intensive glycemic control on fibrinogen, lipids, and lipoproteins: Veterans Affairs Cooperative Study in Type II Diabetes Mellitus. Arch Intern Med. 1998 Dec;158(22):2485–90.

136. Kahn SE; McCulloch DK; Pore D. Insulin secretion in the normal and diabetic human. In: Alberti KZiPDRKH, editor. International Textbook of Diabetes Mellitus. 2nd ed. New York: John Wiley & Sons; 1997. p. 337–54.

137. Melmed, Shlomo;Polonsky, Kenneth; Larsen, P. Reed; Kronenberg H. Williams Textbook of Endocrinology. Twelfth. Phiadelphia: Elsevier; 2011.

138. Indolfi C, Torella D, Cavuto L, Davalli AM, Coppola C, Esposito G, et al. Effects of balloon injury on neointimal hyperplasia in streptozotocin-induced diabetes and in hyperinsulinemic nondiabetic pancreatic islet-transplanted rats. Circulation . 2001 Jun 19;103(24):2980–6.

139. Zhang Q, Lu L, Pu L, Zhang R, Shen J, Zhu Z, et al. Neointimal hyperplasia persists at six months after sirolimus-eluting stent implantation in diabetic porcine. Cardiovasc Diabetol . 2007 Jan;6:16.

140. Zhang Q, Lu L, Pu L, Zhang R, Shen J, Zhu Z, et al. Neointimal hyperplasia persists at six months after sirolimus-eluting stent implantation in diabetic porcine. Cardiovasc Diabetol . 2007 Jun 5;6:16.

141. Pfeifle B, Ditschuneit H. Effect of insulin on growth of cultured human arterial smooth

muscle cells. Diabetologia . 1981 Feb;20(2):155–8.

142. Bornfeldt KE, Raines EW, Nakano T, Graves LM, Krebs EG, Ross R. Insulin-like growth factor-I and platelet-derived growth factor-BB induce directed migration of human arterial smooth muscle cells via signaling pathways that are distinct from those of proliferation. J Clin Invest . 1994 Mar;93(3):1266–74.

143. Murphy LJ, Ghahary A, Chakrabarti S. Insulin regulation of IGF-I expression in rat aorta. Diabetes. 1990 Jun;39(6):657–62.

144. Goalstone ML, Natarajan R, Standley PR, Walsh MF, Leitner JW, Carel K, et al. Insulin potentiates platelet-derived growth factor action in vascular smooth muscle cells. Endocrinology. 1998 Oct;139(10):4067–72.

145. Matthaei S, Stumvoll M, Kellerer M, Haring HU. Pathophysiology and pharmacological treatment of insulin resistance. Endocr Rev. 2000 Dec;21(6):585–618.

146. Kellerer M, Lammers R, Haring HU. Insulin signal transduction: possible mechanisms for insulin resistance. Exp Clin Endocrinol Diabetes. 1999;107(2):97–106.

147. Lee YH, White MF. Insulin receptor substrate proteins and diabetes. Arch Pharm Res. 2004 Apr;27(4):361–70.

148. Cusi K, Maezono K, Osman A, Pendergrass M, Patti ME, Pratipanawatr T, et al. Insulin resistance differentially affects the PI 3-kinase- and MAP kinase-mediated signaling in human muscle. J Clin Invest. 2000 Feb;105(3):311–20.

149. Häring, Hans-Ulrich; Gallwitz B. Insulin Resistance: Pathophysiology, Molecular Mechanisms, Genetic Insights. In: McGuire, Darren;Marx N, editor. Diabetes in Cardiovascular disease: A companion to braunwald's heart disease. 1st ed. Elsevier; 2014. p. 11–23.

150. Sowers JR. Actions of Insulin and Igf-I on Vascular Smooth Muscle Cation and Glucose Metabolism BT - Pharmacological Control of Calcium and Potassium Homeostasis: Biological, Therapeutical, and Clinical Aspects. In: Godfraind T, Mancia G, Abbracchio MP, Aguilar-Bryan L, Govoni S, editors. Dordrecht: Springer Netherlands; 1995. p. 129–37.

151. Brosius FC, Briggs JP, Marcus RG, Barac-Nieto M, Charron MJ. Insulin-responsive glucose transporter expression in renal microvessels and glomeruli. Kidney Int . 1992;42(5):1086–92.

152. Standley PR, Rose KA. Insulin and Insulin-like Growth Factor-1 Modulation of Glucose Transport in Arterial Smooth Muscle Cells: Implication of GLUT-4 in the Vasculature. Am J Hypertens . 1994 Apr 1;7(4_Pt_1):357–62.

153. Boucher J, Kleinridders A, Kahn CR. Insulin Receptor Signaling in Normal and Insulin-Resistant States. Cold Spring Harb Perspect Biol . 2014 Jan;6(1):a009191.

154. Chobanian A V, Bakris GL, Black HR, Cushman WC, Green LA, Izzo JLJ, et al. Seventh report of the Joint National Committee on Prevention, Detection, Evaluation, and Treatment of High Blood Pressure. Hypertens (Dallas, Tex 1979). 2003 Dec;42(6):1206–52.

155. Roger VL, Go AS, Lloyd-Jones DM, Adams RJ, Berry JD, Brown TM, et al. Heart disease and stroke statistics--2011 update: a report from the American Heart Association. Circulation. 2011 Feb;123(4):e18–209.

156. Gürlek A, Dağalp Z, Oral D, Omürlü K, Erol C, Akyol T, et al. Restenosis after transluminal coronary angioplasty: a risk factor analysis. J Cardiovasc Risk . 1995 Feb;2(1):51–5.

157. Gariepy J, Massonneau M, Levenson J, Heudes D, Simon A. Evidence for invivo carotid and femoral wall thickening in human hypertension. Hypertension. 1993;22(1):111–8.

158. Warshaw DM, Mulvany MJ, Halpern W. Mechanical and morphological properties of arterial resistance vessels in young and old spontaneously hypertensive rats. CircRes. 1979;45(2):250–9.

159. Wolinsky H. Response of the rate aortic media to hypertension. Circ Res. 1970;26(20):507–22.

160. Owens GK, Schwartz SM. Alterations in vascular smooth muscle mass in the spontaneously hypertensive rat. Circ Res. 1982;51(1):280–9.

161. Leung DY, Glagov S, Mathews MB. Cyclic stretching stimulates synthesis of matrix components by arterial smooth muscle cells in vitro. Science. 1976 Feb;191(4226):475–7.

162. Dobrin PB. Mechanical factors associated with the development of intimal and medial thickening in vein grafts subjected to arterial pressure. A model of arteries exposed to hypertension. Hypertens (Dallas, Tex 1979). 1995 Jul;26(1):38–43.

163. Sullivan TM, Ainsworth SD, Langan EM, Taylor S, Snyder B, Cull D, et al. Effect of endovascular stent strut geometry on vascular injury, myointimal hyperplasia, and restenosis. J Vasc Surg . 2002 Jul;36(1):143–9.

164. Walker M, Kublin JG, Zunt JR. NIH Public Access. 2009;42(1):115–25.

165. Bennett MR. In-stent stenosis: pathology and implications for the development of drug eluting stents. Heart . 2003;89(2):218.

166. Marks AR. Sirolimus for the prevention of in-stent restenosis in a coronary artery. N Engl J Med . 2003;349(14):1307–9.

167. Martin DM, Boyle FJ. Drug-eluting stents for coronary artery disease: A review. Med Eng Phys . 2011;33(2):148–63.

168. Marx SO, Jayaraman T, Go LO, Marks AR. Rapamycin-FKBP Inhibits Cell Cycle Regulators of Proliferation in Vascular Smooth Muscle Cells. Circ Res . 1995 Mar 1;76(3):412 LP-417.

169. Luo Y, Marx SO, Kiyokawa H, Koff A, Massagué J, Marks AR. Rapamycin resistance tied to defective regulation of p27Kip1. Mol Cell Biol . 1996 Dec 1;16(12):6744–51.

170. Price DJ, Grove, Calvo V, Avruch J, Bierer BE. Rapamycin-induced inhibition of the 70-kilodalton S6 protein kinase. Science (80-) . 1992 Aug 14;257(5072):973 LP-977.

171. Graves LM, Bornfeldt KE, Argast GM, Krebs EG, Kong X, Lin TA, et al. cAMP- and rapamycin-sensitive regulation of the association of eukaryotic initiation factor 4E and the

translational regulator PHAS-I in aortic smooth muscle cells. Proc Natl Acad Sci . 1995 Aug 1;92(16):7222–6.

172. Zhu W, Masaki T, Cheung AK, Kern SE. In-vitro Release of Rapamycin from a Thermosensitive Polymer for the Inhibition of Vascular Smooth Muscle Cell Proliferation. J Bioequiv Availab . 2009 May 9;1:3–12.

173. Voisard R, Zellmann S, Müller F, Fahlisch F, von Müller L, Baur R, et al. Sirolimus inhibits key events of restenosis in vitro/ex vivo: evaluation of the clinical relevance of the data by SI/MPL- and SI/DES-ratio's. BMC Cardiovasc Disord . 2007;7(1):15.

174. Wessely R, Hausleiter J, Michaelis C, Jaschke B, Vogeser M, Milz S, et al. Inhibition of neointima formation by a novel drug-eluting stent system that allows for dose-adjustable, multiple, and on-site stent coating. Arterioscler Thromb Vasc Biol. 2005;25(4):748–53.

175. Caro CG, Fitz-Gerald JM, Schroter RC. Atheroma and Arterial Wall Shear Observation, Correlation and Proposal of a Shear Dependent Mass Transfer Mechanism for Atherogenesis. Proc R Soc London B Biol Sci . 1971;177(1046).

176. Pandolfi A, Grilli A, Cilli C, Patruno A, Giaccari A, Di Silvestre S, et al. Phenotype modulation in cultures of vascular smooth muscle cells from diabetic rats: association with increased nitric oxide synthase expression and superoxide anion generation. J Cell Physiol . 2003 Aug;196(2):378–85.

177. Qi Y-XX, Qu M-JJ, Yan Z-QQ, Zhao D, Jiang X-HH, Shen B-RR, et al. Cyclic strain modulates migration and proliferation of vascular smooth muscle cells via Rho-GDI??, Rac1, and p38 pathway. J Cell Biochem . 2010 Apr 1;109(5):906–14.

178. Qiu J, Zheng Y, Hu J, Liao D, Gregersen H, Deng X, et al. Biomechanical regulation of vascular smooth muscle cell functions: from in vitro to in vivo understanding. J R Soc Interface . 2014 Jan 6;11(90):20130852.

179. Madi HA, Riches K, Warburton P, Regan DJO, Turner NA, Porter KE. Inherent differences in morphology , proliferation , and migration in saphenous vein smooth muscle cells cultured from nondiabetic and Type 2 diabetic patients. 2009;(26):1307–17.

180. Lingman M, Albertsson P, Herlitz J, Bergfeldt L, Lagerqvist B. The Impact of Hypertension and Diabetes on Outcome in Patients Undergoing Percutaneous Coronary Intervention. Am J Med. 2011;124(3):265–75.

181. Hasaneen N a, Zucker S, Cao J, Chiarelli C, Panettieri R a, Foda HD. Cyclic mechanical strain-induced proliferation and migration of human airway smooth muscle cells: role of EMMPRIN and MMPs. FASEB J . 2005;19(11):1507–9.

182. Hu Y, Bock G, Wick G, Xu Q, Böck G, Wick G, et al. Activation of PDGF receptor alpha in vascular smooth muscle cells by mechanical stress. FASEB J . 1998;12(12):1135–42.

183. Stegemann JP, Hong H, Nerem RM. Mechanical, biochemical, and extracellular matrix effects on vascular smooth muscle cell phenotype. J Appl Physiol . 2005;98(6):2321–7.

184. Williams B. Mechanical influences on vascular smooth muscle cell function. J Hypertens . 1998;16(12 Pt 2):1921–9.

185. Papadaki M, Eskin S, McIntire L V. Flow modulation of smooth muscle cells (SMC) proliferation and metabolism. Cardiovasc Pathol. 1996;5(5):292.

186. Ueba H, Kawakami M, Yaginuma T. Shear Stress as an Inhibitor of Vascular Smooth Muscle Cell Proliferation. Arterioscler Thromb Vasc Biol . 1997;17(8).

187. Chiu J-J, Chen L-J, Chen C-N, Lee P-L, Lee C-I. A model for studying the effect of shear stress on interactions between vascular endothelial cells and smooth muscle cells. J Biomech . 2004 Apr;37(4):531–9.

188. Stout RW, Bierman EC, Ross R. Effects of insulin on the proliferation of cultured primate arterial smooth muscle cells. Circ Res. 1975;36(February):319–27.

189. Li F, Xia K, Sheikh MS, Cheng J, Li C, Yang T. Retinol binding protein 4 promotes hyperinsulinism-induced proliferation of rat aortic smooth muscle cells. Mol Med Rep . 2014;1634–40.

190. Lightell DJ, Moss SC, Woods TC. Loss of canonical insulin signaling accelerates vascular smooth muscle cell proliferation and migration through changes in p27Kip1 regulation. Endocrinology. 2011;152(2):651–8.

191. Indolfi C, Torella D, Cavuto L, Davalli AM, Coppola C, Esposito G, et al. Effects of Balloon Injury on Neointimal Hyperplasia in Streptozotocin-Induced Diabetes and in Hyperinsulinemic Nondiabetic Pancreatic Islet–Transplanted Rats. Circulation . 2001;103(24).

192. Chawla V, Simionescu A, Langan EM 3rd, LaBerge M. Influence of clinically relevant mechanical forces on vascular smooth muscle cells under chronic high glucose: An In Vitro Dynamic Disease Model. Ann Vasc Surg. 2016 Apr;

193. Chamley-Campbell J, Campbell GR, Ross R. The smooth muscle cell in culture. Physiol Rev . 1979 Jan;59(1):1–61.

194. Liu B, Qu M-J, Qin K-R, Li H, Li Z-K, Shen B-R, et al. Role of Cyclic Strain Frequency in Regulating the Alignment of Vascular Smooth Muscle Cells In Vitro. Biophys J . 2008;94(4):1497–507.

195. Zhang Y, Cheng Y, Ren X, Hori T, Huber-Keener KJ, Zhang L, et al. Dysfunction of Nucleus Accumbens-1 Activates Cellular Senescence and Inhibits Tumor Cell Proliferation and Oncogenesis. Cancer Res . 2012 Aug 15;72(16):4262–75.

196. Cappione A, Diver L, Gillis K, Technologies G. A Multiplex Assay Approach to Screening Cytoactive Compounds for Cell Cycle Disruption and Apoptotic Activity on the Guava EasyCyte ™ Plus System. 2006;1–6.

197. Mahmood T, Yang P-C. Western blot: technique, theory, and trouble shooting. N Am J Med Sci. 2012 Sep;4(9):429–34.

198. Zhang Y, Cheng Y, Ren X, Hori T, Huber-Keener KJ, Zhang L, et al. Dysfunction of Nucleus Accumbens-1 Activates Cellular Senescence and Inhibits Tumor Cell Proliferation and Oncogenesis. Cancer Res . 2012 Aug 15;72(16):4262–75.

199. Imazu M, Sumii K, Yamamoto H, Toyofuku M, Okimoto T, Gomyo Y, et al.

Hyperinsulinemia as a risk factor for restenosis after coronary balloon angioplasty. Jpn Circ J . 2001 Nov;65(11):947–52.

200. Moussa I, Leon MB, Baim DS, Neill WWO', Popma JJ, Buchbinder M, et al. Impact of Sirolimus-Eluting Stents on Outcome in Diabetic Patients A SIRIUS (SIRolImUS-coated Bx Velocity balloon-expandable stent in the treatment of patients with de novo coronary artery lesions) Substudy.

201. Aronson D, Edelman ER. Revascularization for coronary artery disease in diabetes mellitus: angioplasty, stents and coronary artery bypass grafting. Rev Endocr Metab Disord . 2010 Mar;11(1):75–86.

202. Melmed S, Williams RH. Williams textbook of endocrinology. Elsevier/Saunders; 2011. 1897 p.

203. Braun-Dullaeus RC, Mann MJ, Dzau VJ. Cell Cycle Progression. Circulation . 1998;98(1).

204. Avena R, Mitchell ME, Neville RF, Sidawy AN. The additive effects of glucose and insulin on the proliferation of infragenicular vascular smooth muscle cells. J Vasc Surg. 1998;28(6):1033-1038-1039.

205. Acampora KB, Langan EM 3rd, Miller RS, Laberge M. Development of a novel vascular simulator and injury model to evaluate smooth muscle cell response following balloon angioplasty. Ann Vasc Surg. 2007 Nov;21(6):734–41.

206. Nakazawa T, Chiba T, Kaneko E, Yui K, Yoshida M, Shimokado K. Insulin Signaling in Arteries Prevents Smooth Muscle Apoptosis. Arterioscler Thromb Vasc Biol . 2005;25(4).

207. Thakar RG, Cheng Q, Patel S, Chu J, Nasir M, Liepmann D, et al. Cell-shape regulation of smooth muscle cell proliferation. Biophys J . 2009 Apr 22;96(8):3423–32.

208. Heinonen SE, Genové G, Bengtsson E, Hübschle T, Åkesson L, Hiss K, et al. Animal models of diabetic macrovascular complications: key players in the development of new therapeutic approaches. J Diabetes Res . 2015;2015:404085.

209. Hitomi H, Kaifu K, Fujita Y, Sofue T, Nakano D, Moriwaki K, et al. Angiotensin II shifts insulin signaling into vascular remodeling from glucose metabolism in vascular smooth muscle cells. Am J Hypertens . 2011 Oct;24(10):1149–55.

210. Acampora KB, Nagatomi J, Langan EM, LaBerge M. Increased Synthetic Phenotype Behavior of Smooth Muscle Cells in Response to In Vitro Balloon Angioplasty Injury Model. Ann Vasc Surg. 2010;24(1):116–26.

211. Etienne P, Parés-Herbuté N, Mani-Ponset L, Gabrion J, Rabesandratana H, Herbuté S, et al. Phenotype modulation in primary cultures of aortic smooth muscle cells from streptozotocin-diabetic rats. Differentiation . 1998;63(4):225–36.

212. Carrillo-Sepulveda MA, Matsumoto T. Phenotypic modulation of mesenteric vascular smooth muscle cells from type 2 diabetic rats is associated with decreased caveolin-1 expression. Cell Physiol Biochem . 2014;34(5):1497–506.

213. Lee MG, Jeong MH, Lee KH, Park KH, Sim DS, Yoon HJ, et al. Prognostic impact of diabetes mellitus and hypertension for mid-term outcome of patients with acute myocardial

infarction who underwent percutaneous coronary intervention. J Cardiol . 2012 Oct;60(4):257–63.

214. Spofford CM, Chilian WM. The elastin-laminin receptor functions as a mechanotransducer in vascular smooth muscle. Am J Physiol - Hear Circ Physiol . 2001;280(3).

215. Shaw A, Xu Q. Biomechanical Stress-induced Signaling in Smooth Muscle Cells: An Update. Curr Vasc Pharmacol . 2003 Mar 1;1(1):41–58.

216. Hu B, Song J tao, Qu H yan, Bi C long, Huang X zhen, Liu X xin, et al. Mechanical Stretch Suppresses microRNA-145 Expression by Activating Extracellular Signal-Regulated Kinase 1/2 and Upregulating Angiotensin-Converting Enzyme to Alter Vascular Smooth Muscle Cell Phenotype. Casarini DE, editor. PLoS One . 2014 May 21;9(5):e96338.

217. Butcher JT, Barrett BC, Nerem RM. Equibiaxial strain stimulates fibroblastic phenotype shift in smooth muscle cells in an engineered tissue model of the aortic wall. Biomaterials . 2006 Oct;27(30):5252–8.

218. Wan X-J, Zhao H-C, Zhang P, Huo B, Shen B-R, Yan Z-Q, et al. Involvement of BK channel in differentiation of vascular smooth muscle cells induced by mechanical stretch. Int J Biochem Cell Biol . 2015 Feb;59:21–9.

219. Cheng J, Du J. Mechanical Stretch Simulates Proliferation of Venous Smooth Muscle Cells Through Activation of the Insulin-Like Growth Factor-1 Receptor. Arterioscler Thromb Vasc Biol . 2007;27(8).

220. Standley PR, Camaratta A, Nolan BP, Purgason CT, Stanley MA, Camaratta A. Cyclic stretch induces vascular smooth muscle cell alignment via NO signaling. Am J Physiol - Hear Circ Physiol . 2002 Nov 1;283(5):H1907–14.

221. Liu G, Hitomi H, Hosomi N, Lei B, Nakano D, Deguchi K, et al. Mechanical stretch augments insulin-induced vascular smooth muscle cell proliferation by insulin-like growth factor-1 receptor. Exp Cell Res . 2011 Oct 15;317(17):2420–8.

222. Cattaruzza M, Dimigen C, Ehrenreich H, Hecker M. Stretch-induced endothelin B receptor-mediated apoptosis in vascular smooth muscle cells. FASEB J . 2000 May;14(7):991–8.

223. Wernig F, Mayr M, Xu Q. Mechanical Stretch-Induced Apoptosis in Smooth Muscle Cells Is Mediated by 1-Integrin Signaling Pathways. Hypertension . 2003 Apr 1;41(4):903–11.

224. Cheng W-P, Wang B-W, Chen S-C, Chang H, Shyu K-G. Mechanical stretch induces the apoptosis regulator PUMA in vascular smooth muscle cells. Cardiovasc Res . 2012 Jan 1;93(1):181–9.

225. Wernig F, Mayr M, Xu Q. Mechanical stretch-induced apoptosis in smooth muscle cells is mediated by beta1-integrin signaling pathways. Hypertens (Dallas, Tex 1979) . 2003 Apr 1;41(4):903–11.

226. Cutlip DE, Chauhan MS, Baim DS, Ho KKL, Popma JJ, Carrozza JP, et al. Clinical restenosis after coronary stenting: perspectives from multicenter clinical trials. J Am Coll Cardiol . 2002;40(12):2082–9.

227. Tsihlis ND, Vavra AK, Martinez J, Lee VR, Kibbe MR. Nitric oxide is less effective at

inhibiting neointimal hyperplasia in spontaneously hypertensive rats. Nitric Oxide - Biol Chem . 2013;35:165–74.

228. Grote K, Flach I, Luchtefeld M, Akin E, Holland SM, Drexler H, et al. Mechanical stretch enhances mRNA expression and proenzyme release of matrix metalloproteinase-2 (MMP-2) via NAD(P)H oxidase-derived reactive oxygen species. Circ Res. 2003 Jun;92(11):e80-6.

229. Morrow D, Sweeney C, Birney YA, Cummins PM, Walls D, Redmond EM, et al. Cyclic strain inhibits notch receptor signaling in vascular smooth muscle cells in vitro. Circ Res . 2005 Mar 18;96(5):567–75.

230. Wessely R, Hausleiter J, Michaelis C, Jaschke B, Vogeser M, Milz S, et al. Inhibition of neointima formation by a novel drug-eluting stent system that allows for dose-adjustable, multiple, and on-site stent coating. Arter Thromb Vasc Biol . 2005;25.

231. Dibra A, Kastrati A, Mehilli J, Pache J, Schühlen H, von Beckerath N, et al. Paclitaxel-Eluting or Sirolimus-Eluting Stents to Prevent Restenosis in Diabetic Patients. N Engl J Med . 2005 Aug 18;353(7):663–70.

232. Jain AK, Lotan C, Meredith IT, Feres F, Zambahari R, Sinha N, et al. Twelve-month outcomes in patients with diabetes implanted with a zotarolimus-eluting stent: results from the E-Five Registry. Heart . 2010;96(11):848–53.

233. Silber S, Serruys PW, Leon MB, Meredith IT, Windecker S, Neumann FJ, et al. Clinical outcome of patients with and without diabetes mellitus after percutaneous coronary intervention with the resolute zotarolimus-eluting stent: 2-year results from the prospectively pooled analysis of the International Global RESOLUTE Program. JACC Cardiovasc Interv . 2013;6(4):357–68.

234. Poon M, Marx SO, Gallo R, Badimon JJ, Taubman MB, Marks AR. Rapamycin inhibits vascular smooth muscle cell migration. J Clin Invest . 1996 Nov 15;98(10):2277–83.

235. Hamet P, Richard L, Dam T-V, Teiger E, Orlov SN, Gaboury L, et al. Apoptosis in Target Organs of Hypertension. Hypertension . 1995;26(4).

236. deBlois D, Tea B-S, Dam T-V, Tremblay J, Hamet P. Smooth Muscle Apoptosis During Vascular Regression in Spontaneously Hypertensive Rats. Hypertension . 1997;29(1).

237. Zohlnhöfer D, Nührenberg TG, Neumann F-J, Richter T, May AE, Schmidt R, et al. Rapamycin Effects Transcriptional Programs in Smooth Muscle Cells Controlling Proliferative and Inflammatory Properties. Mol Pharmacol . 2004;65(4).

238. Skowasch D, Jabs A, Andrié R, Dinkelbach S, Schiele TM, Wernert N, et al. Pathogen burden, inflammation, proliferation and apoptosis in human in-stent restenosis. Tissue characteristics compared to primary atherosclerosis. J Vasc Res . 2004;41(6):525–34.

239. Fortuño A, José GS, Moreno MU, Díez J, Zalba G. Oxidative stress and vascular remodelling. Exp Physiol . 2005 Jul;90(4):457–62.

240. Chiu C-Z, Wang B-W, Shyu K-G. Effects of cyclic stretch on the molecular regulation of myocardin in rat aortic vascular smooth muscle cells. J Biomed Sci . 2013 Jul 15;20(1):50.

241. Cheng J, Wang Y, Ma Y, Chan BT, Yang M, Liang A, et al. The mechanical stress-activated serum-, glucocorticoid-regulated kinase 1 contributes to neointima formation in vein grafts. Circ Res . 2010 Nov 12;107(10):1265–74.

242. Zampetaki A, Zhang Z, Hu Y, Xu Q. Biomechanical stress induces IL-6 expression in smooth muscle cells via Ras/Rac1-p38 MAPK-NF- B signaling pathways. AJP Hear Circ Physiol . 2005 Jun 1;288(6):H2946–54.

243. Patel R, Cardneau JD, Colles SM, Graham LM. Synthetic smooth muscle cell phenotype is associated with increased nicotinamide adenine dinucleotide phosphate oxidase activity: Effect on collagen secretion. J Vasc Surg . 2006 Feb;43(2):364–71.